OCS Study
MMS 2000-053

Coastal Marine Institute

Wave Climate and Bottom Boundary Layer Dynamics with Implications for Offshore Sand Mining and Barrier Island Replenishment in South-Central Louisiana

Author

Gregory W. Stone Ph.D.

December 2001

Prepared under MMS Contract
14-35-0001-30660-19911b
by
Louisiana State University
Dept. of Oceanography and Coastal Sciences
Howe-Russell Geoscience Complex
Baton Rouge, Louisiana 70803

Published by

U.S. Department of the Interior
Minerals Management Service
Gulf of Mexico Region

Cooperative Agreement
Coastal Marine Institute
Louisiana State University

Disclaimer

This report was prepared under contract between the Minerals Management Service (MMS) and Louisiana State University. This report has been technically reviewed by the MMS and approved fro publication. Approval does not signify that the contents necessarily reflect the views and policies of the Service nor does mention of trade names or commercial products constitute endorsement or recommendation for use. It is, however, exempt from review and compliance with MMS editorial standards.

Report Availability

Extra copies of the report may be obtained from Public Information Office (MS 5043) at the following address.

U.S. Department of the Interior
Minerals Management Service
Gulf of Mexico OCS Region
Public Information Office (MS 5034)
1201 Elmwood Park Boulevard
New Orleans, Louisiana 70123-2394

Telephone Number: (504) 736-2519 or
1-800-200-GULF

Citation

Stone, G.W. 2001. Wave Climate and bottom boundary layer dynamics with implications for offshore sand mining and barrier island replenishment in south-central Louisiana. OCS Study MMS 2000-053. U.S. Dept. of the Interior, Minerals Mgmt. Service, Gulf of Mexico OCS Region, New Orleans, La. 90 pp.

SUMMARY

The results of a three-year field study of wave climate, wave-current interactions and bottom boundary layer dynamics, and sediment transport on Ship Shoal, off the Isles Dernieres in south-central Louisiana, are presented. Through the procurement and fabricating of bottom boundary layer instrumentation systems, wave characteristics were measured simultaneously at two geographical locations on Ship Shoal to ultimately validate a spectral wave propagation model (STWAVE) used extensively in a previously funded MMS project which concentrated on assessing the potential impacts of mining Ship Shoal off the Louisiana coast. In addition, direct field measurements of temporally- and spatially-varying directional wave spectra were obtained at two locations on the inner shelf. These field measurements were conducted under different wave conditions (storms, fair weather, *etc*.) to facilitate numerical model output validation and to develop a quantitative wave climate for the study area. A third objective involved obtaining direct field measurements of bottom boundary layer hydrodynamic processes and suspended sediment transport. These measurements include total bed shear stress, bed roughness, drag coefficient and their relationship to wave directional spectral characteristics, mean current velocity profile, bedform (*e.g.*, ripples), and suspended sediment concentrations. It is anticipated that the data presented in this report will significantly enhance confidence in numerical modeling of wave conditions on the inner continental shelf . In addition the data presented here are the first on the dynamic characteristics of the bottom boundary layer, directional suspended sediment flux, and the morphodynamic behavior (erosion and accretion) of the bottom in the study area.

TABLE OF CONTENTS

Page

1. INTRODUCTION 1

   Program Overview 1
   Research Objectives 3
   Program Principal Investigator and Support Personnel 3
   Publications Derived from Funded Research 4

2. CONCEPTUAL FRAMEWORK AND STUDY AREA 7

   Introduction 7
   Conceptual Basis for the Research 11
   Study Area 12
   Meteorology 13
   Hydrodynamics and Bottom Boundary Layer Regime 14
   Geology/Geomorphology 15
   Practical Concerns 17

3. METHODOLOGY 19

   Instrumentation and Field Methods 19
   Laboratory Methods 22
   Data Processing and Analytical Methods 23

4. METEOROLOGICAL CONDITIONS DURING THE DEPLOYMENTS 33

   Classification Systems for Meteorological Events 33
   Analysis of Meteorological Events During the Deployment 34
   Meteorological Summary of the Deployment 34

5. HYDRODYNAMICS, BOTTOM BOUNDARY LAYER PARAMETERS AND SEDIMENT TRANSPORT DURING THE ENTIRE DEPLOYMENT PERIOD: TIME- AND FREQUENCY- DOMAIN ANALYSIS AND OVERALL SUMMARY 39

   Introduction 39
   Initial Considerations: Field Observations 39
   Hydrodynamics 42
   Bottom Boundary Layer Parameters 49
   Sediment Suspension and Transport 50

6. COMPARISON OF HYDRODYNAMICS, BOTTOM BOUNDARY LAYER PARAMETERS AND SEDIMENT TRANSPORT DURING STORMS AND FAIR WEATHER CONDITIONS 57

Storm and Fair Weather Hydrodynamics 57
Bottom Boundary Layer Parameters 58
Sediment Transport 61
Sediment Fluxes across Ship Shoal 64

7. VALIDATION OF NUMERICAL WAVE MODEL (STWAVE) 69

Introduction 69
Validation Methods 69
Comparison of *in situ* Modeled Data 70

8. CONCLUSIONS 81

9. REFERENCES 83

LIST OF FIGURES

Figure **Page**

1.1 Map of the Ship Shoal study site off the Isles Dernieres, Louisiana 2
2.1 Results of analysis of sediment from Site 1 16
2.2 Results of analysis of sediment from Site 2 17
3.1 System 2A during deployment at Site 2 20
3.2 System 1B during deployment at Site 1 20
3.3 Location of instrumentation sites at Ship Shoal 21
4.1 Wind speed during the deployment period 35
4.2 Feather plot of hourly wind vectors during the deployment 35
4.3 Power spectrum of wind speed during the deployment 36
5.1 Bed elevation and water level as measured by System 1B during the deployment 40
5.2 Total water depth as measured hourly and smoothed using a 24-h moving average window as measured by System 1B 41
5.3 Across-shelf current flow during the deployment at Sites 1 and 2 as measured by systems 1A and 2A 43
5.4 Significant wave height at Site 1 and Site 2 44
5.5 Peak wave period at Site 1 and Site 2 44
5.6 Flow speed of mean and orbital currents at Site 1 45
5.7 Flow speed of mean and orbital currents At Site 2 46
5.8 Spectrum of current speed at Site 1 46
5.9 Vector plot of mean current direction at Site 1 during the deployment 47
5.10 Cross spectrum of wind and across-shelf current at Site 1 48
5.11 Phase spectrum of northerly wind and northerly current at Site 1 48
5.12 Current and combined wave-current shear velocity as measured at Site 1 49
5.13 Current and combined wave-current shear velocity as measured at Site 2 50
5.14 Suspended sediment concentration at Site 1 50
5.15 Suspended sediment concentration at Site 2 51
5.16 Across-shelf longshore sediment transport for Site 2 as predicted using the GMR method 51
5.17 Along-shelf cross-shore sediment transport for Site 2 as predicted using the GMR method 52
5.18 Across-shelf cross-shore sediment transport for Site 1 as predicted using the GMR method 52
5.19 Along-shelf longshore sediment transport for Site 1 as predicted using the GMR method 53
5.20 Longshore along-shelf bed and suspended load sediment for Site 1 as predicted using the MPM and SCC methods 53
5.21 Cross-shore across-shelf bed and suspended load sediment transport for Site 1 as predicted using the MPM and SCC methods 54
5.22 Cross-shore across-shelf bed load and suspended load transport for Site 2, as predicted using the MPM and SCC methods 54
5.23 Longshore along-shelf bed load and suspended load Transport for Site 2, as predicted using the MPM and SCC methods 55

6.1 Current flux over Ship Shoal 65
6.2 Flux of sediment across Ship Shoal as calculated using the GMR Method 66
6.3 Flux of suspended sediment across Ship Shoal as calculated using the steady current/ concentration method 66
6.4 Flux of bed load across Ship Shoal as calculated using the Meyer-Peter and Muller method 67
7.1 Location of the modeling area at Ship Shoal and instrumentation deployment sites . 70
7.2 Summary of % over prediction of H_s by STWAVE for all stations 71
7.3 Summary of r^2 values for measured and modeled H_s for all stations 71
7.4 Scatter plot of significant wave heights for 1998/99 deployment for all wind directions at Inshore station 72
7.5 Comparison of measured and numerically modeled wave heights for all directions in 1998/99 deployment at Inshore station 72
7.6 Scatter plot of significant wave heights for all wind direction at Inshore station for 2000 deployment 73
7.7 Comparison diagram of numerically modeled and measured wave heights for all wind directions at Inshore station for 2000 deployment 73
7.8 Scatter plot of Hs measured vs. Hs numerically modeled for 2000 deployment at Middle Station 74
7.9 Comparison diagram of numerically modeled and measured wave heights for all wind directions at Middle station for 2000 deployment 74
7.10 Scatter plot of measured and modeled H_s for wind blowing from southwest, south and southeast for 1998/99 deployment at Inshore station 75
7.11 Comparison diagram of numerically modeled and measured wave heights for selected southwest, south, and southeast winds at Inshore tation for 1998/99 deployment 75
7.12 Scatter plot of Hs measured vs. Hs numerically modeled at Inshore station for southwest, south, and southeast wind directions for 2000 deployment 76
7.13 Comparison diagram of numerically modeled and measured wave heights for southwest, south and southeast wind directions at Inshore station for 2000 deployment 76
7.14 Scatter plot of Hs measured vs. numerically modeled Hs at Middle station for southwest, south, and southeast winds for 2000 deployment 77
7.15 Relationship between numerically modeled and measured significant wave heights at Middle station for southwest, south and southeast winds 77
7.16 Scatter plot of Hs measured vs, Hs numerically modeled for southwest wind only at Inshore station for 2000 deployment 78
7.17 Relationship between numerically modeled and measured significant wave heights for southwest wind only at Inshore station 78
7.18 Scatter plot of Hs measured vs. Hs numerically modeled for southwest wind only at Middle station for 2000 deployment 79
7.19 Relationship between numerically modeled and measured significant wave heights for southwest wind only at Middle station 79

LIST OF TABLES

Table **Page**

3.1 Sampling schemes used in data collection 21
3.2 Segment, window, and overlap lengths used in spectral analysis 23
3.3 Summary of methods used to calculate shear velocity and sediment transport 25
4.1 Classification of storms during the deployment on the basis of the methods discussed 37
5.1 Summary of hydrodynamics parameters recorded by the systems throughout the deployment 42
6.1 Summary of storm and fair weather hydrodynamic measurements taken at Site 1 using System 1B 58
6.2 Summary of storm and fair weather hydrodynamic measurements taken at Site 2 using System 2A 58
6.3 Summary of bottom boundary layer parameters calculated based on System 1B data for storms and fair weather conditions 59
6.4 Summary of bottom boundary layer parameters calculated based on data from the offshore ADV for storms and fair conditions 59
6.5 Summary of bottom boundary layer parameters calculated based on the System 2A data for storms and fair weather conditions at Site 2 60
6.6 Summary of sediment transport estimates within and above the wave boundary layer for storms and fair weather conditions at the offshore Site 61
6.7 Predicted sediment transport and bed level change for Site 1 based on data from System 1A analyzed using several models 62
6.8 Predicted sediment transport and bed level change for Site 2 based on several models 62
6.9 Co-spectral estimates of suspended transport at System 1A 63
6.10 Co-spectral estimates of suspended sediment transport at System 2A 88
6.11 Sediment flux across Ship Shoal during storms and fair weather as predicted from Systems 1A and 2A using spectral methods and the GMR and MPM methods 67
7.1 Percentage of over prediction of H_s by STWAVE when compared to *in situ* measurements at two locations on Ship Shoal, based on 590 model run 71

1. INTRODUCTION

Program Overview

Coastal erosion and wetland loss in Louisiana have been a serious threat to the coastal ecosystem and local economy. Degradation of Louisiana's barrier shorelines is interconnected with massive wetland loss (McBride *et al.*, (1989); Williams *et al.*, 1992; Stone et al., 1997; Stone and McBride, 1998). Among the most promising mitigative techniques to temporarily offset further deterioration of the barrier island system, thereby reducing wetland loss, involves increasing the subaerial volume of barrier islands located primarily west of the Mississippi River. The most economically and technically feasible source of sediment appears to be Ship Shoal, a shore-parallel sand body with approximately 1.25 x 10^9 m^3 of fine sand (Suter *et al.*, 1989) located 15 km offshore off the Isles Dernieres (Figure 1). In 1994, MMS funded the first phase of a multi-year project designed to numerically model the impacts of shoal removal on the wave field (Stone and Xu, 1996). The results of that project are summarized below:

1. Removal of Ship Shoal will alter wave propagation, dissipation and wave energy distribution. The magnitude and spatial distribution of the alteration depends on the initial wave conditions, and initial wave direction is not an important factor in determining the wave climate change. During severe storms (Case 1; H_s=6 m, T_p=11 sec.) and strong storms (Case 2; H_s=4 m, T_p=9 sec.), the propagating waves reach breaking conditions seaward of the west part of Ship Shoal. Therefore, removal of Ship Shoal causes a maximum increase of the significant wave height over the shoal complex and its lee flank. Wave breaking does not occur on the east part of Ship Shoal because of much deeper water, and the magnitude of the wave height increase due to shoal removal is secondary on comparison with the value on the west flank of the shoal. During weak storms (Case 3; H_s=2 m, T_p=6 sec.) and fair weather conditions (Case 4; H_s=1 m, T_p=5 sec.), waves never reach breaking conditions over any part of Ship Shoal. The magnitude of the significant wave height increase due to the removal of the shoal is considerably smaller, and the magnitudes of the wave height increase on the east part of the shoal are minimal.

2. The nearshore wave fields are largely dependent on the offshore wave conditions. Numerical simulations indicate that under high energy conditions (Case 1 and Case 2) removal of Ship Shoal may result in larger breaking wave heights and, therefore, displacement of the breaker zone offshore by 0.5 - 1.0 km. Energy levels however do not show a marked increase in the nearshore zone due to post-breaking frictional dissipation, when the shoal is removed. This is even less apparent under the weaker energy conditions in Case 3 and Case 4.

3. Inclusion of a wind forcing function in the numerical model significantly enhances the overall significant wave height. A 20 m/s wind (Case 1) in the wave direction causes an increase of the significant wave height by as much as 1.0 m . A 5 m/s wind in Case 4, also in the wave direction, can increase the wave height by 0.2 m. Consequently, the width of the surf zone is also increased significantly during "local" winds.

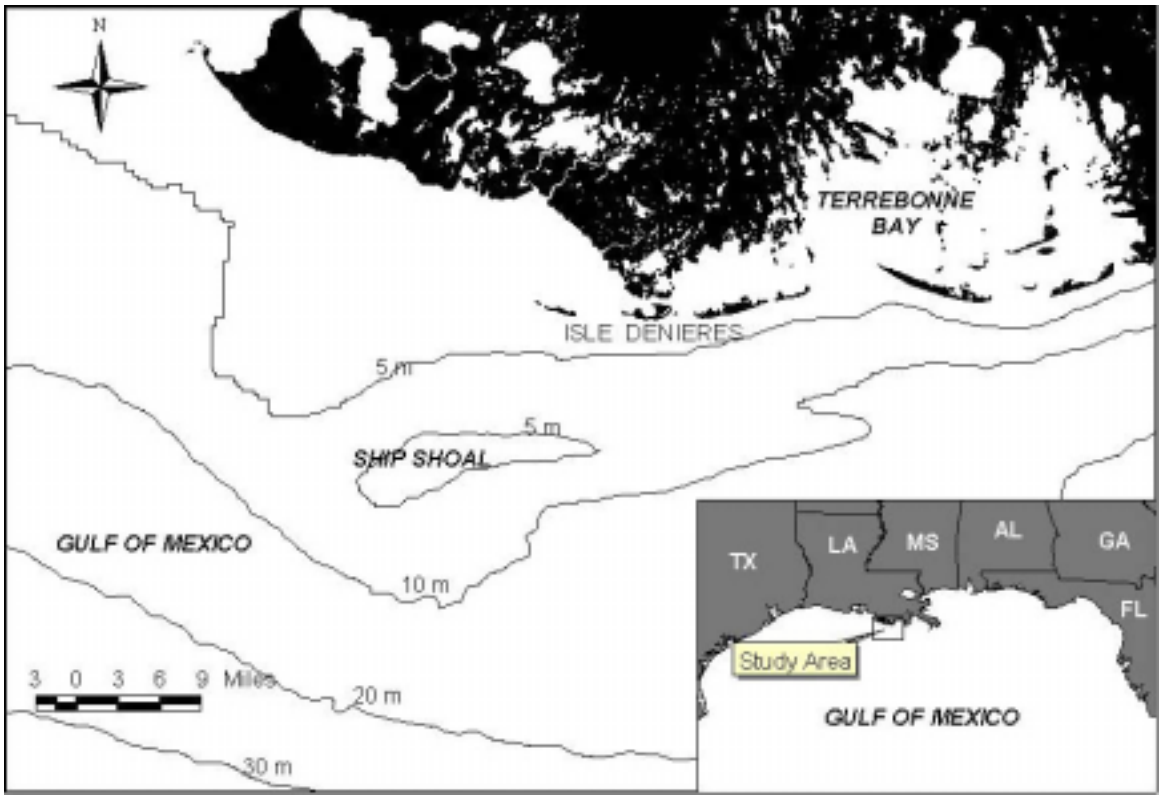

Figure 1.1. Map of the Ship Shoal study site off the Isles Dernieres, Louisiana.

Although the results obtained from the numerical modeling phase will provide guidance in management decision making and developing the Environmental Impact Statement pertaining to Ship Shoal, three critical questions remain unanswered:

1. **To what extent does the numerical model realistically represent conditions in the field?**

As stated explicitly in phase 1 of this study, a comprehensive field data set from which the wave climate, among other things, can be constructed for the study area off the Isles Dernieres on the inner shelf will be necessary to help check and validate model output. The data necessary to accomplish this are not available at present. Although the model (STWAVE) has gained acceptance in the scientific and engineering literature (Kraus *et al*., 1991; McKee et al., 1999), comparisons with measurements obtained from *in situ* measurement is necessary on applying the model locally;

2. **What are the dynamic characteristics of the bottom boundary layer in the region? How do they control the suspension and transport of bed sediment?**

3. **If Ship Shoal is mined, what will be the transport dynamics of sediment introduced to the inner shelf from the shoal on dredging completion, and what changes will occur to the bottom boundary layer? How will this ultimately affect the distribution and fate of sediment along the nourished coast?**

This report describes the findings of a three year study that directly addresses these questions. The project is unique in that it is the first research effort that concentrates on the dynamic characteristics of the bottom boundary layer, directional suspended sediment flux, and the morphodynamic behavior (erosion and accretion) of the bottom.

Research Objectives

This report presents the data and interpretation of a three-year field study of wave climate, wave-current interactions and bottom boundary layer dynamics, and sediment transport in the Ship Shoal area, landward to the inner shelf adjacent to the Isles Dernieres. The primary objectives of this research are as follows:

1. *Obtain direct field measurements of bottom boundary layer hydrodynamic processes and suspended sediment transport*.

These measurements include total bed shear stress, bed roughness, drag coefficient and their relationship to wave directional spectral characteristics, mean current velocity profile, bedform (*e.g.*, ripples), and suspended sediment concentrations.

2. O*btain direct field measurements of temporally- and spatially-varying directional wave parameters at several locations on Ship Shoal*.

These field measurements were obtained under different wave conditions (storms and fair weather) to facilitate skill assessment of the numerical model output and to develop a quantitative wave climate for the study area.

Program Principal Investigator and Support Personnel

All aspects of this program, including preparation of this report, have been carried out by the principal investigator, Dr. Gregory W. Stone (Louisiana State University). David Pepper (CSI) has developed much of the bottom boundary layer data into a hydrodynamic-sediment transport model as part of a Ph.D. dissertation and has contributed to this report and provided field support. Xiongping Zhang (CSI) has assisted in running and skill assessing the numerical wave model (STWAVE) and has contributed to this report also. Dr. Ping Wang (CSI) has assisted in field work and data interpretation. Field deployments were accomplished through the Coastal Studies Institute's Field Support Group who also fabricated the bottom boundary layer instrumentation arrays.

Publications Derived from Funded Research

The following publications have dealt specifically with the data obtained from this research:

Stone, G. W., J. P. Xu, and X. P. Zhang. 1995. Estimation of the wave field during Hurricane Andrew and morphological impacts along the Louisiana coast. In: Stone, G.W. and C.W. Finkle, eds. Impacts of Hurricane Andrew on the Coastal Zones of Florida and Louisiana: *Journal Coastal Research Special Issue* 21:234-253.

Stone, G.W. and J.P. Xu. 1995. Wave Climate Modeling and Evaluation Relative to Sand Mining on Ship Shoal, Offshore Louisiana, for Coastal and Barrier Island Restoration. Report prepared for Minerals Management Service. Coastal Morphodynamics Laboratory Technical Paper 95-3, 21 pp.

Stone, G.W. and J. P. Xu. 1995. Wave and nearshore transport modelling Louisiana coast. Coastal Morphodynamics Laboratory Technical Paper 95-5, 18 pp.

Stone, G.W., J. P. Xu, and X. P. Zhang. 1995. Wave climate modeling and evaluation relative to sand mining on Ship Shoal, offshore Louisiana, for coastal and barrier island restoration. U.S. Minerals Management Service International Transfer Meeting, New Orleans, LA. (invited).

Xu, J.P., G. W. Stone and X. P. Zhang. 1995. Impacts of Ship Shoal on storm wave propagation across south-central Louisiana shelf, a simulation study. Geological Society of America Annual Meeting, New Orleans, LA.

Stone, G.W., J. P. Xu and X. P. Zhang. 1996. Ship shoal wave climate modeling and evaluation. *Transactions*, International Transfer Meeting, Minerals Management Service, Gulf of Mexico OCS Region, New Orleans, LA.

Stone, G.W., J. P. Xu and X. P. Zhang. 1996. Physical and environmental studies within the Ship Shoal area: wave climate study and ongoing physical field study. U.S. Minerals Management Service International Transfer meeting, New Orleans, LA. (invited).

Xu, J.P. and G. W. Stone. 1996. Wave climate modeling and evaluation relative to sand mining on Ship Shoal, offshore Louisiana, for coastal barrier island restoration. American Geophysical Spring Meeting, Baltimore, MD.

Zhang, X.P. and G. W. Stone. 1997. Application of GIS to assist in wave modeling for the central Louisiana coast. 13th. Louisiana remote Sensing and Geographical Information Systems Conference, Lafayette, LA.

Stone, G.W. 1998. The significance of frontal boundaries, tropical storms and hurricanes on the morphodynamics of Gulf Coast barriers, USA." International Coastal Symposium, West Palm Beach, FL.

Stone, G.W. 1998. Numerical wave modeling of wave energy increases in Louisiana's bays, USA. International Coastal Symposium, West Palm Beach, FL.

Stone, G.W. and R. A. McBride. 1998. Louisiana barrier islands and their importance in wetland protection: forecasting shoreline change and subsequent response of wave climate. *Journal of Coastal Research* 14, 3, 900-916.

Stone, G.W., X. P. Zhang and P. Wang. 1998. Forecasting wave energy changes along the Louisiana coast and implications for accelerated wetland loss. International Deltas Symposium, New Orleans, LA.

Pepper, D.A., G. W. Stone and P. Wang. 1998. A preliminary assessment of wave and sediment interaction on the Louisiana shoreface adjacent to Ship Shoal and the Isles Dernieres. Recent Research in Coastal Louisiana, Lafayette, LA.

Zhang, X.P. and G. W. Stone. 1998. Development of a Louisiana coastal processes geographic information system. Recent Research in Coastal Louisiana, Lafayette, LA.

Stone, G.W. and P. Wang. 1999. The importance of cyclogenesis on the short-term evolution of Gulf Coast barriers. *Transactions*, Gulf Coast Association of Geological Societies, Lafayette, LA., XLIX:478-486.

Pepper, D.A., G. W. Stone and P. Wang. 1999. Boundary layer parameters and sediment transport on the Louisiana inner shelf during cold front passages. *Transactions*, Gulf Coast Association of Geological Societies, Lafayette, LA., XLIX: 432-438

Stone, G.W. 1999. The importance of cyclogenesis on the short-term evolution of Gulf Coast Barriers. Association of American Geographers, 95th Annual Meeting, Honolulu, HI.

Stone, G.W. 1999. Storm impacts and the importance of subsidence on the Mississippi River delta plain, Louisiana, USA. 52nd NGMSO Lecture Series, University of Utrecht, The Netherlands.

Stone, G.W. and P. Wang. 1999. The importance of cyclogenesis on the short-term evolution of Gulf Coast barriers. Gulf Coast Association of Geological Societies, Lafayette, LA.

Stone, G.W., P. Wang and D. Pepper. 1999. Importance of hurricanes, tropical storms and mid-latitude cyclones on the short-term evolution of Gulf Coast barriers: the impact of Hurricane Camille: A Storm Impacts Symposium to Mark the 30 th Anniversary, New Orleans, LA.

Stone, G.W., P. Wang and X. P. Zhang. 1999. Development of a wave-current information system for Louisiana bay-shelf environments. Estuarine Research Federation'99, 15th Biennial International Conference, New Orleans, LA.

Pepper, D.A., G. W. Stone and P. Wang. 1999. Bottom boundary layer parameters and predicted sediment transport. Association of American Geographers, 95th Annual Meeting, Honolulu, HI.

Pepper, D.A., G. W. Stone and P. Wang. 1999. The significance of mid latitude cyclones on the inner continental shelf of the northern Gulf of Mexico: the impact of Hurricane Camille: A Storm Impacts Symposium to Mark the 30 th Anniversary, New Orleans, LA.

Pepper, D.A., G. W. Stone and P. Wang. 1999. Boundary layer parameters and sediment transport on the Louisiana inner shelf during cold front passages. Gulf Coast Association of Geological Societies, Lafayette, LA.

Pepper, D.A., G. W. Stone P. Wang. 2000 A preliminary assessment of wave, current, and Sediment Interaction on the Louisiana Shoreface Adjacent to the Isles Dernieres. *Estuaries* (in press).

2. CONCEPTUAL FRAMEWORK AND STUDY AREA

Introduction

The inner shelf is the region adjacent to the coast where the entire water column is dominated by friction with the overlying air and the underlying seabed. In spatial terms, it lies between the shoreline and the mid-continental shelf, with the surf zone as its most landward portion. The dominant hydrodynamic variables that operate in this environment are infragravity and wind waves, as well as currents generated by winds and tides. These hydrodynamic influences jointly exert stress on the water column and seabed, causing sediment to be mobilized and transported along the bed or in suspension (Kim *et al.*, 1997). Given the importance of wind as a forcing mechanism, it follows that the passage of atmospheric storms often results in hydrodynamic responses, bottom boundary layer modification, and sediment transport on inner shelves. Not surprisingly, therefore, field research has often demonstrated that storm events can be responsible for transporting very large quantities of sediment in comparison with fair weather conditions.

The general model for inner shelf sediment transport that has emerged is one in which fair weather wave asymmetry gradually moves sediment onshore, while during storms, high wave orbital currents suspend sediment that is then transported offshore by downwelling mean flows (Wright et al, 1991; Nittrouer and Wright, 1994). Furthermore, it is commonly assumed that alongshelf transport of suspended sediment during both fair weather and storm conditions is much higher than across-shelf transport, owing to stronger mean flows in the alongshore direction. Considerable deviation from these general models results, however, from variability in meteorological conditions, local geology, bathymetry, and physical oceanography. Additionally, a variety of complex and poorly-understood interactions and feedback mechanisms operate in the bottom boundary layer. For example, while it is sometimes assumed that waves provide the shear stress (or “stirring mechanism”) that entrains sediment that is then transported by mean currents, recent research has demonstrated that waves and currents interact in a highly non-linear fashion, complicating sediment transport predictions (Grant and Madsen, 1979, 1986).

The Louisiana inner shelf is an example of a low-energy environment where significant hydrodynamic activity is generated almost exclusively by local storms, including both tropical (summer) and extratropical (winter) storms. Furthermore, the Louisiana coast is somewhat unique as a result of its high rates of subsidence and land loss. Bearing this uniqueness in mind, however, the following paragraphs are intended to serve as a discussion of field research conducted on inner shelves around the world, highlighting “typical” hydrodynamic, bottom boundary layer and sedimentary responses to meteorological forcing, and the sources of deviation from these usual responses.

A large proportion of research dealing with continental-shelf response to meteorological forcing emphasizes the importance of storms in generating high bed stress due to the combined effects of waves and currents, and causing large increases in sediment transport, which varies in direction. Nittrouer and Wright (1994) state, for example, that sediment particles can be transported tens of kilometers seaward during storms, in contrast to fair weather conditions,

when sediment transport may be landward, or may not occur at all. Lyne *et al*. (1990a, 1990b) estimated that 91% of sediment transport along the mid-continental shelf of the U.S. Atlantic coast occurs during storms due to strong bed stresses resulting from wave and current interaction. Niedoroda and Swift (1981) and Niedoroda *et al*. (1984) stated that winter storm activity provides an important contribution to the long-term retreat of the Long Island coast. They observed offshore and alongshore transport as a result of the combination of high wave energy and strong downwelling currents at the peak of a winter storm, while during the waning phases of the storm, when upwelling occurred, the waves were generally too low to entrain sediment. Fair weather periods were characterized by wave asymmetry that transported sediment landward at depths shallower than 10m. In contrast, Vincent *et al.* (1983) suggested that winter storms produce a net onshore bedload sediment transport in the same region, accompanied by a shore-parallel transport of fine suspended sediment. The researchers did note, however, that offshore transport components were measured during one winter storm, suggesting that there may be considerable variability in transport direction, depending on the specific wind conditions accompanying a storm.

Despite well-documented differences in oceanographic regime, the continental shelf of the Pacific coast of North America seems to be characterized by similar storm-driven responses. According to Cacchione and Drake (1990), over 50% of sediment transport in a one-year period on the northern California inner shelf occurred during that year's 20 stormiest days. The authors propose that, during storms, sediment transport is predominantly offshore at depths less than 50m, as a result of strong wave activity combined with downwelling, and alongshore in deeper water. They note that transport is almost always the result of an interaction between factors, most often mean and wave-orbital flows. Finally, they point out that transport rates and directions are strongly dependent upon the location and intensity of the storm, the regional pattern of wind stress, the magnitude of sea-level setup and the bottom gradient. These results were corroborated by Cacchione et al. (1994), who calculated that offshore transport on the same shelf reached a maximum of 0.5 g $cm^{-1}s^{-1}$ during an early-March storm event. Cacchione et al. (1987) concluded that the repeated occurrence of winter storms on the California coast generates high bottom stresses due to the combined effects of waves and currents, and that this is ultimately an important factor in controlling the spatial distribution of bottom sediment.

Lynch et al (1996) showed that sediment transport was dominated by large storms during an eight-week winter deployment in 90 m of water off the California shelf. Transport was predominantly along-shelf, although offshore, and occasionally, onshore components were recorded. Interestingly, although sediment concentrations of up to 0.75 g l^{-1} were measured, these did not necessarily correlate with high transport rates, since high concentrations were sometimes accompanied by weak mean currents. According to Gross et al. (1991), suspended sediment concentrations of 0.030 g l^{-1} over the California shelf are caused by high orbital velocities generated by winter storms, and as a result, 75% of the total annual sediment flux occurred between December and March. The researchers observed statistically-significant logarithmic current profiles, even under strong wave-orbital flows, and calculated apparent bottom roughness (z_{0c}) of up to 18 cm during winter storms. This was more than 25 times the typical non-storm value, and appears to have been the result of wave-current interaction. Similarly, Cacchione and Drake (1982) observed large increases in shear velocity and apparent

bottom roughness (maximum values of 6.9 cm s^{-1} and 8.6 cm, respectively) at a depth of 18 m on the continental shelf of Alaska during a storm.

Research from Canada, New Zealand and the United Kingdom has also provided important contributions to the understanding of storm-induced bottom boundary layer and sedimentary processes. Li et al. (1997) measured two to threefold increases in shear stress, order of magnitude increases in apparent bed roughness, and two to three order of magnitude increases in sediment transport on eastern Canada's Scotian shelf during storms. Although fair weather sediment transport in the region is determined almost exclusively by tidal flows, the researchers found that transport direction during storms was dependent on the direction of both waves and wind-driven currents, and showed a high degree of inter- and intra-storm variability. Amos et al. (1999) measured sediment transport maxima of 0.027 and 0.035 g $cm^{-1}s^{-1}$ at a 22-m deep location on the Scotian Shelf during two storms. Amos and Judge (1991) used the sediment transport model SEDTRANS in combination with field data to predict sediment transport at several sites on the eastern Canadian continental shelf. They concluded that long-term sediment transport varies over a range of temporal scales. At one site, for example, transport was dominated by storms of the longest return interval (32 yrs.) and would thus not be well predicted using the patterns that occur during a "typical" winter storm. On the other hand, at more easterly sites, transport appeared to be dominated by waves and wind-driven currents generated by storms of a one-year return interval (a "typical" strong winter storm). Certain exceptions were noted in channels, however, where tidal currents were shown to be the dominant long-term influence. Manighetti and Carter (1999) described a complex system in the Hauraki Gulf, New Zealand, in which sediment may be transported offshore at times, but remains in the shelf system as a result of rotating tidal currents, until it is ultimately lost through an adjacent channel to deep water. The authors stress that storms are the dominant agents of sediment transport in the region, although the specific effect of an individual storm at a particular location is highly dependent upon local coastal geography. Green et al (1995) discussed numerous responses to the passage of a severe winter storm from a 25-m deep site on the macrotidal British North Sea shelf. They found that apparent bed roughness and sediment transport was two orders of magnitude higher during the storm than fair weather conditions. High suspended sediment concentrations resulted from incident wave and wave group activity, although transport resulting from wave orbital flows was minimal. Instead, net transport over the course of the storm was largely a result of sediment being suspended by waves and transported off- and alongshore by steady wind-driven flows that distorted the tidal ellipse.

A series of papers by Wright and others describes the influence of the passage of "Northeasters" (extratropical storms) over the inner shelf of the Mid-Atlantic Bight in terms of distinct storm phases, or in some cases, storm types. Wright *et al.* (1986) measured a net seaward flux of suspended sediment accompanied by a bed level change of 15 cm in the Middle Atlantic Bight during a single storm. Bed level response was characterized by four distinct stages: 1) negligible response to an initial peak in wind and current speed and suspended sediment concentration; 2) gradual erosion of the bed following this initial peak; 3) slow bed accretion during the second and stronger peak of the storm; 4) rapid bed accretion during the waning phases of the storm.

Madsen *et al.* (1993) and Wright *et al.* (1994) reported maximum suspended sediment concentrations of 1 g l^{-1} within the lowest meter of the water column during a severe Northeaster. Suspended sediment transport during this event was highly dependent on the phase of the storm. During the storm's main phase, sediment flux was seaward as a result of strong downwelling in response to onshore winds. The later swell-dominated phase of the storm was characterized by the deployment's highest shear velocity as well as high suspended sediment concentration, although only low onshore fluxes occurred, owing to the presence of weak mean flows. Kim *et al*. (1997) characterized a Northeaster over the Mid-Atlantic Bight in terms of four phases: 1) an initial calm period when non-diffusive sediment transport was confined to the thin wave boundary layer (wbl); 2) the storm's onset, when the wbl thickened dramatically and suspended sediment transport increased; 3) the storm's peak, when bed stress, wbl thickness, and suspended sediment transport were at a maximum, causing the onset of sheet flow; and 4) the post-storm phase, when suspended sediment transport was confined to the thick wbl, owing to low current shear. Wright et al. (1991) summarized results from three years of field deployments in 7-17 m water depths on the Middle Atlantic Bight. They found that measurable contributions to sediment transport were made by mean flows, infragravity oscillations and incident waves. During storms, downwelling mean flows caused sediment to be transported offshore, while during fair weather and moderate energy conditions, mean currents transported sediment both on- and offshore. During all conditions, incident waves were the primary source of shear stress, and fluxes at both incident and infragravity frequencies were just as commonly onshore as offshore. Xu and Wright (1998) identified two significantly different storm types and their associated currents on the North Carolina shoreface. Southerly storms caused coastal set-down and upwelling, while northeasterly storms were associated with coastal set-up and downwelling**.** It is clear from this research that considerable variability may occur during various stages of an individual storm as well as between different storms.

In addition to the complications to bottom boundary layer response and sediment transport introduced by local differences in geographic, geological, oceanographic factors, important influences are exerted by negative feedback, and other non-linear mechanisms, some of which will be introduced briefly in this paragraph. Glenn and Grant (1987) demonstrated by means of a sophisticated mathematical model that storms may result in enhanced turbulent mixing owing to wave-current interaction, which can, in turn, cause a reduction in shear stress owing to the stable stratification of the water column by suspended sediment. Bed armoring occurs when sediment in size classes with a low critical entrainment stress is winnowed from the bed, leaving a higher bed concentration of less-easily-entrained size-fractions. Sediment stratification and bed armoring have both been shown to reduce sediment transport on the inner shelf during high-suspension events such as storms (Lyne *et al*., 1990b; Wiberg *et al.*, 1994).

The morphology of the bed is also an important factor influencing bottom boundary layer parameters and sediment transport. Li et al. (1996) described feedback between bed forms and suspended sediment transport during various meteorological conditions in the Middle Atlantic Bight. They found that during fair weather, bed ripple roughness, shear stress, and the amount of sediment suspended by vortices were directly related. During moderate storms, bed roughness reached a "breakoff point" where it, and hence vortex activity, began to decline with increasing shear stress. During severe storms, ripples on the bed were completely washed out, vortex activity was eliminated, and sheet flow prevailed. These results are supported by subsequent

research at a 39-m deep location on the Canadian continental shelf by Li and Amos (1999). They observed the disappearance of large wave ripples during the strong combined flows that accompanied storm activity, and their subsequent re-formation as sediment fell out of suspension following the peak of the storm. Vincent and Green (1990) demonstrated that wave vortices may have somewhat unpredictable effects on sediment transport over a rippled bed on the tide-dominated inner shelf of north Norfolk, U.K. Vortices were responsible for phase differences in sediment concentration and flow at various levels above the bed. As a result, sediment transport was onshore near the bed, slightly offshore between five and 10 cm above the bed, and onshore higher in the water column. Boon et al. (1996) highlighted an interesting shallow-water (11.5 m) phenomenon in which interacting wave trains of swell and sea frequencies in an estuary caused an enhancement of sediment transport by a factor of $2^{-0.5}$. Clearly, therefore, bottom boundary layer responses to hydrodynamic forcing are seldom simple and linear and researchers must be cognizant of a variety of potentially complicated interactions.

Three general conclusions of the research discussed in the previous paragraphs are evident. First, storm-induced transport is often so high that it dominates total long-term sediment transport on a particular inner shelf, despite the fact that storm activity may account for only a small fraction of time. Second, certain responses to storm conditions on the continental shelf are fairly universal and are to some degree predictable. Common bottom boundary layer responses include changes in bed form morphology and apparent bottom roughness, and increases in shear velocity and suspended sediment concentration. Sediment transport rate during storms tends to increase, while transport direction is largely determined by wave asymmetry, wind-driven flows, and barotropic currents. Finally, hydrodynamic, bottom boundary layer and sedimentary responses to storm events are extremely sensitive to the duration, intensity, track, and wind structure of the storm as well as to the characteristics of the coastal environment itself, including its geology, bathymetry, coastal orientation and physical oceanography. These responses are further complicated by poorly-understood interactions between variables and complex negative feedback mechanisms such as stratification and bed modification. Thus, the general model of large off- and alongshore fluxes of sediment being generated by the passage of storms, while useful, must be used with caution in the context of a specific inner-shelf site.

Conceptual Basis for the Research

It has been demonstrated in the preceding section that many issues regarding hydrodynamic, bottom boundary layer, and sedimentary responses to meteorological forcing on inner shelves are poorly understood. Further, it has been noted that the response of a particular inner shelf environment is sensitive to a variety of local and regional factors. The inner shelf of Louisiana is unique in comparison with many previously-studied oceanic shelves in that it is exposed to a much lower mean level of hydrodynamic energy, it is dominated by higher frequency waves, and it has a different orientation relative to mean and storm wind directions. Furthermore, it is an important component of a system that is experiencing some of the highest rates of land loss in the world. Finally, a submerged Holocene sand body (i.e. Ship Shoal) is a conspicuous local bathymetric feature whose influence on hydrodynamics and sediment transport is poorly understood. Thus, there are both theoretical and pragmatic reasons for this study.

Ultimately, the goal of this project is to describe and quantify hydrodynamic variables, bottom boundary layer parameters, and directional sediment transport in the context of meteorological forcing on the south-central Louisiana inner shelf in the vicinity of Ship Shoal. Although many variables will be considered, particular emphasis will be placed upon wave height and period, mean and orbital flow velocity, current and combined wave-current shear velocity, and across-shelf (i.e. on and offshore) sediment transport. This project will address these variables in the context of the following specific objectives:

1. **To illustrate the episodic, storm-dominated, nature of the inner shelf in the region during the winter by quantifying the differences between storms and fair weather**.

2. **To demonstrate the variability between individual storms with different meteorological characteristics, and to suggest reasons for this variability.**

3. **To specify the differences between the seaward and landward sides of Ship Shoal, thereby elucidating its influence on regional hydrodynamics and sediment transport.**

4. **To estimate the overall flux of sediment across Ship Shoal over a short time scale. This will permit a quantitative evaluation of event-scale erosion, accretion and migration of the shoal, and will allow forcing mechanisms to be identified and placed within the context of the shoal's long-term evolution.**

5. **To utilize the hydrodynamic measurements, primarily wave characteristics, to skill assess the numerical wave model STWAVE.**

The fulfillment of these objectives will provide a unique and useful evaluation of the influence of both winter storms, which are arguably the most significant regional forcing mechanism, as well as Ship Shoal, which is undoubtedly the region's most prominent morpho-sedimentary feature. Additionally, it is hoped that this analysis will enhance overall understanding of bottom boundary layer, sediment transport and wave models for inner-shelf environments worldwide, where research has been limited in both quantity and geographical coverage.

Study Area

The study area is located on the south-central Louisiana inner shelf, seaward of the Isles Dernieres, in water depths of six to nine meters (Fig. 1.1). Two deployment sites were chosen so as to occupy both the seaward and landward margins of Ship Shoal, the area's most prominent bathymetric feature. The co-ordinates of the seaward location (Site 1) are 28° 50.68'N, 91° 07.52'W, and those of the landward site (Site 2) are 28° 55.74' N, 91° 01.73'W. This chapter will discuss the specific characteristics of these study sites as well as provide a brief overview of pertinent regional considerations.

Meteorology

A primary focus of this work is to investigate the influence of meteorological conditions, and in particular, high-energy wind events (storms), on inner shelf processes in Louisiana. Annually, average wind speed in coastal Louisiana is approximately 3 m s^{-1} from the southeast. Since wind conditions vary considerably over the course of the year, however, storm climatology is most conveniently represented by means of two "seasons"—a summer season lasting roughly from April to November, and a winter season comprising the remainder of the year.

During the summer months, coastal Louisiana's weather is dominated by Maritime Tropical air masses centered over the Gulf of Mexico. This almost always results in uniformly hot, humid, and calm weather, aside from localized convectional thunderstorm activity. Infrequent but often very powerful tropical cyclones (tropical storms and hurricanes), do occur, however, during this time. Tropical storms and hurricanes have made landfall on the Louisiana coast during the past century once every 3.3 and 4.0 years, respectively, with the highest frequency in September (Stone *et al*., 1997). Tropical cyclones can obviously be extremely high-energy events; for example, sustained winds during Hurricane Camille, which struck the Louisiana coast in 1969, were in excess of 100 m s^{-1} (Stone et al., 1997). The impact of such storms on a particular section of coast, while potentially dramatic however, is highly variable, and depends upon the intensity, duration, and track of the individual cyclone. Since no tropical cyclones influenced the study area during the deployment period, however, no further discussion of such events is included.

From approximately November to April, extratropical, or mid-latitude, meteorological systems dominate coastal Louisiana's weather. Since mid-latitude meteorology is controlled by a complex interrelationship of air masses, cyclones, anticyclones and fronts, only a brief overview is offered here, although more detailed references are abundant (e.g. Moran and Morgan, 1994). Ultimately, extratropical storms are the result of Rossby waves generated by heat transfer along the polar front, which forms the global boundary between tropical and polar air masses (Henderson-Sellers and Robinson, 1986). Synoptic-scale storms are initiated along this front through cyclogenesis, a regular sequence of events that commences when an area of strong divergence in the upper atmosphere causes a drop in surface air pressure and the formation of a low-pressure cell, or "Low" (Moran and Morgan, 1994). Clockwise, or cyclonic, circulation develops around this Low, and the cyclone begins to migrate eastward. As this occurs, the portion of the polar front to the east of the Low moves northward as a warm front, while the portion to the west moves southward as a cold front. The process of cyclogenesis tends to occur in particular geographic locations, and although there are several such source regions in North America, the most important for coastal Louisiana are on the lee side of the Rocky Mountains and in the western Gulf of Mexico (Chaney, 1999).

Since any portion of a mid-latitude system may impact the Louisiana coast during any stage of development, the general term *extratropical storm* is used in this dissertation to include all meteorological phenomena that originate in the mid-latitudes and generate high, sustained, wind speeds for several hours. It should be noted, however, that other authors have used different nomenclature to identify these events. For example, the terms cold front (Roberts, et al., 1987, 1989; Chaney, 1999), cold air outbreak (Chuang and Wiseman, 1983), episodic

atmospheric forcing (Armbruster et al., 1997), Nor'easter (Wright et al., 1986), winter storm (Drake and Cacchione, 1991) as well as mid-latitude, and extratropical cyclone, refer to phenomena that are called extratropical storms in this dissertation.

Extratropical storms are extremely important meteorological forcing mechanisms in the northern Gulf of Mexico. While they tend to be less intense than tropical storms, they are much more frequent, occurring roughly 20 to 30 times per year, with a maximum frequency in January (Roberts et al, 1987, 1989). Given their complex evolution and their spatial and temporal variability, it is not surprising that individual extratropical storms that pass a particular location may differ widely in terms of their meteorological characteristics. Wind speed may exceed 25 m s^{-1}, as estimated for the "Storm of the Century" in 1993 (Chaney, 1999), but may be only slightly above average for weaker events. Generally, extratropical storms are characterized by a clockwise rotation of wind direction from the south to the north, with high wind speeds occurring both prior to, and following the passage of the cold front (Chaney, 1999). This results in a general shift from onshore to offshore winds along the coast of the Gulf of Mexico, unlike that which occurs on the north-south aligned Atlantic or Pacific coasts, a factor which presumably has implications for wave growth and propagation, current flow, and sediment transport.

Hydrodynamics and Bottom Boundary Layer Regime

The northern Gulf of Mexico is a microtidal environment characterized by low hydrodynamic energy, except during storms (Penland et al., 1988; Wright, 1995; Jaffe *et al*., 1997, Wright et al., 1997). Average significant deep-water wave height and peak period are approximately 1 m and 5-6 s, respectively, while the dominant angle of wave approach is from the southeast (Penland et al., 1988; Jaffe *et al*., 1997). Wave dissipation and refraction occur across the shallow Louisiana shelf, however, modifying these parameters closer to shore (Stone et al., 1995). Most notably, this causes a decrease in wave height. According to Ritchie and Penland (1988) average wave height seaward of the Isles Dernieres (immediately landward of the present study area) is only about 0.6 m. On the other hand, wave characteristics during storms tend to be markedly different from those measured during fair weather. During winter cold fronts, for example, significant wave heights of 2-3 m may occur (Dingler et al., 1993). A typical, although variable, sequence of wave responses to these frontal passages includes the propagation of high, long-period waves from offshore during the pre-frontal phase, followed by the presence of sea-like conditions, with variable wave heights, periods and directions, during the post-frontal phase (Roberts et al., 1987). Tropical storms and hurricanes generate a variety of wave conditions depending upon their track and intensity, including waves several meters in height and greater than ten seconds in period (Stone et al., 1997).

Tides in the study area are diurnal, with a tropic range of roughly 40 cm, resulting in only weak tidal currents (Wright, 1995; Wright et al., 1997). On the other hand, storm surges associated with wind-events play a significant, but highly variable, role in modulating sea level over the shelf and in nearshore environments (Chuang and Wiseman, 1983; Biocourt et al., 1998). For example, water level set-up along the coast may reach 0.9 m during extratropical storms (Ritchie and Penland, 1988) and 7.0 m during hurricanes (Stone et al., 1997).

As would be expected from the hydrodynamic regime, only low-energy processes operate the majority of the time in the bottom boundary layer of the Louisiana shelf (Wright, 1995; Wright et al., 1997). Several field studies conducted on the mid- and outer shelf have indicated that mean near-bottom flows and bed stresses are not strong enough to re-suspend sediment during typical conditions (Adams et al, 1987; Halper and McGrail, 1988). Even on the inner shelf, in depths of 15-20m, Wright et al. (1997) estimated a mean combined wave-current shear velocity of less than 0.7 cm s^{-1}, an apparent bottom roughness of 0.011-0.015 cm, and a mean drag coefficient of 3.6 x 10^{-3}, during fair weather conditions. They concluded that variations in suspended particulate concentration are generally the result of the advection of sediment plumes from nearby rivers. On the other hand, a few authors have evaluated field data with mathematical models that suggest that bottom stress may be large enough to suspend bottom sediment under certain conditions. For example, Crout and Hamiter (1979) analyzed pressure transducer data from a 10-m deep location on the inner shelf of western Louisiana using the model of Komar and Miller (1975), and estimated that summer storms, winter cold front passages and southeasterly wind events during the spring could generate sufficient stress to suspend bottom sediment. Jaffe et al.(1997) used the Glenn-Grant-Madsen model (Grant and Madsen, 1979; Glenn and Grant, 1987) to predict sand resuspension on the shoreface adjacent to the Isles Dernieres during a variety of conditions. They concluded that bottom stress would be incapable suspending a significant amount of sediment except during storm conditions. Specifically they emphasized that sediment transport rates on the Louisiana inner shelf during normal fair weather conditions would be more than 10^3 times lower than during large storms, such as major cold front passages, and more than 10^4 times lower than during hurricanes. This analysis indicated that extreme events are probably responsible for the vast majority of long-term sediment transport in the region, even considering their relative infrequency. In summary, therefore, the few studies conducted on the Louisiana shelf have indicated that its bottom boundary layer is characterized by low hydraulic energy, except during storms, when bed stresses may increase to a level capable of suspending and transporting bottom sediment.

Geology/Geomorphology

The geology of the Louisiana continental shelf is extremely complex, and also very well documented. A comprehensive discussion, which would necessarily include features as diverse as diapirs, salt domes, and any number of muddy, silty and sandy sedimentary structures, is therefore clearly beyond the scope of this dissertation, although excellent reviews may be found in Kolb and Van Lopik (1958), Scruton (1960), Frazier (1967) and Coleman et al. (1998).

The geology of the Louisiana inner shelf has been largely dominated during the past several thousand years by the influence of the Mississippi River system and its associated delta cycle (Scruton, 1960). This cycle consists of quasi-periodic delta-switching, which occurs roughly every 1000 years, and smaller-scale switching associated with subdeltas, bayfills, and crevasse splays, which occur with frequencies from hundreds of years to a few decades (Coleman et al., 1998). During this cycle, coastal progradation of up to 100m yr^{-1} takes place while a delta or lobe is active (regression). Following abandonment, the delta gradually becomes submerged due to subsidence and the shoreline retreats (transgression). This cycle has created an alternating succession of transgressive and regressive sedimentary features that dominate Louisiana's coastal geology. Only two areas of Louisiana's coast, the Birdfoot and

Atchafalaya/Wax Lake Deltas, are presently experiencing the regression phase of this cycle, while the majority of the coast, including the study area, is undergoing relative sea level rise at a rate of roughly 1.0-1.1 cm yr^{-1} (Penland and Ramsey, 1990).

Ship Shoal is a sand body that is approximately 50 km long and 12 km wide at its western end, where the minimum overlying water depth is 3 m. It is asymmetric in profile, with steep landward slopes of 1:90 to 1:750 and shallower seaward slopes of 1:900 to 1:2,000 (Penland et al., 1988). Penland et al. (1988) attempted to account for coastal features associated with deltaic transgression in Louisiana in terms of a three-stage model that included the development of: 1. an erosional headland with flanking barriers; 2. a transgressive barrier island arc; 3. an inner shelf shoal. According to this classification, Ship Shoal is a typical stage 3 feature that formed from the transgression and submergence of a former barrier shoreline, while the adjacent Isles Dernieres chain is a transgressive barrier island arc (Penland et al., 1988). Bathymetric surveys suggest that Ship Shoal is migrating landward across deposits from the abandoned Maringouin Delta at a rate of between 15 m yr^{-1} in the west, and 7 m yr^{-1} in the east .

Unlike many of Louisiana's coastal environments which are dominated by silt and mud, bed sediment in the study area is clean quartz sand with a mean grain diameter of 0.12-0.13 mm. Complete results of the analysis of bottom sediment from both study sites are shown in Figs.2.1 and 2.2.

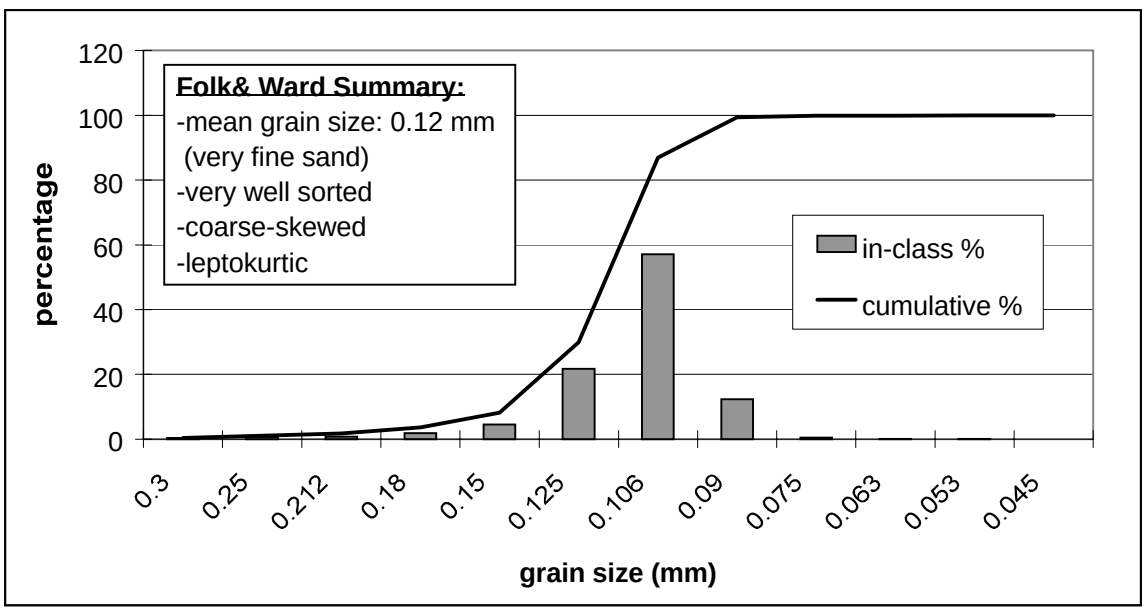

Figure 2.1. Results of analysis of sediment from Site 1 (the Offshore site; see Fig. 3.3 for location).

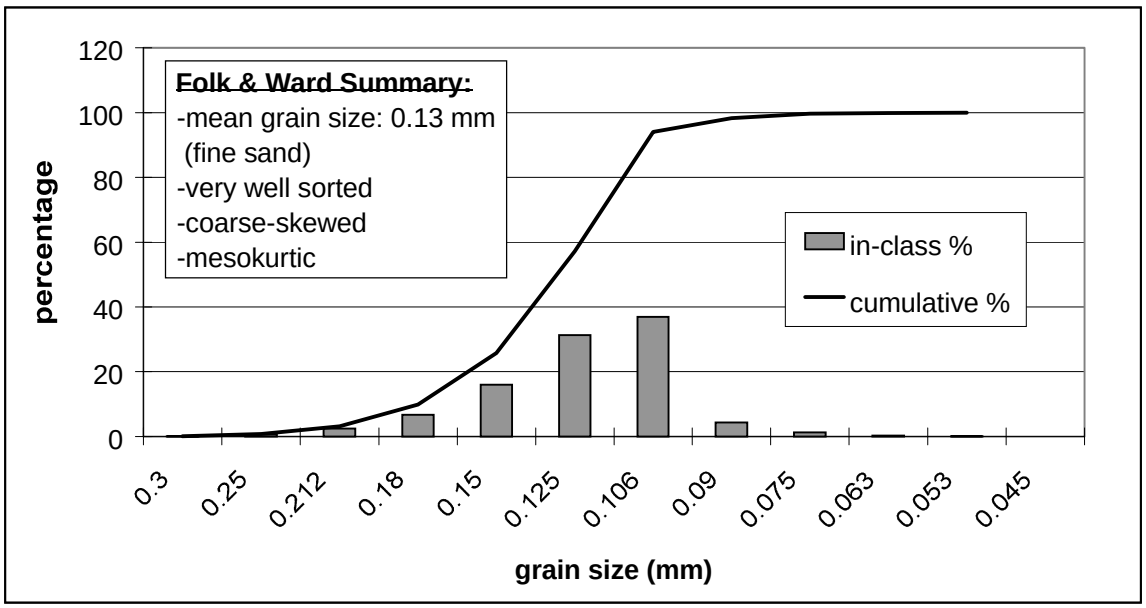

Figure 2.2. Results of analysis of sediment from Site 2 (the Inshore site; see Fig. 3.3 for location).

Practical Concerns

The unique characteristics of the Louisiana coastal zone have been widely discussed in the literature, including, but not limited to oceanographic, geological, ecological, geographical, and policy-oriented sources. Obviously, relative sea level rise and coastal land loss are primary concerns. One prominent proposal has been to artificially maintain the volume of eroding offshore barrier island chains to act as a protective barrier against wave energy for the adjacent coast. The possible means by which to do so include the implementation of hard structures, such as breakwaters, and artificial nourishment using sediment from distant sources. Ship Shoal, with its large quantity of clean, quartz sand, is considered a viable source for this sediment. With the exception of an extensive numerical modeling effort of the wave field (Stone and Xu, 1996), the shoal's influence on waves, currents, bottom boundary layer dynamics, and sediment transport in the region is largely unknown. Clearly, therefore, a knowledge of hydrodynamic and sedimentary processes on the south-central Louisiana inner shelf is of great practical, as well as theoretical concern.

3. METHODOLOGY

Instrumentation and Field Methods

The primary component of the field research was the deployment of instrumentation during a period of several weeks, beginning November 24, 1998. Three bottom-mounted instrumentation systems were used, two of which (Systems 1A and 1B) were deployed a few meters away from each other at Site 1, while the other (System 2A) was deployed at Site 2. System 2A was retrieved on January 12, 1999, and the others remained at Site 1 until February 2, 1999. Due to memory constraints, however, System 1A ceased logging on January 20, 1999. During each deployment and retrieval, divers collected sediment from the bed, and water samples from the water column, and observed and measured any visible bed forms. An additional deployment occurred on February 9 through March 13, 2000. Data measured during these and the previous deployments were used for model comparison and are evaluated later in this report.

The instrumentation consisted of two types of frame-mounted system, both of which included a self-contained data recorder module. The primary components of Systems 1A and 2A (Fig.3.1) were Sontek$_{TM}$ downward-looking Acoustic Doppler Velocimeters (ADV's) that measured seabed elevation, relative particulate concentration and 3-dimensional currents at an elevation of 20 cm above the bed. System 1A was programmed to sample at 25 Hz, the maximum rate achievable by the sensor, since such a high sampling rate had seldom, if ever, been used in an inner-shelf environment (see Table 3.1, at the end of this section, for all instrument sampling rates). Unfortunately, storage of these data necessitated that a burst interval of only 81 seconds every three hours be used. It was thought that since System 1B was deployed in the immediate vicinity, potential gains achieved by detecting high-frequency turbulent fluctuations that had not previously been reported would outweigh losses incurred by using a short burst interval. System 2A included a Paroscientific pressure sensor in addition to the ADV, and was programmed to sample at 4Hz for 8.5 minutes every three hours. Systems 1A and 2A included internal compasses and tilt and roll sensors to enable the rotation of directional measurements into a planetary frame of reference.

System 1B was a unique multi-sensor package nicknamed WADMAS (Fig 3.2). It consisted of a Paroscientific pressure sensor, a sonar altimeter, and a vertical array of three co-located Marsh-McBirney electromagnetic current meters and Seapoint optical backscatter sensors (OBS's). This instrumentation enabled WADMAS to measure water level, directional wave parameters, and seabed elevation, as well as current velocity and suspended sediment concentration at heights of 20, 60, and 100 cm above the seabed. To conserve battery power and recorder memory, all of the sensors on WADMAS were programmed for burst-mode (i.e. discontinuous) sampling. Specifically, the sonar altimeter collected one measurement every 15 minutes, while all other sensors sampled for 8.5 minutes per hour at a frequency of 4 Hz.

Figure 3.1. System 2A during deployment at Site 2. Key: (A) Acoustic Doppler Velocitmeter (ADV); (B) Pressure Sensor; (C) Enclosed cylinder containing recorder module, compass and power supply. System 1A was identical except that it did not include a pressure sensor.

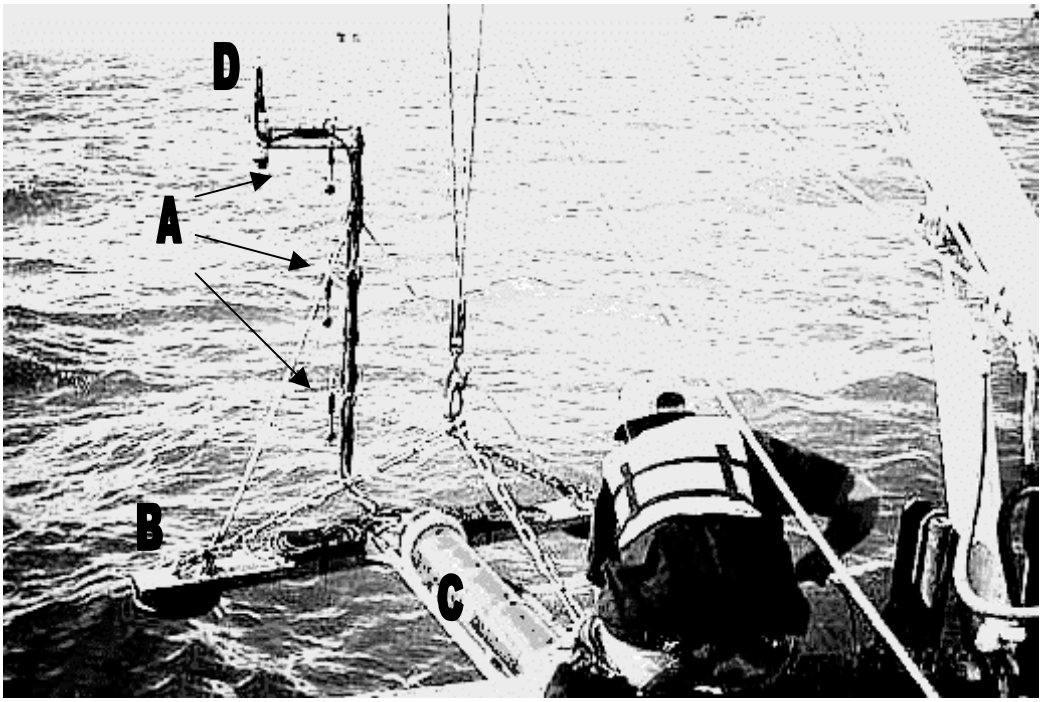

Figure 3.2. System 1B during deployment at Site 1. Key: (A) Stacked array of co-located electromagnetic current meters and optical backscatter sensors; (B) Pressure Sensor; (C) Water-tight cylinder containing recorder module, compass and power supply; (D) Sonar altimeter.

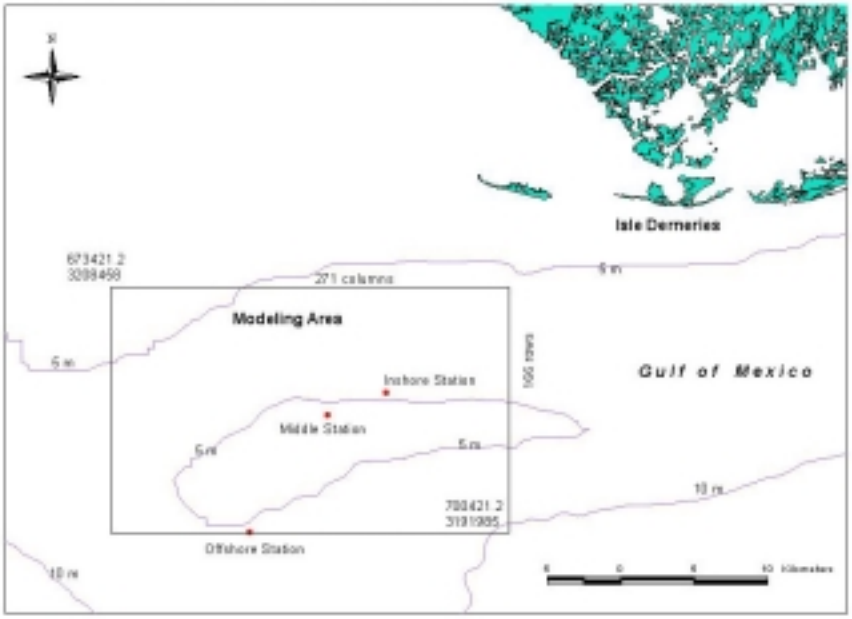

Figure 3.3. Location of instrumentation sites at Ship Shoal; Site 1 = Offshore Station, Site 2 = Inshore Station. An additional site (Middle Station) was established for the 2000 deployment.

Table 3.1: Sampling schemes used in data collection. * Note: Sampling scheme shown for the meteorological station indicates GDIL1 data selected for use in this study, and not the entire data set collected by NOAA, which was more comprehensive.

System	***Sensor/ Measurement***	***Hours between Bursts***	***Samples/ Burst***	***Burst Duration (min)***	***Rate (Hz)***
1A (ADV)	Pressure	3	2048	8.5	4
	3-D Current	3	2048	8.5	4
	Suspended Sediment Concentration	3	2048	8.5	4
	Bed Level	3	1	-	-
2A (ADV)	3-D Current	3	2048	1.35	25
	Suspended Sediment Concentration	3	2048	1.35	25
	Bed Level	3	1	-	-
1B (WADMAS)	Pressure	1	2048	8.5	4
	Current	1	2048	8.5	4
	OBS	1	2048	8.5	4
	Sonar Altimeter	0.25	1	-	-
GDIL1 (NOAA)	Wind	1*	1	10	-

Unlike many comparable instrumentation packages that have been deployed on inner shelves, the systems used in this study are notable in that they do not employ a traditional tripod or tetrapod-type frame design. Instead, sensors are supported by thinner, less-obtrusive metal supports that allow them to remain separated from the heavy bottom-mounted frames. The intent of this design was to minimize the interference of the equipment with the parameters being measured; in particular. In particular design of System 1B allowed the sonar altimeter to measure bed elevation at a distance of nearly 1 m from the bottom-mounted section of the frame, bed level changes relative to it could, in certain cases, be localized effects, such as ripple migration, that did not effect the entire instrument.

Hourly wind data for the deployment period were obtained from the National Oceanographic and Atmospheric Administration (NOAA) station located on Grand Isle, Louisiana at $29^{o}27'$ N, 89° 96' W (GDIL1). These measurements were supplemented by daily national weather maps obtained from the National Weather Service, which were inspected visually to verify the occurrence of cold front passages.

Laboratory Methods

Laboratory procedures for this project included two components: 1) instrument calibration, testing and preparation, and 2) analysis of sediment and water samples from the field site. All instrumentation was calibrated, prior to deployment, by the Coastal Studies Institute Field Support Group in their testing facilities. Since optical backscatter sensors are more sensitive to fine than to coarse sediment, while the reverse is true for acoustic systems, appropriate field conversion factors were established using bottom sediment from the study sites. This procedure consisted of exposing the sensors to a series of uniformly-stirred mixtures of distilled water and known concentrations of field sediment. The voltage output from the sensors was then related to the sediment concentration by using regression to fit a calibration curve to a scatter-plot of these variables. Since the field data from the optical backscatter sensors were ultimately found to be faulty, OBS calibration results will not be discussed. Field data from the ADV's appeared to be reliable, however, and as such, the electronic signal strength was converted from the calibration curve obtained in the laboratory, which took the form:

$$C=7.20197 \times 10^{-10} (10^{0.043SS}) \qquad (3.1)$$

where C is the volumetric concentration of sediment and SS is the ADV signal strength.

Dry sieving at 0.25 ϕ intervals was conducted to determine the grain-size composition of the samples of bottom sediment. The water samples, collected at the surface and at 0.5, 2 and 4 m above the bed, were filtered through 0.7-m paper using a pump-operated filtration system, dried in an oven at 60°C, and weighed to determine the sediment concentration.

Data Processing and Analytical Methods

Spectral Analysis

An initial discussion of spectral analysis is warranted since it played a prominent and varied role in this project. Spectral plots of individual variables and cross-spectral plots of paired variables were generated on several time-scales. In addition, plots of coherence and phase spectra were derived from the cross-spectra of the paired variables. Generally speaking, the purpose of spectral, or frequency-domain, representation is to identify periodicities (essentially recurrence intervals) over which phenomena fluctuate. Power spectra indicate the frequency ranges over which an individual variable fluctuates whereas cross-spectra do the same for the cross-product of two variables. Coherence spectra illustrate, on a scale of 0 to 1, the correlation between two variables at different frequencies, while phase spectra show the lead or lag of one variable in relation to a second.

Spectral analysis generally involves the application of smoothing, segmenting, or windowing techniques to increase the confidence level of the results. The Welch method, in which a single data series is initially subdivided into several shorter segments with a specified overlap length, was used in this study. A Hanning window was then applied to smooth these series, and Fourier series expansion was used to convert these series from the frequency to the time domain. Since spectral techniques have been applied in this project in situations where sampling schemes and record lengths have varied widely, the details of analysis techniques are summarized in Table 3.2.

Table 3.2: Segment, window, and overlap lengths used in spectral analysis**.**

System	*Series Length*	*Samples*	*Freqency*	*Segment Length*	*Window Length*	*Overlap Length*
1A	81 s	2048	25 Hz	256	256	128
1B & 2A	8.5 min	2048	4 Hz	256	256	128
1A	56 d	448	8 day^{-1}	64	32	0
1B & GDIL1	65.5 d	1574	24 day^{-1}	256	256	128
2A	49 d	392	8 day^{-1}	64	32	0

Directional Wave Processing

Directional wave parameters were calculated from the pressure and current-meter data by using a spectral approach to generate the first five coefficients (a_0, a_1, b_1, a_2, and b_2) of the directional Fourier series (Earle *et al*., 1995). To compensate for the effect of depth attenuation, wave-pressure and horizontal-velocity-amplitude correction factors (*Rp* and *Ru*, respectively) were applied to the coefficients. These correction factors were calculated for each frequency (*f*) using:

$$Rp(f) = \frac{\cosh[k(z_d + d)]}{\cosh(kd)} \quad (3.2)$$

$$Ru(f) = \frac{\cosh[k(z_d + d)]}{\sinh(kd)} \quad (3.3)$$

where z_d and d are the mean sensor and total water depths, and wave number (k) was calculated iteratively using the dispersion equation:

$$(2\pi f)^2 = (gk)\tanh(kd) \quad (3.4)$$

The five Fourier coefficients were calculated by generating all possible combinations of the cross-spectra (Cxy) of the pressure (p) and horizontal velocity components (u_c and v_c), and using the following formulas:

$$a_0(f) = \frac{Cpp(f)}{Rp^2(f)p} \quad (3.5)$$

$$a_1(f) = \frac{Cpu_c(f)}{Rp(f)Ru(f)(2pf)p} \quad (3.6) \qquad b_1(f) = \frac{Cpv_c(f)}{Rp(f)Ru(f)(2pf)p} \quad (3.7)$$

$$a_2(f) = \frac{(Cu_c u_c(f) - Cv_c v_c(f))}{Ru^2(f)(2pf)^2 p} \quad (3.8) \qquad b_2(f) = \frac{Cu_c v_c(f)}{Ru^2(f)(2pf)^2 p} \quad (3.9)$$

It should be noted that the correction factors Rp and Ru are frequency-dependent, and thus will approach zero as the frequency increases. As such, a high-frequency "cut-off" value of 0.35 Hz was selected in accordance with Long and Oltman-Shay (1991).

Mean and principal wave direction (Φ_1 and Φ_2) were calculated using:

$$\Phi_1 = \arctan(b_1/a_1) \quad (3.10)$$

and

$$\Phi_2 = 0.5 \arctan(b_2/a_2) \quad (3.11)$$

These Cartesian directions were converted to geographical directions on the basis of the instrument orientation measured by the compasses included on the systems.

Peak wave period (Tp) and significant wave height (H_{mo}) were calculated using the non-directional wave spectrum, Czz, which is equal to the product of a_0 and B. Peak period is simply the reciprocal of the spectral frequency at which the highest energy occurs (i.e. where Czz is the highest). Significant wave height was computed from:

$$H_{mo} = 4.0\sqrt{m_0} \quad (3.12)$$

where the zero moment of the non-directional spectrum (m_0) is the summation of spectral energy over the total number (Nb) of frequency bands of bandwidth df:

$$m_0 = \sum_{n=1}^{Nb} Czz(f)df \quad (3.13)$$

This calculation is commonly used in wave analysis, although it may yield estimates 5-10% higher than the traditional definition of significant wave height ($H_{1/3}$), calculated using the highest one-third of the waves in the wave field (Longuet-Higgins, 1980).

Calculation of Bottom Boundary Layer Parameters and Sediment Transport

This section describes the procedures used to calculate bottom boundary layer parameters and predict flow, sediment suspension and sediment transport. Since it is a lengthy and detailed section, a few initial notes of explanation are warranted to clarify how each technique relates to the overall structure of the research.

Two methods were used to calculate an initial value of shear velocity, depending on the system used. Values from Systems 1A and 2A were obtained using the Reynolds Stress technique (RS), while values from System 1B were calculated on the basis of the logarithmic profile (LOG) method. Sediment transport was calculated using essentially three techniques, called, for the purposes of this project, the Grant-Madsen-Rouse (GMR), the Meyer-Peter and Muller (MPM), and the spectral cross-product (SCP) methods. The first two of these (GMR and MPM) were based on the concept of shear velocity, while the SCP method was based on instantaneous field measurements. It was assumed in this study that sediment transport could be subdivided into bed and suspended load modes, as is very commonly done, despite the somewhat arbitrary nature of this classification scheme (Davies and Li, 1997). Bed load is generally defined as all sediment that maintains occasional contact with the bed, while moving horizontally at a measurably slower rate than the flow, while suspended sediment is assumed to remain above the bed at all times and to be transported horizontally at approximately the fluid velocity. In this study, the MPM method was employed to calculate bed load transport, while the GMR and SCP methods were used to calculate suspended sediment transport. Table 3.3 summarizes the methods used to calculate shear velocity and sediment transport. Finally, although the relevant equations in this section are presented sequentially, the reader should bear in mind that the actual physical processes they represent are interrelated by feedback mechanisms, and therefore, calculations were often performed iteratively.

Table 3.3: Summary of methods used to calculate shear velocity and sediment transport. * Although all sensors were used to make these calculations, results from all sensors are not necessarily presented.

Abbreviation	***Full Name***	***System***	***Mode***	***Basis***
Shear Velocity				
LOG	Logarithmic profile	1B		
RS	Reynolds stress	1A, 2A		
Sediment Transport				
GMR	Grant-Madsen-Rouse	All*	suspended	shear velocity
SCP	Spectral cross product	All*	suspended	sensor
MPM	Meyer-Peter and Muller	All*	bed	shear velocity

Bottom Boundary Layer (BBL Parameters

Two important parameters in bottom boundary layer modeling, particularly with respect to sediment transport, are the apparent bottom roughness length, z_{0c} and the shear velocity, defined as $u_* = (\tau/\rho)^{0.5}$, where Δ is the density of seawater (1.025 g cm^{-3}), and τ is the shear stress. Two approaches were used to calculate these parameters in this study. For System 1B (WADMAS) data, velocity profiles were initially estimated from log-linear regression of the burst-averaged current meter velocities (the "log-profile" method). Two conditions must be satisfied for a profile to be considered logarithmic in a statistically significant sense: first, the correlation coefficient (r^2) must be equal to or greater than 0.994 (Drake and Cacchione, 1992); second, the variation in mean direction between current meters must be less than 20°. Shear velocity and apparent bottom-roughness length were calculated for all logarithmic profiles using the von Karman-Prandtl equation:

$$u(z) = u_*/\kappa \, ln(z/z_{0c}) \qquad (3.14)$$

where $u(z)$ is the horizontal velocity at height z above the bed, and κ is von Karman's constant (0.4).

The Reynolds stress, or eddy correlation, technique was used to estimate bottom boundary layer parameters from the ADV data (Systems 1A and 2A). The total horizontal and vertical velocities (u and w) were represented as the sum of mean ($\bar{u}$ or $\bar{w}$), periodic (u_p or w_p), and turbulent (u' or w') components:

$$u = \bar{u} + u_p + u' \qquad (3.15)$$

and

$$w = \bar{w} + w_p + w' \qquad (3.16)$$

which is based on the assumption that turbulent and mean velocities are uncorrelated at all frequencies. The turbulent velocity was isolated by subtracting the periodic (wave-orbital) velocity component from the total-velocity-power spectrum (Green, 1992). To do so, wave orbital velocity was defined as the portion of the velocity spectrum (P_{UU}) that was coherent with pressure:

$$P_{u_w u_w}(f) = \gamma^2 U_p(f) P_{UU}(f) \qquad (3.17)$$

where $P_{u_w u_w}$ is the wave-driven component of the velocity spectrum and $\gamma^2 \; U_p$ is the coherence between pressure and velocity (note that the same was done for the vertical, w, component). Obviously, this also has the effect of removing any turbulence that is coherent with pressure, including wave-induced secondary flows. Although such flows were not directly observed during this study, they may have been present at certain times. However, it is assumed that their influence can be neglected in calculating shear stress and bed roughness, since these parameters are based on diffusive, rather than convective processes. When measurements are taken in the constant stress layer, shear velocity is defined as:

$$u_* = -\sqrt{\overline{u'w'}} \tag{3.18}$$

Bottom roughness was calculated by applying these results to Equation 3.14.

The Combined Effect of Waves and Currents

Numerous field studies have demonstrated that the superimposition of waves and currents enhances bottom shear stress and apparent bottom roughness (Wiberg and Smith, 1983; Cacchione *et al.*, 1987; Lyne *et al.*, 1990a; Drake and Cacchione, 1992; Kim *et al.*, 1997). Wave-current interaction is a highly non-linear and poorly-understood phenomenon, and various approaches have been applied to model it. According to Dyer and Soulsby (1988) the following four categories of models are commonly applied in combined wave and current situations: 1. Prescribed mixing-length distribution; 2. Prescribed eddy viscosity distribution; 3. Momentum deficit integral; 4. Turbulent kinetic-energy closure. These model categories differ widely not only in their assumptions and inputs, but also in the results they may produce. Since a field comparison of these model-types, not to mention all available models themselves, would constitute a project unto itself, the Grant-Madsen model (1979, 1986) was used in this study, owing to its widespread familiarity and high level of empirical verification (Cacchione *et al.*, 1987; Lyne *et al.*, 1990a). According to the model, a wave boundary layer (wbl) of thickness (d_w) develops during wave activity and the velocity profile is defined separately within and above this layer as:

$$u_c = \frac{u_{*c}}{k}\left(\frac{u_{*c}}{u_{*cw}}\right) ln\frac{z}{z_0} \ , \qquad z \le d_w \tag{3.19}$$

where

$$u_c = \frac{u_{*c}}{k} ln\frac{z}{z_{0c}} \ , \qquad z \ge d_w \tag{3.20}$$

u_{*c} and u_{*cw} are the current-, and combined wave-current-induced shear velocities. z_0 is the roughness produced by the sand grains, defined as D/30, where D is the mean grain diameter, and z_{0c} is the apparent bottom roughness experienced by the current above the wave boundary layer. Wave boundary layer thickness is defined by the equation:

$$\delta_w = n\, u_{*cw}\, \omega \tag{3.21}$$

where n has a value of 1-2, depending upon the reference, and ω is the wave radian frequency, $2\pi/Tp$. Apparent bottom roughness, z_{0c}, is used because the current experiences drag due to the combined influences of physical elements (grain roughness and bed forms) as well as non-linear interaction with the wave boundary and mobile bedload layers (Gross *et al.*, 1992). Equation 3.14 was used to determine u_{*c} and z_{0c}, and u_{*cw} was calculated using an iterative procedure involving the following equations:

$$u_{*cw} = u_{*wm}\,[1 + 2(u_{*c}/u_{*wm})^2 cosf + (u_{*c}/u_{*wm})^4]^{1/4} = \sqrt{C_R}\,u_{*wm} \tag{3.22}$$

where u_{*wm} is the wave shear velocity, ϕ is the acute angle between the waves and the current (waves were considered to be bi-directional, thus $\phi \le 90^\circ$), and C_R is a coefficient initially assumed to equal one. A wave friction factor (f_w) was then defined through:

$$u_{*wm} = \sqrt{C_R}\sqrt{f_w/2}\,u_b \tag{3.23}$$

and $$\frac{1}{4\sqrt{f_w}} + \log\frac{1}{4\sqrt{f_w}} = \log\left(\frac{C_R u_b}{z_0\omega}\right) - 1.65 + 0.24(4\sqrt{f_w}) \tag{3.24}$$

where u_b is the maximum near-bottom orbital velocity per wave period.

The current-induced shear velocity, u_{*c}, was assumed to act in the same direction as the mean current, while the direction of u_{*cw} was expected to oscillate during the course of the wave cycle. When the wave orbital velocity was at a minimum (near zero) the direction of u_{*cw} was the same as that of the current; when it was at its maximum, its direction ($\varphi_{\max}$) was between the wave and current directions, specified by (modified from Cacchione et al., 1994):

$$\varphi_{\max} = \arctan\left(\frac{\sin\phi}{\cos\phi + \frac{u_b}{\bar{u}}}\right) \tag{3.25}$$

Obviously, the direction of u_{*cw} has implications for sediment transport within the wave boundary layer, which will be discussed in greater detail in a subsequent section.

Sediment Suspension, Flow Stratification, and Bed Armoring

Sediment transport occurs when the shear stress (τ) exerted by the fluid on grains of size-class n, exceeds the critical shear stress (τ_{ncrit}) required to initiate sediment motion. In practice, determination of the critical shear stress of seabed sediment is problematic, as a result of three general factors outlined by Drake and Cacchione (1986). First, the grain-size distribution of shelf sediment may be quite broad, although this is not the case for the study area. Second, the presence of even a small fraction of clay-sized sediment may cause cohesiveness, which increases τ_{ncrit}. Finally, benthic organisms exert a significant, but poorly understood, influence on the properties of bed sediment. Not surprisingly, various methods may be used to determine τ_{ncrit} under combined flows, including the modified Yalin method, which was used in this study following (Li *et al.*, 1996). The Yalin parameter (Ξ_n) is defined by:

$$\Xi = [(\rho_s - \rho)gD^3/\rho\nu^2]^{0.5} \tag{3.26}$$

where ρ_s and ρ are the densities of sediment (2.65 gcm^{-3}) and seawater (1.025 g cm^{-3}), D is the grain diameter, and < is the kinematic fluid viscosity (0.013 cm^2 s^{-1}). The Yalin parameter was first used to calculate a critical Shield's criterion (2_{crit}), and then τ_{crit} using:

$$\log\theta_{\text{crit}} = 0.041(\log\Xi)^2 - 0.356\log\Xi - 0.977 \tag{3.27}$$

and

$$\tau_{\text{crit}} = \theta_{\text{crit}}(\rho_s - \rho)gD \tag{3.28}$$

Critical shear velocity was then simply calculated by: $u_{*crit} = (\tau_{cri\tau}/\rho)^{1/2}$. An additional parameter to be used in this study was the normalized excess shear stress (*S'*):

$$S' = \left(\frac{\tau - \tau_{crit}}{\tau_{crit}} \right) \qquad (3.29)$$

where τ is the observed shear stress.

The sediment suspension profile over a sandy bottom was shown by Lynch et al. (1997) to be well represented by the standard Rouse equation, even under combined wave and current flows. This profile is the result of a balance between the upward-diffusive and downward-settling fluxes of sediment. It is represented by:

$$C(z) = C\ (z_a)\left(\frac{z}{z_a}\right)^{-\alpha}, \qquad \text{where} \qquad \alpha = \frac{\gamma w_s}{\kappa u_*} \qquad (3.30)$$

$C(z_a)$ is the reference concentration at height z_a, γ is the ratio of the eddy diffusivity of sediment to that of momentum (~1), and w_s is the sediment fall velocity. These equations are based on the somewhat vaguely defined concept of a reference concentration of sediment near the bed. The concentration $C(z_a)$ is commonly defined by the equation from Glenn and Grant (1987):

$$C(z) = C\ (z_a)\left(\frac{z}{z_a}\right)^{-\alpha}, \qquad \text{where} \qquad \alpha = \frac{\gamma w_s}{\kappa u_*} \qquad (3.31)$$

where C_{bed} is the sediment concentration in the bed (0.65 for the sum of all size classes) and γ_0 is an empirical constant with a value of approximately 1.3 x 10^{-4}.

Under certain conditions, suspended sediment may cause the water column to become stable-stratified, increasing the vertical velocity gradient, but inhibiting the upward diffusion of mass and momentum (Smith and McLean, 1977; Adams and Weatherly, 1981; Glenn and Grant, 1987; Huntley *et al.*, 1994). Some authors have suggested that this phenomenon should be represented numerically by modifying von Karman's constant (Adams and Weatherly, 1981; Gust and Southard, 1983). The more common approach, however, as was used in this study, is to apply a stratification correction to the velocity profile based on the predicted sediment concentration. As suggested by Glenn and Grant (1987), it was applied only above the wave boundary layer and took the form:

$$u_z = \left(\frac{u_{*c}}{\kappa}\right)[\ln(z/z_0) + \beta z/L] \qquad (3.32)$$

where is an empirical constant with a suggested value of 4.7 (Glenn and Grant, 1987), and L is the Monin-Obukhov length scale, defined by:

$$L = \frac{u_{*c}^{\ 3}}{zkg((r_s - r)/r)w_s C} \qquad (3.33).$$

Bed armoring occurs when sediment in size classes with a low critical entrainment stress is winnowed from the bed, leaving a higher bed concentration of less-easily-entrained size-

fractions. This phenomenon, which serves as a negative feedback mechanism for sediment transport, has been observed on the inner shelf during high-suspension events such as storms (Lyne *et al*., 1990b; Wiberg *et al.*, 1994). Its possible effect was included in the analysis by incorporating the mixing-depth limitation ($_{mix}$) suggested by Green et al. (1990):

$$\delta_{mix} = 2.5\ S'/(\rho_s - \rho)g \qquad (3.34)$$

Sediment Transport

Suspended sediment transport is represented mathematically by time- and depth-integrating the product of the horizontal velocity and suspended sediment concentration. As simple as this may seem, it is a very complex problem in combined-flow regimes, owing to phase differences in velocity and concentration, and the possible occurrence of secondary flows including ejected vortices (Agrawal and Aubrey, 1992; Osborne and Greenwood, 1993; Davies, 1995). As a result, the time-scale chosen for this integration procedure is of great importance. In fact, Osborne and Vincent (1996) indicated that not only may the magnitude of transport vary on the basis of averaging period, but in some cases the direction may be completely reversed. On the other hand, the use of instantaneous measurements is problematic, since the time scales of velocity- and suspended-sediment-profile development are different (Davidson et al., 1993). Lesht (1979) and Shauer (1987), for example, recommend scales of several minutes for the establishment of logarithmic velocity profiles. As such, two approaches were employed in this study, the first based on time-averaged values and the second on instantaneous field measurements.

The first technique, which was earlier labeled the GMR approach, was to multiply the burst-averaged velocity and concentration profiles as calculated on the basis of the shear velocity. This approach has often been employed in wave-dominated environments (e.g. Vincent *et al*., 1983; Kim *et al*., 1996) despite the fact that it assumes temporally-uniform values, a condition that may not be satisfied during unsteady oscillatory flow. The profiles were integrated both within and above the wave boundary layer using:

$$Q_{sn} = \frac{1}{t}\int_{z=d_w}^{z=h}\int_0^t uC_n\ dzdt \qquad \text{for} \qquad z > \delta_w \qquad (3.35)$$

$$Q_{sn} = \frac{1}{t}\int_{z=z_0}^{z=d_w}\int_0^t uC_n\ dzdt \qquad \text{for} \qquad z < \delta_w \qquad (3.36)$$

where η is the sea surface elevation.

The cross-product of instantaneous values (i.e. every 0.04 s or 0.25s) of velocity and concentration from Systems 1 and 2A were also used to calculate suspended sediment transport. This had the advantage of accounting for time-varying effects of waves on the sediment suspension and velocity profiles as well as allowing transport to be analyzed according to frequency components. However, quantitative assessments were made less reliable since it was necessary to assume (very simplistically) that the mean sediment concentration and flow velocity throughout the water column were equal to the burst-averaged values measured at the sensor.

Bed load transport rate (Q_{bl}) was calculated by using the combined wave-current shear stress as an input the empirical formula of Meyer-Peter and Muller (1948) as adapted by Wiberg *et al.* (1994):

$$Q_{bl} = 8\frac{(t - t_{crit})^{3/2}}{(r_s - r)g} \tag{3.37}$$

The direction of bedload transport under the combined flow of waves and currents is as yet an inadequately resolved issue. Cacchione *et al.* (1994) assumed that bedload transport would occur in same direction as that of the maximum shear stress ($_{max}$) within the wbl. Although this seems to be a somewhat simplistic assumption since the direction of stress may vary up to 180° over the course of a wave cycle, these workers were able to reasonably represent observed trends of bed form migration. As such, this method was adopted for this study.

A wide variety of methods have been presented in this section, many of which involve important assumptions that have not necessarily been well tested in the field. All have a solid grounding in the literature, however, and as will be apparent in later sections, the trends they produce are similar in most instances. Nonetheless, the choice of the most reliable method must, to some degree, be left to the discretion of the reader.

4. METEOROLOGICAL CONDITIONS DURING THE DEPLOYMENTS

Classification Systems for Meteorological Events

One objective of this project was to differentiate between various meteorological conditions that occurred during the study period and to associate these with hydrodynamic, bottom boundary layer and sedimentary responses. It is useful, therefore, to establish a classification system by which to characterize atmospheric conditions, specifically those related to winter extratropical storms and fair weather in the northern Gulf of Mexico. Numerous classification schemes have been proposed to categorize atmospheric conditions in a variety of environments—however, since meteorological processes are inherently complicated, these are of necessity based on criteria that suit a particular purpose. Depending on the requirements of a specific study, for example, a classification scheme may be based on local atmospheric measurements, on synoptic or global-scale atmospheric circulation, or on the effect of atmospheric forcing on some aspect of the physical or human environment. The system employed in this project was ultimately designed to differentiate between: (1) fair weather and storm conditions; (2) different phases of extratropical storms; (3) extratropical storms of different intensities and synoptic types. As such, it draws upon several classification systems suggested in the literature, as well as criteria specific to the research, and employs both hourly wind velocity data and daily national weather maps.

Storm magnitude scales, such as the Saffir-Simpson scale for hurricanes and the Fujita scale for tornadoes, are a fairly simple and familiar type of meteorological classification system based largely on wind speed and barometric pressure. Although magnitude scales for extratropical storms are somewhat less familiar, several have been proposed. One example is the Northeast storm scale of Halsey (1986), who ranked storms in the Atlantic qualitatively, on the basis of their effect (damage potential) on coastal beaches. More recently, Dolan and Davis (1992a, 1992b) suggested a scale for Atlantic coast Northeast storms (Nor'easters) that was also based on coastal damage potential, but included, in addition, a quantitative index of storm power calculated using the square of the significant wave height times the duration of the storm. Hsu (1993) proposed a classification system for extratropical cyclones in the Gulf of Mexico. This scale is based on the minimum central pressure of a Gulf cyclone and the predicted maximum wind speed, and is thus more fundamental than the scales proposed for Atlantic storms. Chaney (1999) used a simple measure of magnitude for Gulf Coast storms known as the V square value, which is based on the sum of the squares of the hourly wind velocity during a storm event, thus incorporating the influence of both storm wind duration and speed.

Synoptic-scale classification systems have also been applied to the meteorology of the northern Gulf of Mexico. Notably, Muller (1977) subdivided New Orleans weather into eight synoptic types that included both storms and fair weather. Roberts et al. (1987) identified two end member types of extratropical storms in coastal Louisiana: the migrating cyclone, characterized by the passage of a cold front aligned oblique to the coast, and the arctic surge, in which a front is aligned parallel to the coast. Chaney (1999) subdivided characteristic synoptic weather patterns responsible for extratropical storms over the northern Gulf of Mexico into seven categories: 1) Primary Front (P) 2) Secondary Front (S) 3) Secondary Gulf Front (SG) 4)

Secondary Gulf Low (SL) 5) Gulf Front (GF) 6) Gulf Low (GL) and 7) Primary Low (PL). The first two of these were found to account for approximately 90% of storm activity along the northern Gulf of Mexico.

The "cold front cycle" has commonly been used to characterize the sequence of events that accompanies a "typical" extratropical storm passage (e.g., Roberts et al., 1987; Roberts et al., 1989; Armbruster et al., 1997; Chaney 1999). Initially a pre-frontal phase occurs during which, strong, warm, moist winds blow from the southerly quadrant. The ensuing frontal phase is characterized by a sudden drop in air pressure, erratic winds, and short-lived, but occasionally intense, squalls. Finally, a post-frontal phase occurs, during which temperature and humidity drop, air pressure rises, and winds are strong and northwesterly to northeasterly. It should be noted, however, that this sequence, although considered typical, exhibits considerable variability. This will become apparent in the discussion of the data from this study.

Analysis of Meteorological Events During the Deployment

Aspects from several of the sources discussed above were used to characterize extratropical storms during the study period. Since wind velocity is a critical meteorological variable in coastal systems, the onset of storm conditions was considered to occur when a threshold wind speed was exceeded. The value assigned to this threshold was 7.4 m s^{-1}, which was equal to one standard deviation above the mean speed for the study period. The end of the storm was identified as the hour that wind speeds fell, and subsequently remained, below the threshold for six hours or more. Wind direction was also analyzed to identify phases of extratropical storm passages that corresponded to the cold front cycle described in the previous paragraph. Pre-frontal storm winds were defined as those that blew from a direction between 90 and 270° and appeared, from weather maps, to occur prior to a cold front passage. The post-frontal phase included the period subsequent to the frontal passage when storm winds blew from a direction between 270 and 90°. All other wind conditions were considered fair weather. Furthermore, storms were classified on the basis of intensity and synoptic characteristics according to several of the classification systems discussed earlier.

Meteorological Summary of the Deployment

Wind speed during the deployment averaged 4.8 m s^{-1} and had a mean direction toward the Southwest (228°). It is important to note that the oceanographic and not the meteorological convention is used for wind direction in this project; thus, the stated direction indicates the direction *toward which* the wind was blowing. Hourly wind speed and direction for the deployment period are shown in Figures 4.1 and 4.2. These figures clearly demonstrate the increases in wind speed characteristic of extratropical storms, as well as the clockwise rotation of wind direction during their passage.

Spectral analysis of the wind speed over the 61-day deployment period shows a statistically significant peak in energy at a frequency of roughly every five days, or approximately the same as that of extratropical storm passages (Fig.4.3). This suggests that extratropical storms were responsible for most of the variability in wind speed during this time, a

result consistent with other published research for the northern Gulf of Mexico (e.g. Chuang and Wiseman, 1983).

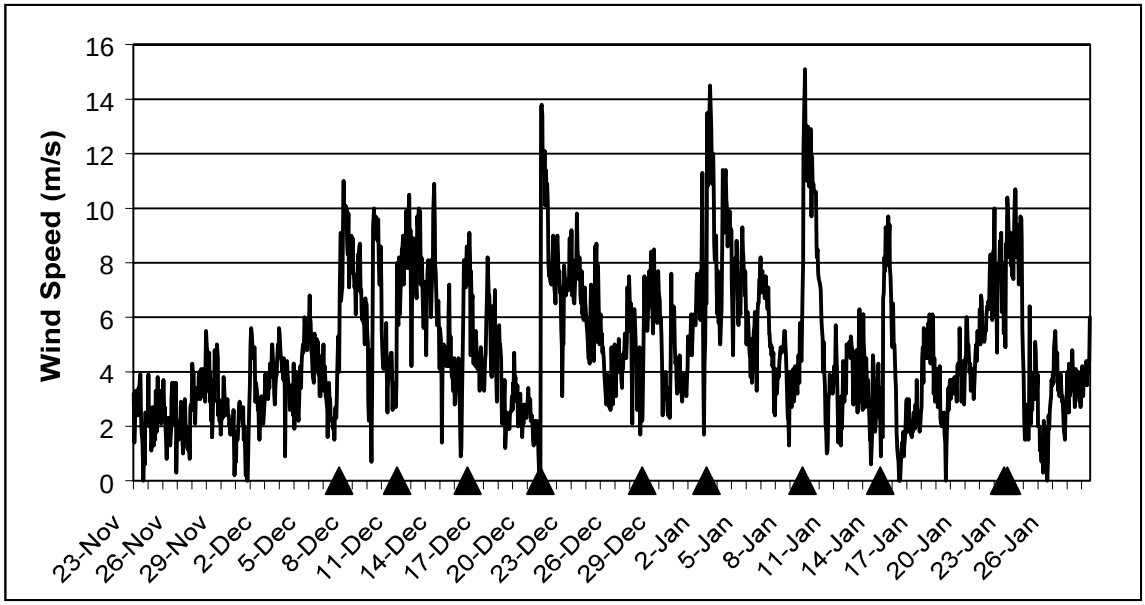

Figure 4.1. Wind speed during the deployment period. The time of the cold front passages associated with extratropical storms is indicated by black arrows.

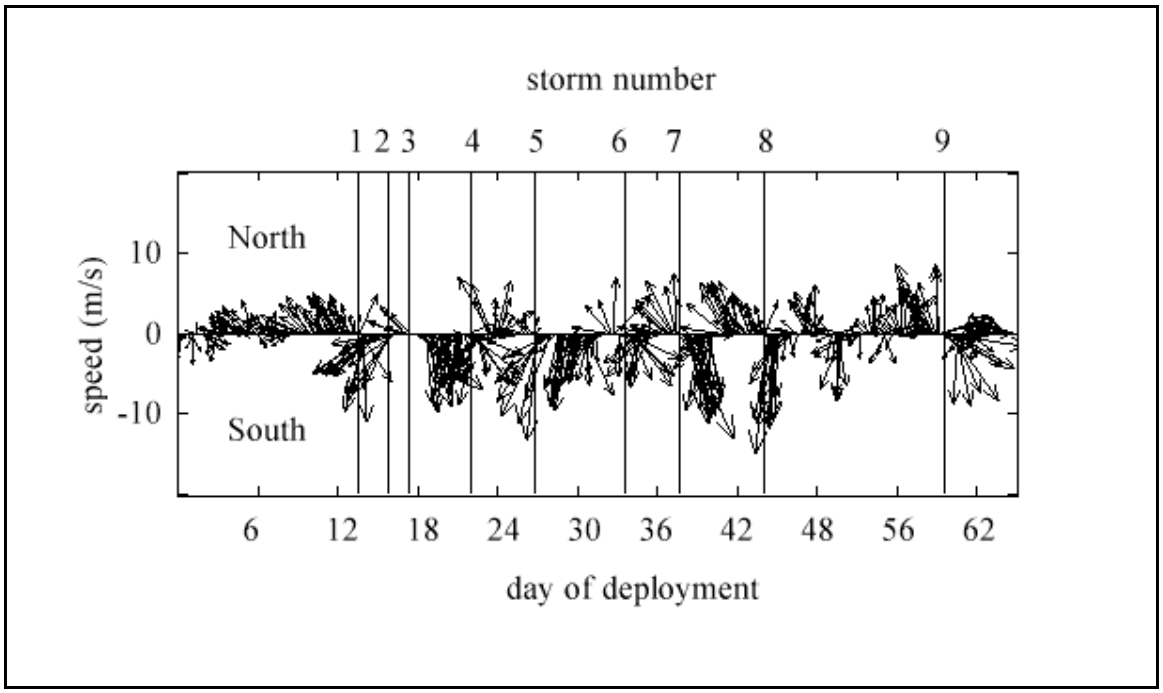

Figure 4.2. Feather plot of hourly wind vectors during the deployment.

According to the quantitative definition outlined previously, nine storms occurred during the 61-day deployment, a frequency of one every 6.8 days. Mean wind speed and direction were 8.1 m s^{-1} and 174° during storms and 3.8 m s^{-1} and 293° during fair weather. On the whole, therefore, storms during the period were characterized by strong winds blowing toward the south, while the mean wind direction during fair weather was westerly.

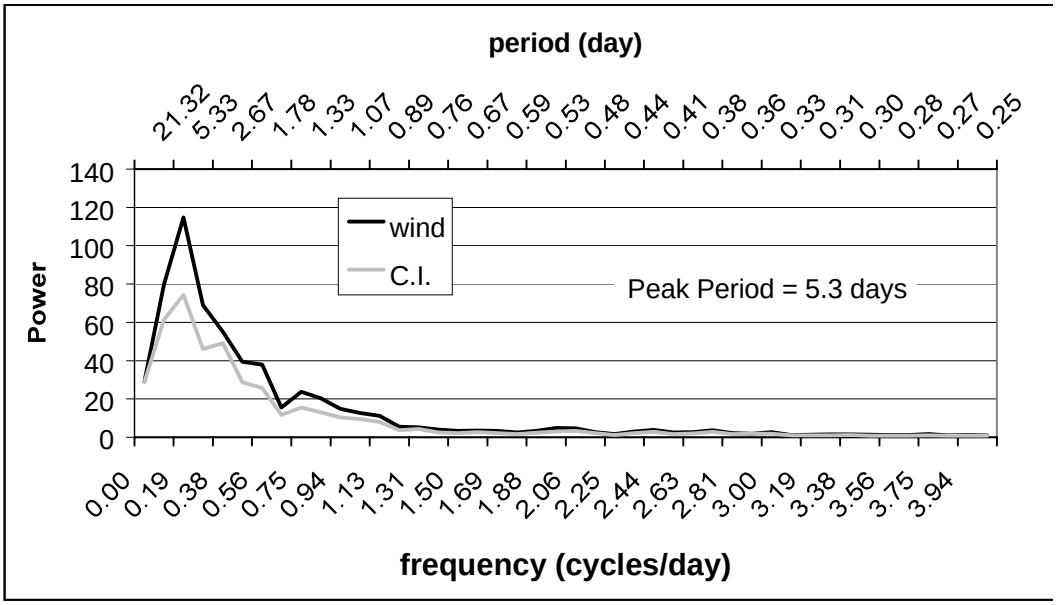

Figure 4.3. Power spectrum of wind speed during the deployment. C.I. represents the 90% confidence interval.

Classification of the storms that occurred during this study, using the described previously, is shown in Table 4.1. Several results are evident. First, analysis of the synoptic types associated with storms indicates that the majority of cold fronts affecting the coast were aligned oblique to it (i.e. the migrating cyclone of Roberts, et al., 1989). Six of the nine storms were classified as the Primary front type described by Chaney (1999), while an additional two were of the Secondary Front type. Despite the sequence of atmospheric events that "typically" accompany cold front passages, strong, winds did not often blow toward the north during this study, and as such, only two storms were considered to have a notable pre-frontal phase at all. On the other hand, all storms had a marked post-frontal phase during which strong winds blew from north to south.

Clearly, there was considerable variation in the intensity of storm events, with maximum wind speeds varying by as much as a factor of two, Power V varying by nearly an order of magnitude and Dolan and Davis values ranging by more than two orders of magnitude. Storms 3 and 5 were particularly weak, while Storms 2, 4, 7, and 9, and especially, Storm 6, were energetic. This is an important factor to bear in mind, since it will be demonstrated in later sections that the relative strength of storms is a key element in determining their influence on the marine environment.

Table 4.1. Classification of storms during the deployment on the basis of the methods discussed. In all cases, rank is based on a five-point scale.

Storm Number	***Month/ Day-hour***	***Orientation***	***Maximum Velocity (south)***	***Maximum Velocity (north)***	***Type (Chaney 1999)***	***V^2 (h ms^{-1}) [Rank]***	***Hsu Rank***	***Dolan & Davis [Rank]***	***Stages***
1	12/8-18	Oblique	5.3	11.0	P	2402[2]	2	18[1]	Post
2	12/12-17	Perp.	5.8	10.5	SG	4106[3]	1	31[1]	Post
3	12/17-13	Oblique	6.1	9.1	P	774[1]	1	1[1]	Post
4	12/22-14	Oblique	8.2	13.8	P	4779[3]	2	40[1]	Post
5	12/29-12	Parallel	7.5	8.5	S	1224[1]	1	3[1]	Post
6	1/2-22	Perp.	11.5	14.5	S	5712[4]	2	52[1]	All
7	1/9-12	Oblique	5.8	15.1	P	3392[3]	3	27[1]	Post
8	1/14-20	Oblique	6.3	9.7	P	852[1]	1	8[1]	Post
9	1/23-13	Perp.	10.0	10.7	P	3616[3]	1	178[3]	All
All	**-**	**-**	**7.4**	**11.4**	**-**	**2984**	**-**	**40**	**-**

According to both the Dolan and Davis and Hsu scales, storms that occurred during this study tended to be weak with only one Rank 3 event taking place during the deployment in each case (Table 4.1). There are several reasons for this. Magnitude of the Dolan and Davis scale was based on measured wave height in the Atlantic, which would presumably be much greater than in the Gulf of Mexico as a result of regional oceanographic considerations. The Hsu scale was based on the maximum wind speed calculated from the lowest central pressure of a Low in the Gulf of Mexico, whereas this study employs the maximum wind speed at a particular location. Clearly, site-specific wind measurements would be lower unless the Low passed directly over the study area.

The Power V rating (Chaney, 1999) appears to have been the most useful representation of storm intensity for present purposes. Unlike the system used in this study, however, where a value of one standard deviation above the mean was used to define storms, Chaney included all winds that exceeded the mean. According to this classification, three storms were weak (Rank 1), five were moderate to significant (Rank 2-3), while only Storm 6 was severe (Rank 4). These results should be noted by the reader, since Power V classifications will be often referenced during later sections of this project to differentiate between the storms that occurred during the deployment.

5. HYDRODYNAMICS, BOTTOM BOUNDARY LAYER PARAMETERS AND SEDIMENT TRANSPORT DURING THE ENTIRE DEPLOYMENT PERIOD: TIME- AND FREQUENCY-DOMAIN ANALYSIS AND OVERALL SUMMARY

Introduction

Long-term measurements in the bottom boundary layer of inner shelves are fairly rare, and published results are often confined to a single storm. Furthermore, as discussed previously, the only research conducted in coastal Louisiana that employed a similar methodology to the present study consisted of two summer deployments devoid of appreciable storm activity (Wright et al., 1997). Thus, an important objective of this research is to summarize prevailing winter hydrodynamic, bottom boundary layer, and sediment transport patterns in the region, thus helping to establish a "climate" from which regularities may be drawn in the future. This section will therefore focus on the results of the entire deployment by means of general summaries, as well as time-series and spectral (frequency domain) representations. Although the connection between atmospheric forcing mechanisms and marine and sedimentary processes will become evident, more detailed representations of these linkages are reserved for later sections.

Initial Considerations: Field Observations

Divers characterized the bed at the field sites as being largely free of bed forms during both the emplacement and retrieval stages of the deployment. While they did report bed irregularities with an estimated height of 1 cm during the emplacement phase, these were apparently localized, non-periodic, and were thus not likely the result of organized wave or current activity. Unfortunately, it was unrealistic for divers to monitor the bed throughout the duration of the deployment, owing to obvious logistical, financial, and, most importantly, environmental limitations. Video camera surveillance was also impossible as a result of extremely poor visibility. Therefore, the assumption adopted during this project is that the bed at the study sites was essentially flat (i.e. free of bed forms), unless data from bed level sensors suggested otherwise.

The initial trip to the field sites to retrieve all instrumentation occurred on January 12, 1999. Diver recognizance revealed that all systems, which had initially rested on the bed, were submerged beneath at least 20 cm of sediment, impeding their safe return to the research vessel. Only System 2A, located at the nearshore site and submerged to a lesser extent than the two offshore systems, was retrieved that day. Several subsequent attempts were made to recover the systems at Site 1, and eventually, on February 2, 1999, both were successfully retrieved. The sedimentary material overlying the instrumentation upon recovery was fine sand, similar to typical bed sediment in the study area. Although the cause of the burial of the systems was unclear at the time, two hypotheses were considered for further investigation: (1) overlying deposition of sediment (i.e., bed level increase) or (2) scouring or sinkage of the instruments into the bed (i.e. sensor level decrease).

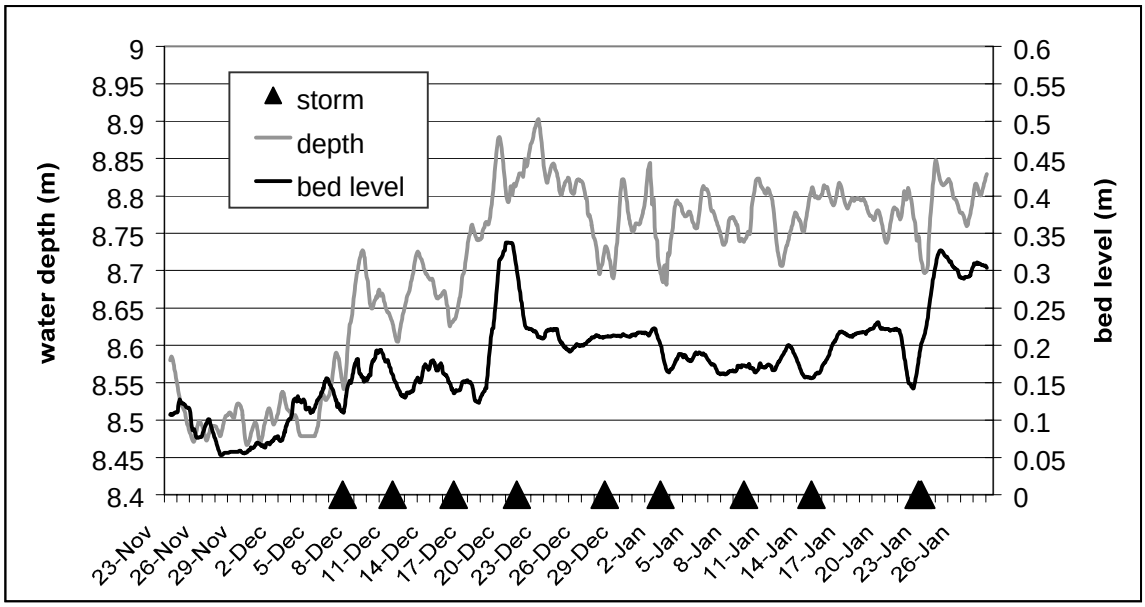

Figure 5.1. Bed elevation and water level (smoothed using a 24-h moving average window), as measured by System 1B during the deployment. Storms are indicated with black arrows, as will be the case in subsequent figures.

Recorded data from all systems were used to investigate these hypotheses. Since results from all systems were similar, data from only System 1B, specifically, bed level (relative to the sonar altimeter) and water depth (to the pressure sensor) will be considered in this section. Time series of these data are shown in Fig. 5.1. One important, but probably safe, assumption that should be noted was that the instrumentation system moved as a contiguous unit (i.e. it did not warp or bend), and thus the relative location of the sensors was constant. Although large short term-fluctuations (which will be discussed later) are evident in the time series of bed level, overall, it corroborates the field observations, indicating a total increase of approximately 20 cm during the deployment. Unfortunately, this trend is not particularly enlightening by itself since it could be a result of either hypothesized mechanism. Specifically, deposition of sediment would cause the bed to move closer to the (fixed) sensor, whereas downward motion of the entire instrument through sinkage or scour would cause the sensor to move closer to the (fixed) bed.

However, the pressure gauge also enabled the distance from the system to the sea surface to be quantified. There is no reason to believe that the water level at the site increased over the course of the deployment, beyond obvious short-term fluctuations due to tides and wind forcing. This is supported by NOAA data from Grand Isle (GDIL1), which indicated little change in water level between the beginning and end of the deployment period for the research. The time series of 24-h moving average water level at System 1B, however, did indicate a 20-cm increase during the period, and was strikingly similar to the time-series of bed level. Therefore, when the sum of the depth to the sensor and the distance from the sensor to the bed (i.e. the total water depth) was considered, no appreciable long-term trend over the course of the deployment was evident (Fig.5.2). Thus, it would appear that there was probably no appreciable long-term

change in bed level at the sites, but instead, a downward displacement of the instruments relative to it. All calculations of water level or total depth were therefore corrected for the influence of deployment-length instrument level change.

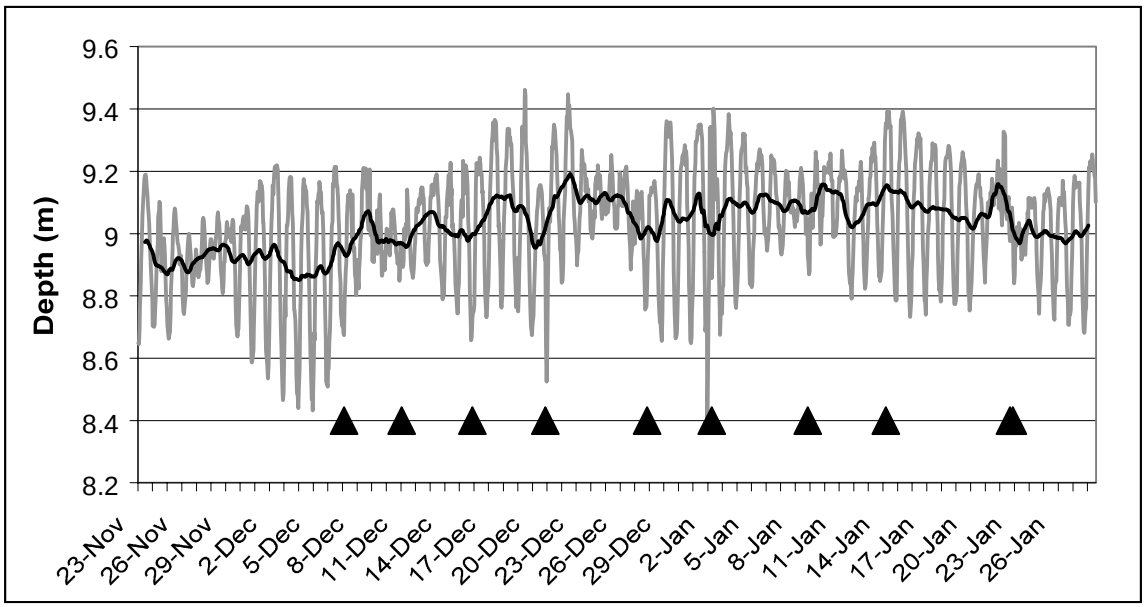

Figure 5.2. Total water depth (to the bed) measured hourly and smoothed using a 24-h moving average window as measured by System 1B.

Two possible causes for the downward displacement of the instruments were suggested previously: in-place sinkage; and scouring and immediate re-deposition of sediment around the instruments' bases, likely as a result of energetic wave-orbital currents. The second of these possibilities is far more likely, for two reasons. First, sinkage appears somewhat implausible, since the frames of the systems were wide and stable and the seabed in the study area was flat and sandy. Second, the vertical motion of the instruments was highly episodic, suggesting the importance of forcing mechanisms that vary considerably over time, such as hydrodynamic processes. Sinkage, driven essentially by the constant force of gravity, would be expected to be relatively steady over time. It appears, therefore, that scour was an important factor around the bases of the instruments. However, it is important to point out that flow modification and scour does not appear (with a few exceptions to be noted) to have influenced the sensors themselves, which were separated by tens of centimeters from the heaviest, most-intrustive, parts of the instrument frames.

As noted previously, short-term fluctuations of the bed level, both up and down, appear in the deployment record. Unlike episodic deposition of sediment, which can be interpreted from the data record as either bed or instrument displacement, decreases in bed elevation are less ambiguous to interpret since sediment cannot plausibly accumulate under the bases of instrumentation systems. Low rates of episodic bed erosion must have occurred locally beneath the bed sensors. It appears, therefore, that in addition to the movement of the systems themselves, short-term bed fluctuations in bed level caused by erosion and accretion occurred

during the deployment, suggesting that sedimentary processes during the winter are quite dynamic at these sites.

Hydrodynamics

An overall summary of hydrodynamic parameters for the entire deployment is shown in Table 5.1. Important points to note include the total depth, which was 1.5-2 m deeper offshore (Site 1) than nearshore (Site 2), and the depth range, which was slightly more than 1 m at both sites. Significant wave height and wave orbital velocity were higher at Site 1 than at Site 2, by 36 and 18 %, respectively, which is consistent with the expectation that waves crossing Ship Shoal are attenuated as a result of depth-limited energy dissipation. Wave period was also higher at the offshore site, which likely reflects the reduced importance of northward-propagating long-period swell waves, also due to attenuation, relative to locally generated sea.

Table 5.1. Summary of hydrodynamic parameters recorded by the systems throughout the deployment. It should be noted (as discussed previously) that the final recording dates of the instruments were different and that the sensors on System 1A were buried for several hours during the deployment.

Location		***Site 1 (Offshore)***		***Site 2 (Nearshore)***
System	***Statistic***	***1A (ADV)***	***1B (WADMAS)***	***2A (ADV)***
Total Depth (m)	Mean	8.8	9.0	7.3
	Minimum	8.2	8.4	6.7
	Maximum	9.2	9.5	7.8
Hs (m)	Mean	n/a	0.61	0.45
	Minimum	n/a	0.07	0.10
	Maximum	n/a	2.80	1.53
Tp (s)	Mean	n/a	5.3	5.0
	Minimum	n/a	3.6	3.6
	Maximum	n/a	9.1	9.1
Orbital Velocity ($cm\ s^{-1}$)	Mean	11.7	10.6	9.9
	Minimum	2.6	0.8	0.0
	Maximum	35.9	53.1	36.5
Current Speed ($cm\ s^{-1}$) (~0.3m above bed)	Mean	5.8	4.6	6.3
	Minimum	0.1	0.1	0.0
	Maximum	44.8	34.2	47.6
Current Speed ($cm\ s^{-1}$) (~1m above bed)	Mean	12.4	8.0	13.9
	Minimum	0.1	0.1	0.0
	Maximum	72.4	53.2	62.3
Current Direction	Mean	245	240	292

In contrast to the somewhat predictable differences in wave parameters between sites, current velocity differences, while equally evident, were less expected and in some senses, less explicable. Interestingly, for example, the inter-site comparison in wave energy described above

was reversed in the case of current energy, with mean current speed being approximately 10% higher at Site 2 (nearshore) than Site 1 (offshore). Current direction had a strong westerly component at both sites, which is consistent with general trends suggested in previous research. More notably, however, the across shelf component was seaward at the offshore site and landward at the nearshore site (Fig 5.3). Since the two sites are separated by only a few kilometers and are thus influenced by nearly equivalent atmospheric and tidal forcing mechanisms, this was apparently the result of flow modulation by the bathymetry associated with Ship Shoal. The reasons for this are not entirely clear, although one likely possibility is that westward flowing currents are steered downslope by gravity when they encounter the shallow shoal, thus resulting in an onshore flow to the north and an offshore flow to the south. Unfortunately, it is difficult to verify the cause of the observed behavior from the available data set, although preliminary results from a more recent deployment that included an instrument located in the center of the shoal suggest that this interpretation is correct. Nonetheless, it is clear that Ship Shoal exerts a measurable influence on mean current flow that requires further quantification.

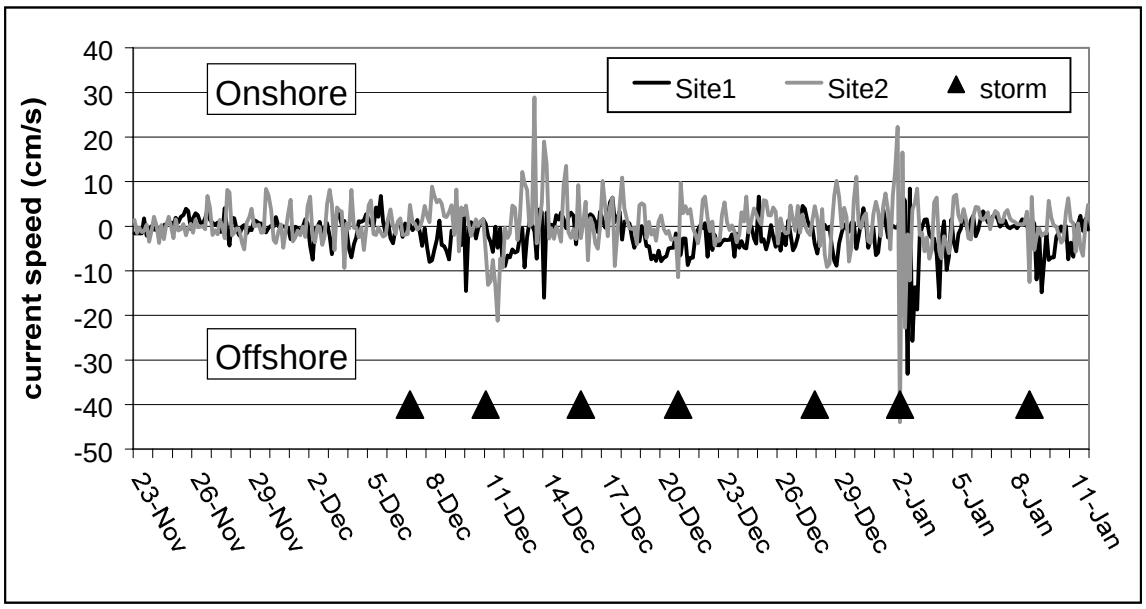

Figure 5.3. Across-shelf current flow during the deployment at Sites 1 and 2 (at ~20 cm above the bed) as measured by Systems 1A and 2A.

Obviously, Ship Shoal has an important effect on regional hydrodynamics, an influence that is presumably also significant on any inner shelf that includes submerged sand bodies or other prominent bathymetric features. Furthermore, this has important implications for bottom boundary layer dynamics and sediment transport on the south-central Louisiana inner shelf, a point that will be discussed further in subsequent sections of this project. Time-series plots clearly illustrate the importance of storms in generating episodic increases in hydrodynamic energy, as well as the differences in hydrodynamic response between the study sites. Figures 5.4 and 5.5 show wave parameters at the offshore and nearshore sites, highlighting not only the differences between storms and fair weather, but also the changes in wave characteristics caused by Ship Shoal.

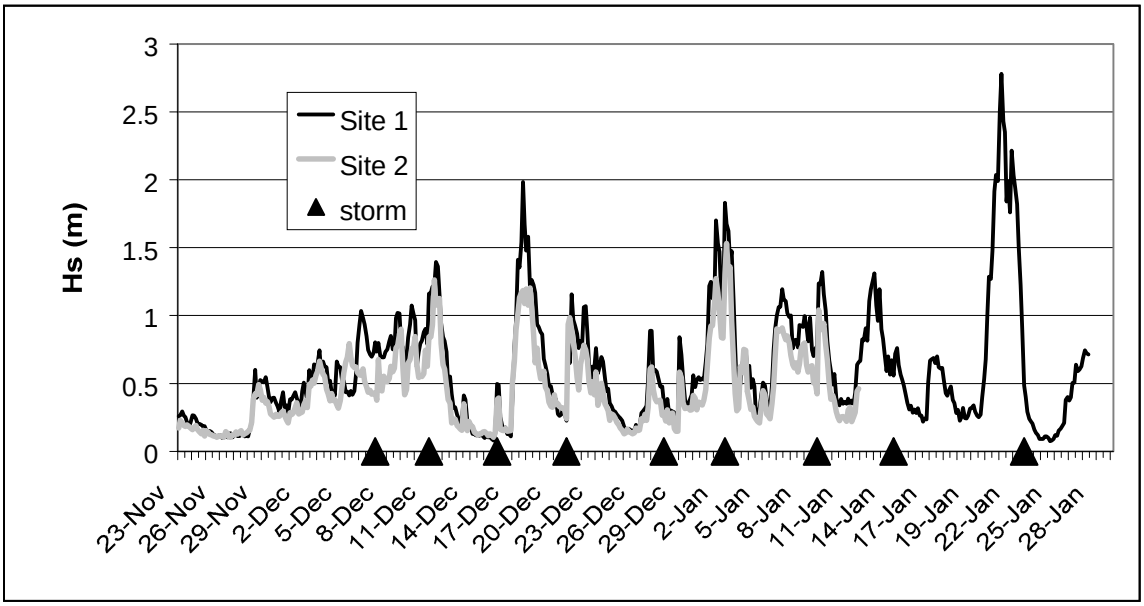

Figure 5.4. Significant wave height (Hs) at Site 1 and Site 2.

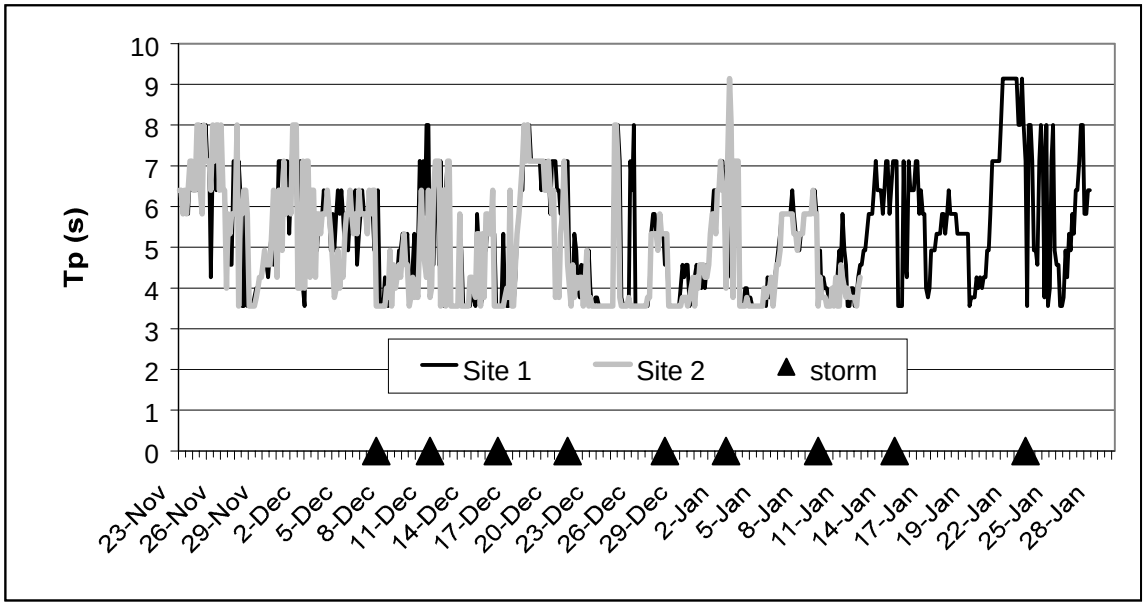

Figure 5.5. Peak wave period (Tp) at Site 1 and Site 2.

Figures 5.6 and 5.7 illustrate mean current and wave orbital speed at Sites 1 and 2, respectively, revealing several regularities. First, dramatic increases in both mean and wave-driven flow tended to accompany storms, particularly during Storm 6. Second, although mean and orbital current speeds were similar overall, each attained a relatively higher level at Three peaks in wave height are particularly noteworthy, two associated with Storms 6 and 9, respectively, and the other occurring during the fairly brief interval between Storms 3 and 4 (it

should be noted that later sections will demonstrate that Storm 4 was responsible for the majority of the observed response, and as such, this interval will be referred to as Storm 4 for the remainder of this section). Significant wave height during these storms was several times the mean fair weather value and was clearly higher at Site 1 (offshore) than at Site 2 (nearshore), supporting the conclusion that Ship Shoal is responsible for measurable wave energy attenuation. Trends in peak wave period are not especially clear from the time series, although it appears to have fluctuated in a temporally similar manner at the two sites. As such, it will be considered further in later sections. different times during the deployment, apparently as a result of meteorological forcing mechanisms. For example, while wave orbital flows were dominant at both sites during Storm 4, comparatively stronger mean currents accompanied Storm 6. The situation therefore contrasts both with surf zones, where orbital flows are nearly always dominant, and outer continental shelves, where mean currents are expected to be much more important than orbital flows. This highlights the uncertainty inherent in the study of sediment transport on the inner continental shelf, since either of these hydrodynamic forcing mechanisms may dominate depending on a complex interaction of a variety of geographical and oceanographic factors. The near parity between these hydrodynamic mechanisms also has clear implications for sediment suspension, which is thought to be closely related to wave orbital flow, and suspended sediment transport, which, requires the presence of a mean current (in addition, of course, to the presence of suspended sediment).

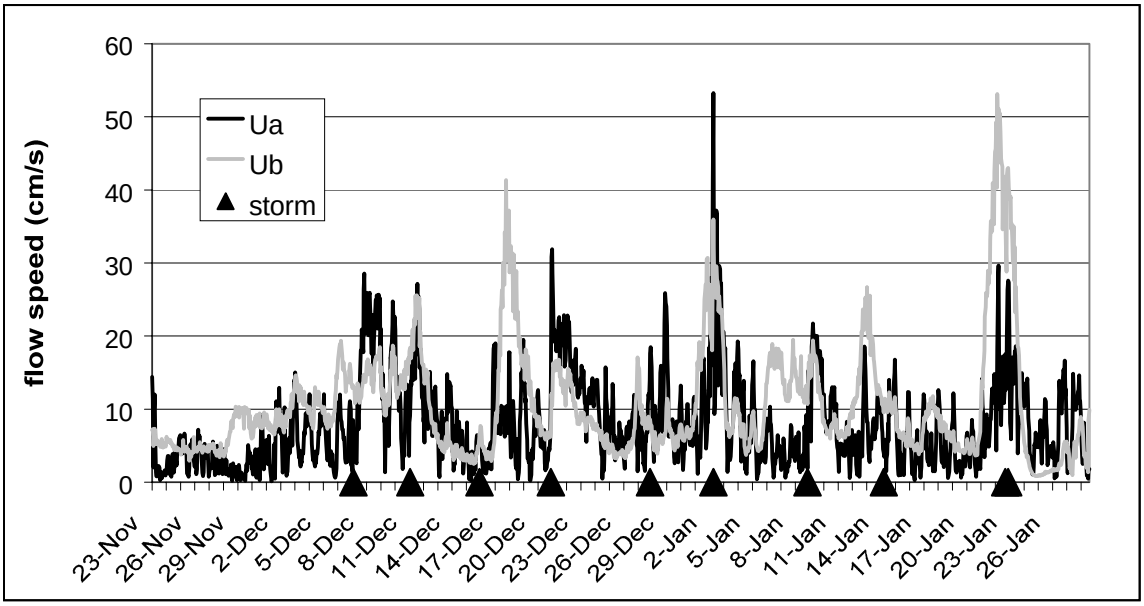

Figure 5.6. Flow speed of mean (Ua) and orbital (Ub) currents at Site 1.

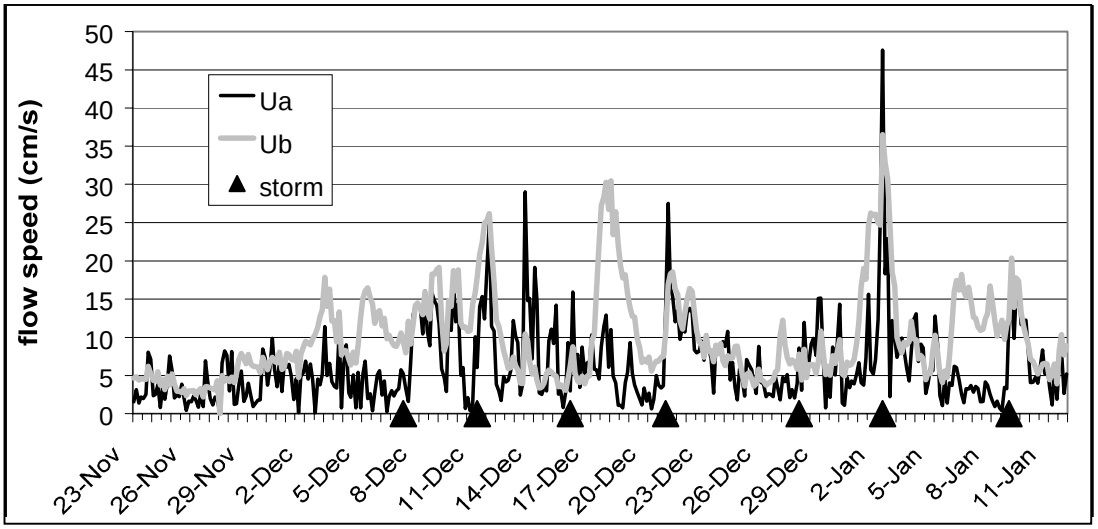

Figure 5.7. Flow speed of mean (Ua) and orbital (Ub) currents at Site 2.

Frequency-domain analysis shows the important time-scales over which across-shelf mean currents fluctuated. Figure 5.8 is a spectral plot of current speed during the deployment. Several statistically significant peaks are evident. The highest (i.e. most energetic) peak is at a period of 5.3-10.7 days, which reflects the importance of quasi-periodic extratropical storm passages in generating currents in the area. The next-highest peak occurs at a period of approximately 24 hours, illustrating the influence of diurnal tides, and possibly inertial currents, a phenomenon that will be discussed in more detail in subsequent sections. A minor peak is also evident at 12 hours, equivalent to that of the lunar tide, which is known to be much less important than the diurnal tidal signal, given the diurnal tidal regime in the area.

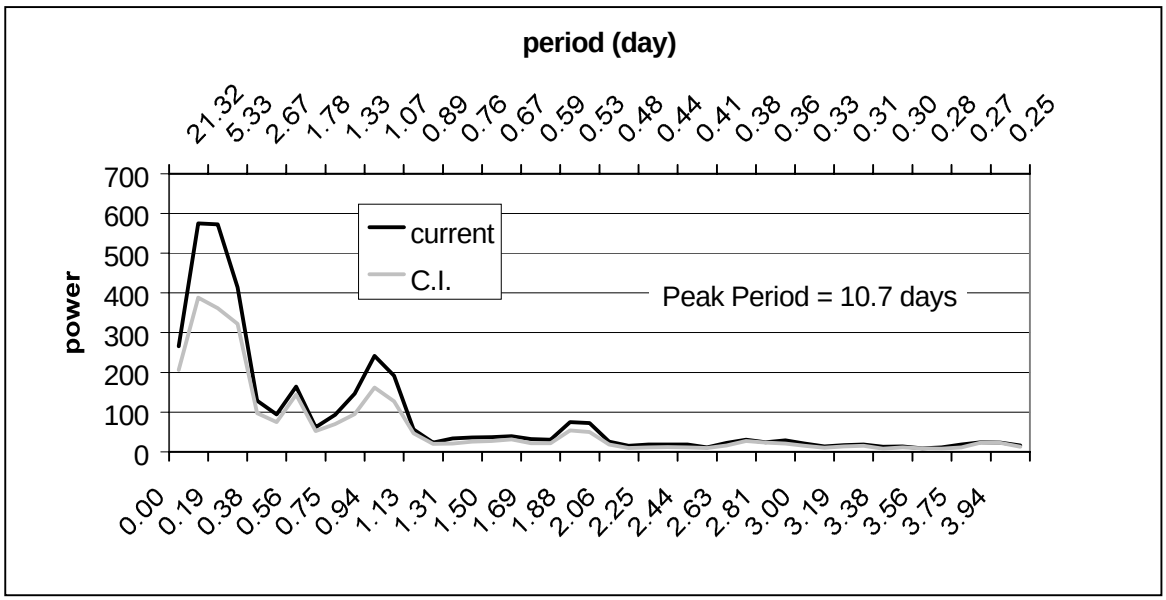

Figure 5.8. Spectrum of current speed at Site 1.

Figure 5.9 is a vector plot of near-bed current velocity at Site 1. Although the figures clearly indicate that currents rotated during the deployment, the expected time-scales of 5-10 days, reflecting the influence of extratropical storms, and 24 hours, indicating the presence of tidal currents, are difficult to visualize. On the other hand, detailed inspection of the figures suggests that wind and near-bottom current generally moved in the same direction, presumably as a result of direct wind stress on the water column. This is supported by cross-spectral analysis. Figure 5.10 shows that a statistically-significant, positive, peak between across-shelf winds and currents was present at periods of 5-10 days (the extratropical storm band) while the phase spectrum indicates that there was little or no phase difference between these variables (Fig. 5.11). In other words, northerly winds were coincident with northerly currents, and southerly winds were coincident with southerly currents, with extratropical storms providing the major energy input. The same relationship appears to be true of along-shelf winds and along-shelf currents, although the cross-spectrum was not statistically significant over most frequencies. Cross-spectra of winds and currents at 90° to each other did suggest possible Ekman effects at storm frequencies farther out on the shelf, however these results were not statistically significant.

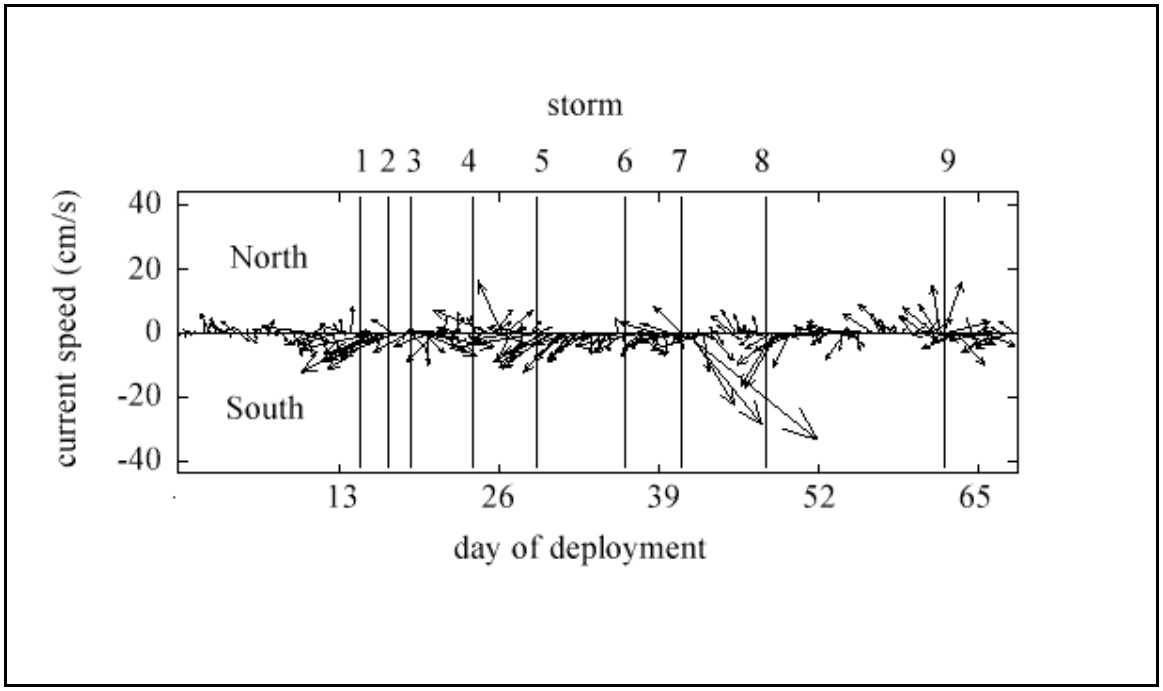

Figure 5.9. Vector plot of mean current direction at Site 1 during the deployment.

These results are somewhat puzzling since most research, as discussed previously, indicates that onshore storm winds normally generate coastal set-up which causes downwelling (offshore) mean flows near the bottom, while the reverse is true for offshore winds. Clearly, on the basis of mass conservation and an impenetrable coastal boundary, either return bottom flow or spatially-variable along-shelf flow are necessary if across-shelf currents are to flow in the same direction for an extended period of time. Inertial currents, which result when a wind blowing steadily in one direction ceases (Pond and Pickard, 1983), are a possible explanation for the observed behavior. Such currents continue to flow despite the removal of a forcing mechanism, with their direction and intensity modified by Coriolis force and friction. Daddio

(1977) stated that his study site in south-central Louisiana was sufficiently far from the coast (25 km) for the effect of sea surface slope (i.e. set up) to be negligible. Instead, Coriolis-driven inertial currents, which rotated clockwise with a period of approximately 24 h, accompanied frontal passages. This effect was enhanced where sudden removal of onshore wind forcing released sea surface set-up. It is possible that the near-bottom currents measured in the present study were at least partially the result of this effect, and not exclusively a product of direct wind forcing. Unfortunately, the lack of on-site wind data preclude a more detailed analysis of causal mechanisms. Despite this, the sequence of mean flow patterns that accompanied extratropical storm passages was distinctive, and has clear implications for inner-shelf sediment transport.

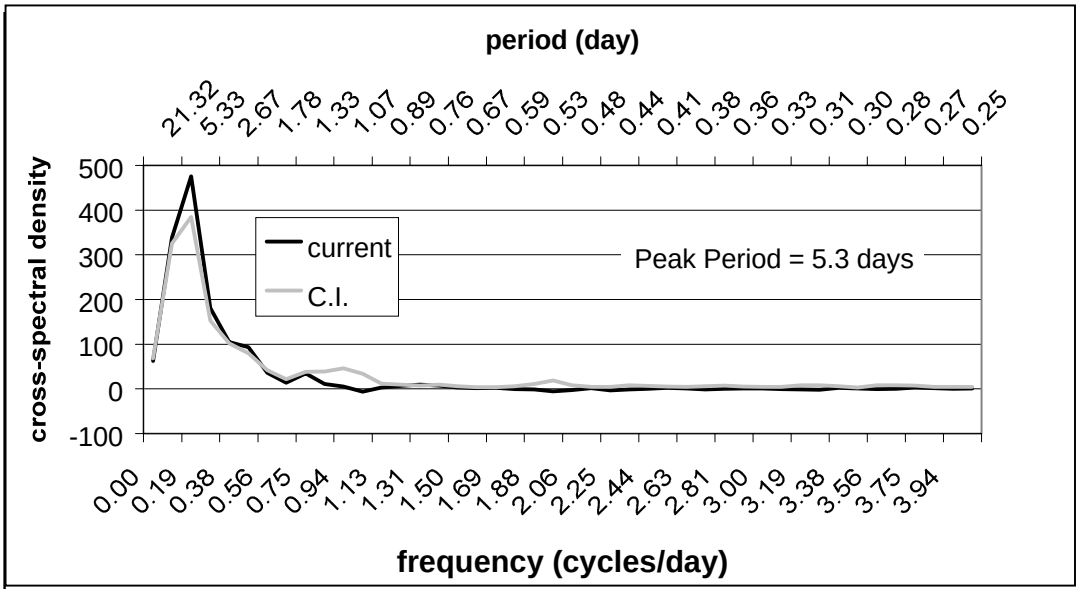

Figure 5.10. Cross spectrum of wind and across-shelf current at Site 1.

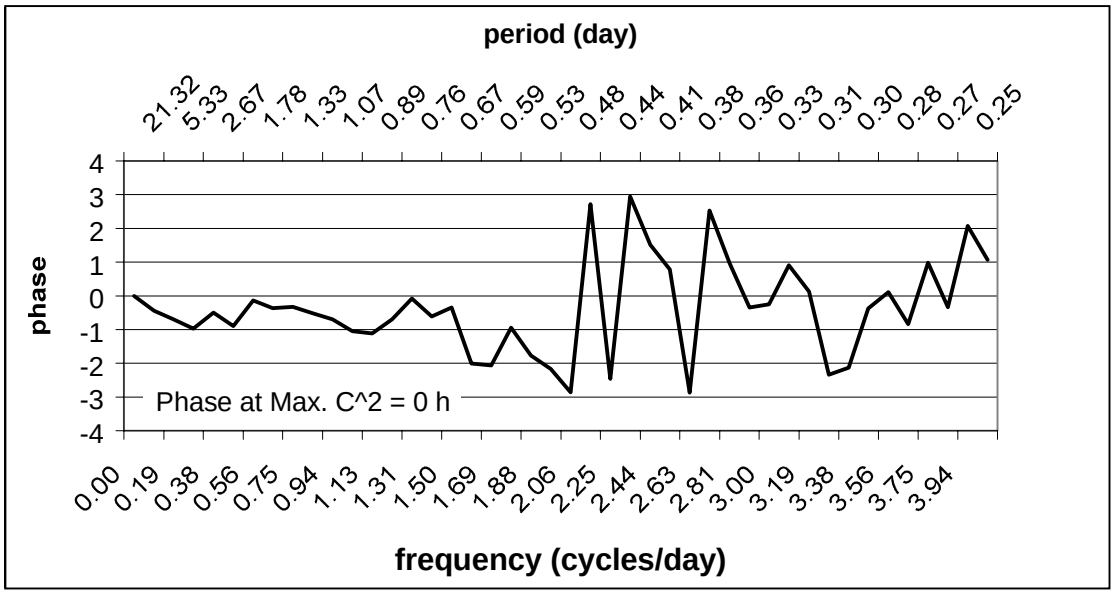

Figure 5.11. Phase spectrum of northerly wind and northerly current at Site 1.

Bottom Boundary Layer Parameters

As outlined previously, several methods were used to calculate bottom boundary layer parameters, depending at least partially on the instrumentation used. In this case, results from the Reynolds Stress (RS) method are shown. Although the values computed using this method are probably higher than those derived using other means, magnitudes during storm and fair weather conditions and between sites are useful for comparative purposes.

Not surprisingly, episodic increases in current- and wave-current shear velocity were associated with storm activity (Figs. 5.12 and 5.13). Shear velocity was particularly high during the period of strong wave-orbital flow between Storms 3 and 4, as well as during Storm 6, when mean flows were particularly strong. The interval of very high shear velocity that accompanied Storm 8 is somewhat difficult to explain, however, given that neither mean nor orbital currents were especially strong. As discussed previously, however, shear velocity is a complex parameter that is related not only to the flow, but also to non-linear wave and current interaction, physical bottom roughness and sediment transport. It is notable, in light of these considerations, that Storm 8 was, in fact, characterized by a particularly high apparent bottom roughness value, which could account for the high shear velocity values. Trends in other bottom boundary layer parameters, such as bottom roughness, drag coefficient and wave friction factor were unfortunately not particularly clear from time series representations. As such, their discussion is reserved for later sections.

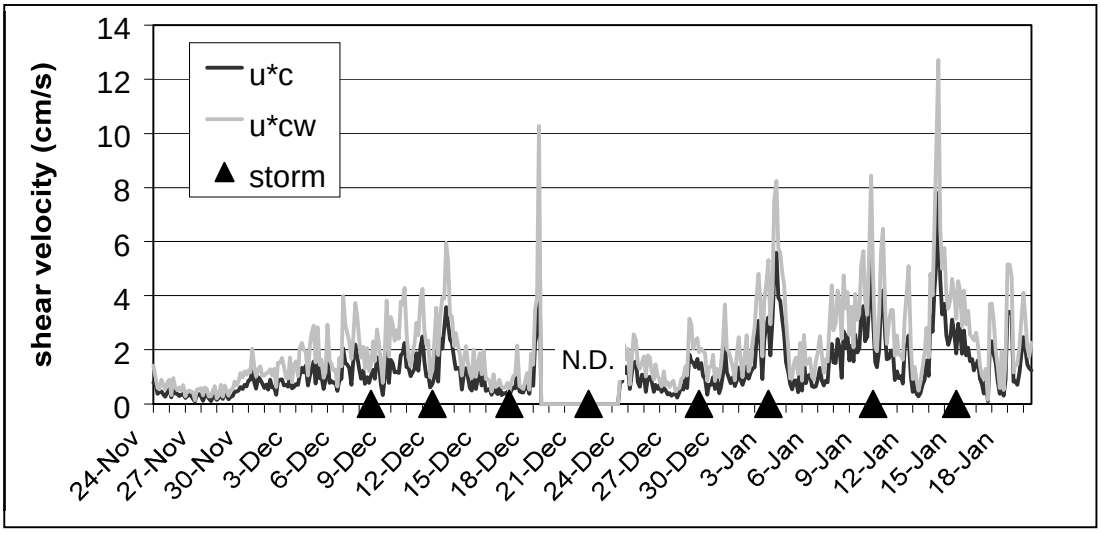

Figure 5.12. Current and combined wave-current shear velocity as measured at Site 1.

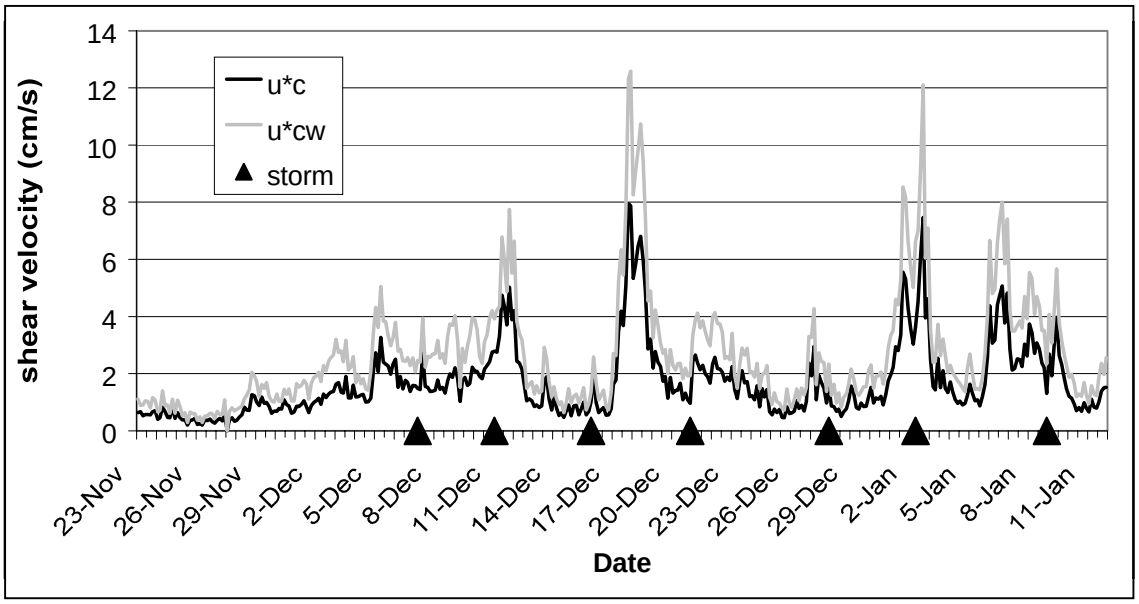

Figure 5.13. Current and combined wave-current shear velocity as measured at Site 2.

Sediment Suspension and Transport

Suspended sediment concentration at each site is shown in Figs. 5.14 and 5.15. It is clear that sediment suspension was episodic, and increased dramatically as a result of extratropical storm influences. At Site 1, Storm 4 and, to a lesser degree, Storm 6, had the highest measured concentrations, while at Site 2, the maximum concentration clearly occurred during Storm 6. Maximum concentrations were slightly higher at the offshore than the nearshore location, possibly as a result of the higher waves that occurred there during the majority of the deployment.

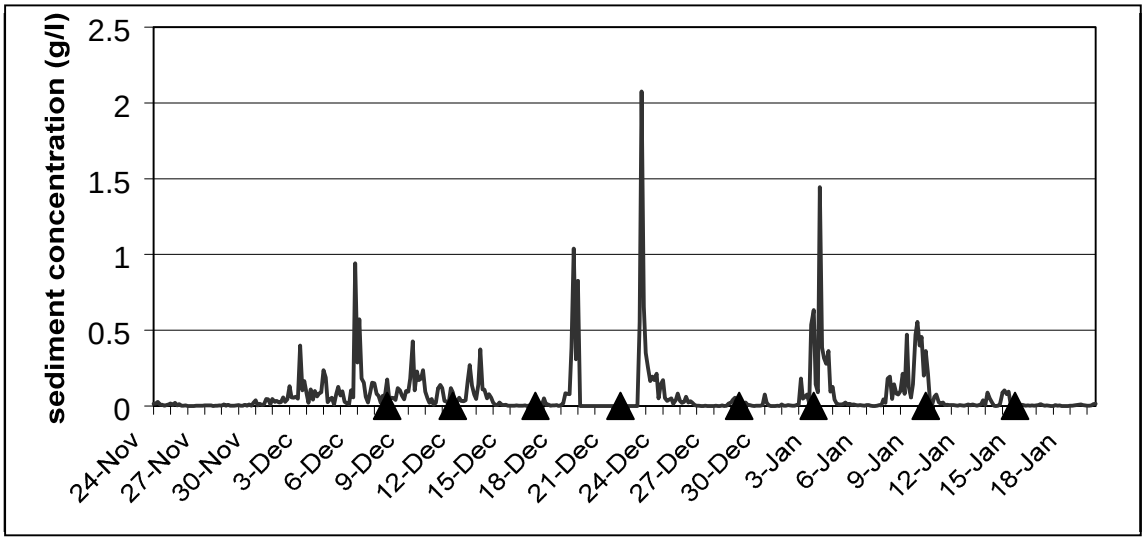

Figure 5.14. Suspended sediment concentration at Site 1 (System 1A).

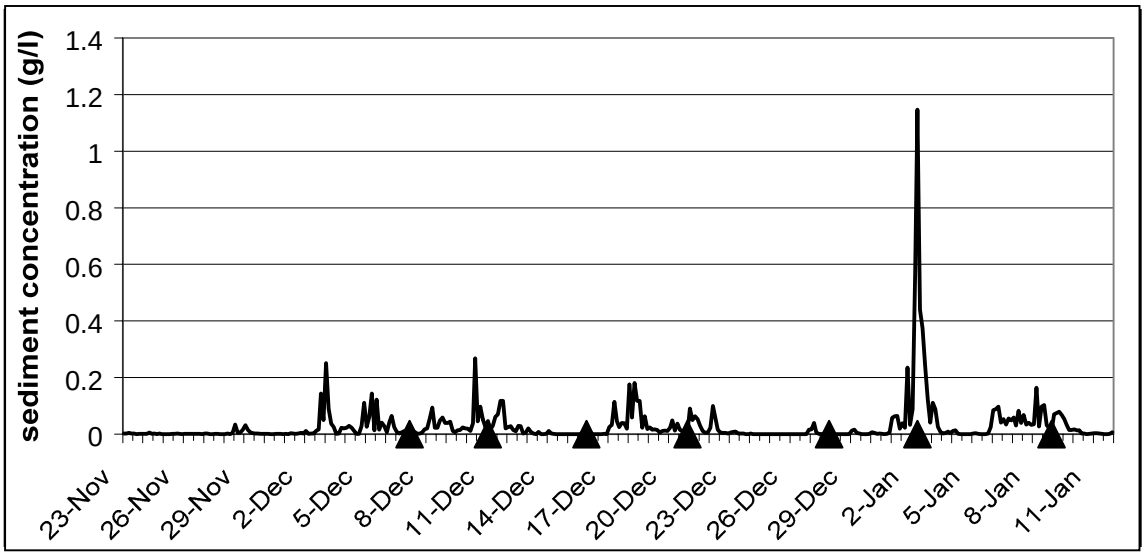

Figure 5.15. Suspended sediment concentration at Site 2 (System 2A).

Sediment transport was episodic and storm-driven at both locations and in both the across-shore and along-shore directions (Figs. 5.16-5.19). Enhancement due to storms was much more dramatic than for hydrodynamic parameters or shear velocity, for two reasons: first, sediment suspension is subject to a threshold value, below which transport is zero; and second, sediment transport, depending on how it is calculated, is subject to a power law, such that increases in flow velocity lead to exponential increases in transport.

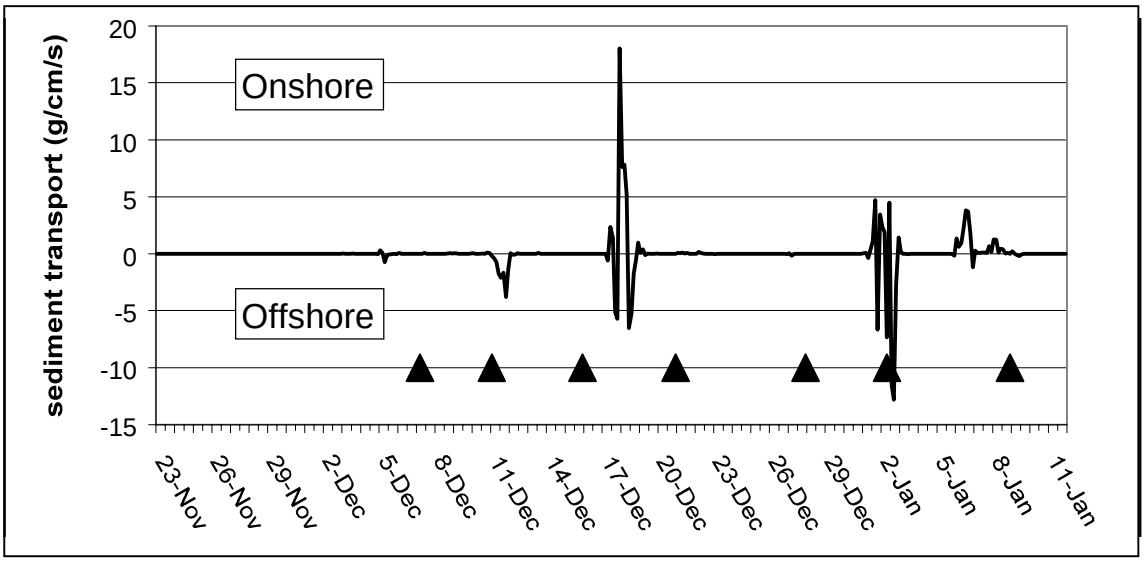

Figure 5.16. Across-shelf longshore sediment transport for Site 2 as predicted using the GMR method.

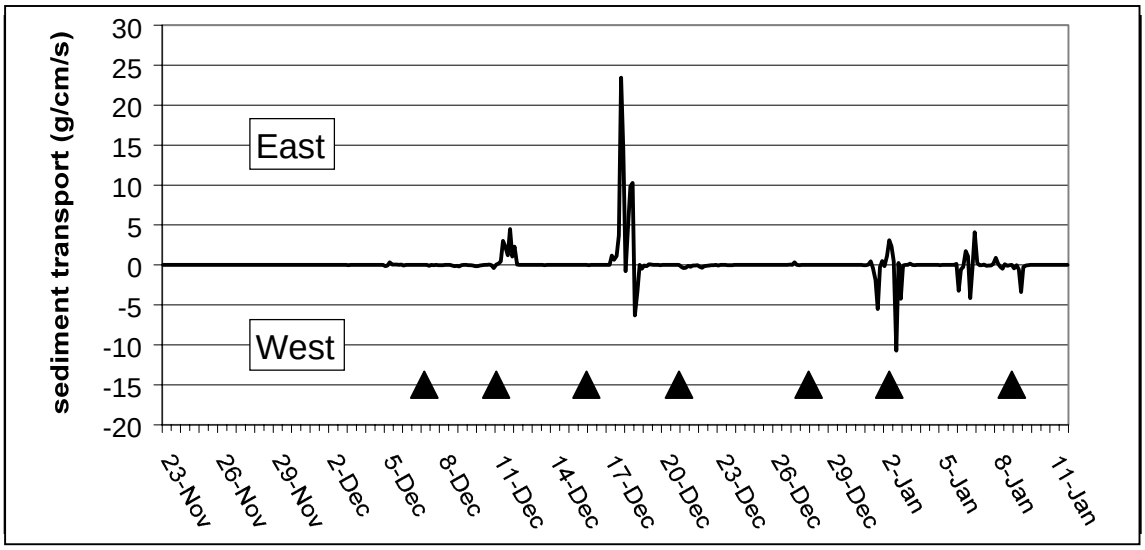

Figure 5.17. Along-shelf cross-shore sediment transport for Site 2 as predicted using the GMR method.

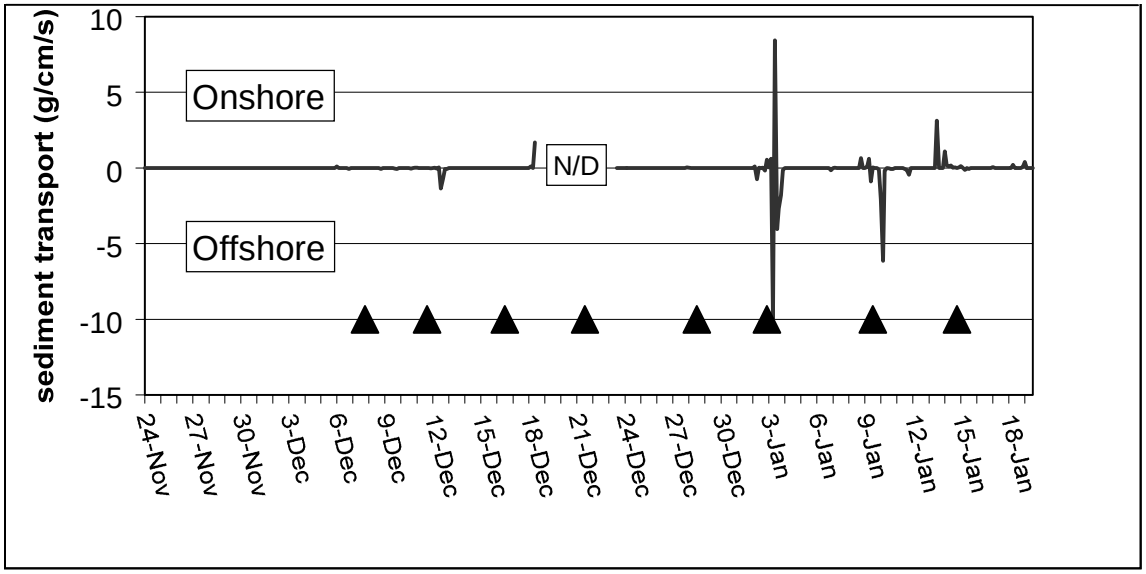

Figure 5.18. Across-shelf cross-shore sediment transport for Site 1 (System 1A) as predicted using the GMR method.

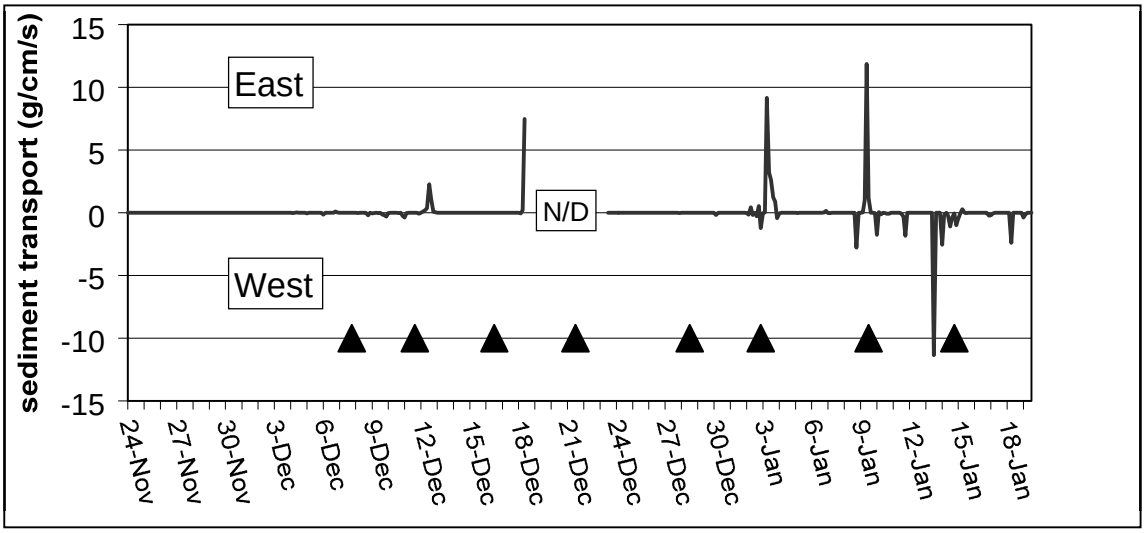

Figure 5.19. Along-shelf longshore sediment transport for Site 1 (System 1A) as predicted using the GMR method.

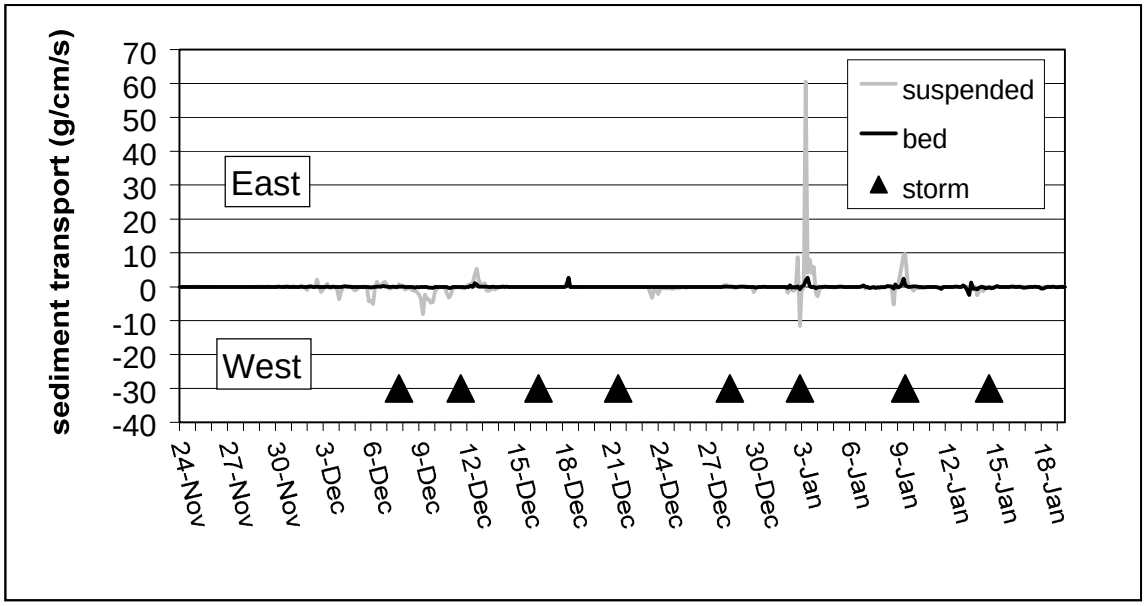

Figure 5.20. Longshore long-shelf bed and suspended load sediment transport for Site 1 (System 1A) as predicted using the MPM and SCC methods (respectively).

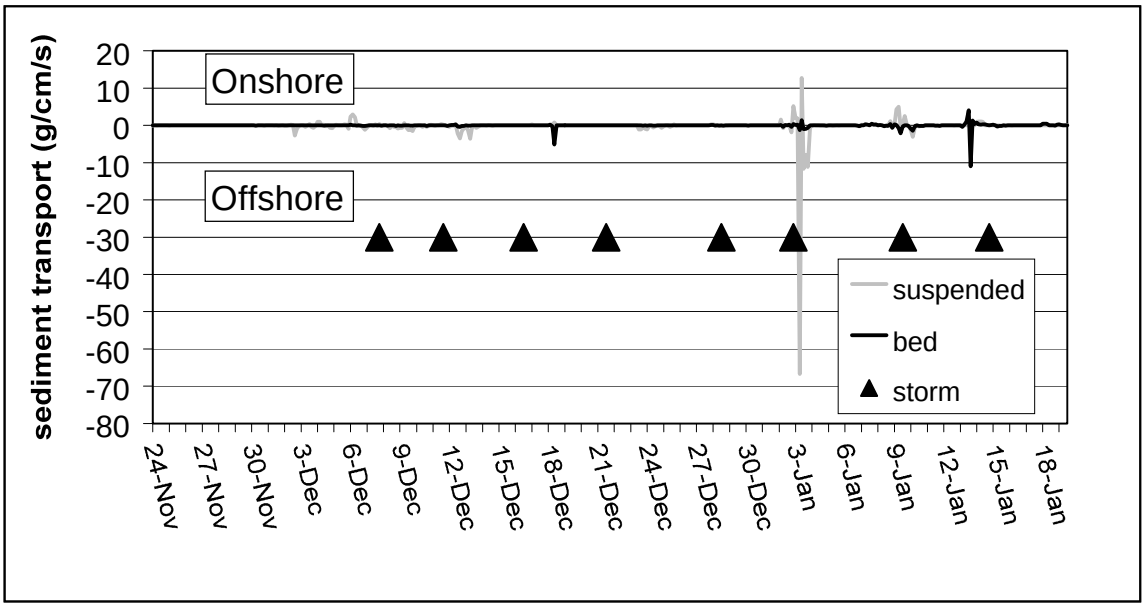

Figure 5.21. Cross-shore across-shelf bed and suspended load sediment transport for Site 1 (System 1A) as predicted using the MPM and SCC methods (respectively).

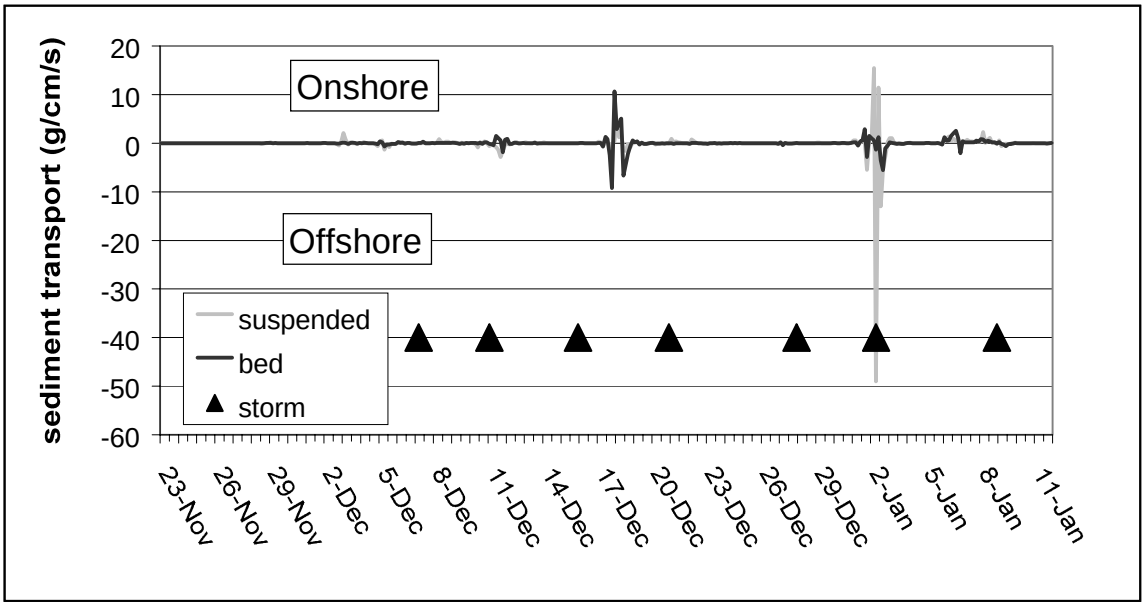

Figure 5.22. Cross-shore across-shelf bed load and suspended load transport for Site 2, as predicted using the MPM and SCC methods (respectively).

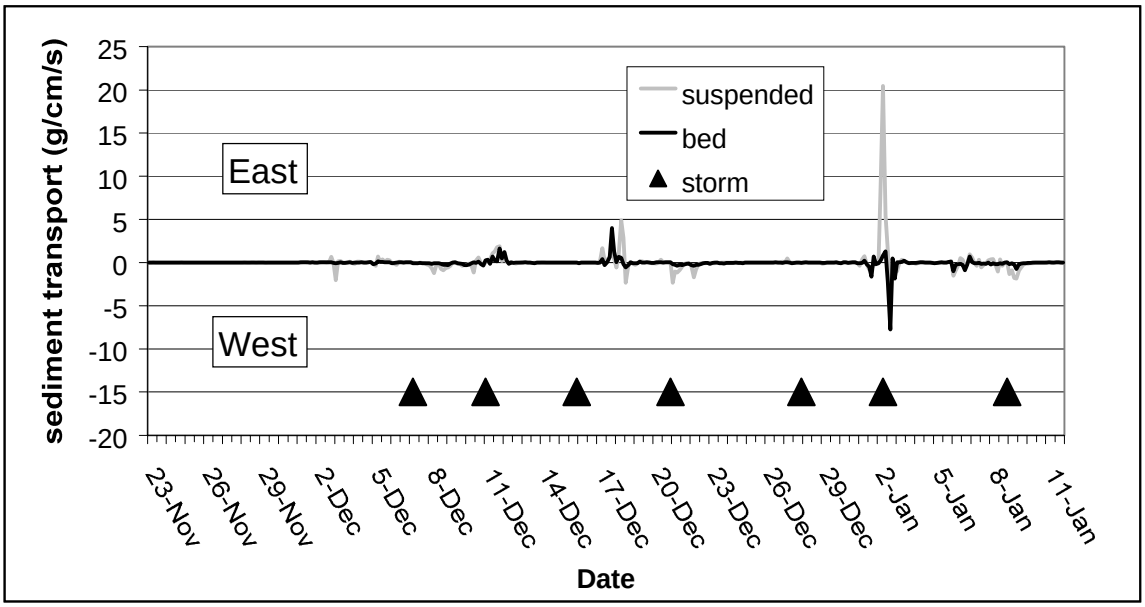

Figure 5.23. Longshore along-shelf bed load and suspended load transport for Site 2, as predicted using the MPM and SCC methods (respectively).

Four high sediment transport events are notable from Figs. 5.16-5.23, which show transport as predicted using the Grant-Madsen-Rouse (GMR), Meyer-Peter and Muller (MPM), and steady current concentration (SCC) methods. Results predicted using other methods were similar, and are thus not presented. High rates of sediment transport were generally associated with storms, specifically Storms 2, 4, 6 and 7. Sediment transport direction varied considerably between storms as well as during individual storms. Two of the most significant storms (4 and 6), were characterized by opposing trends in sediment transport direction—while onshore and eastward (i.e., NE) transport dominated during Storm 4, offshore and westward (i.e., SW) transport dominated during Storm 6. Within these storms, transport direction fluctuated by 180° on a very short time scale (i.e. several times per storm). This may have been related to diurnal fluctuations resulting from either tidal or inertial current flow, or to other variations in relative wave and current energy and direction. This question clearly requires further investigation.

This section has demonstrated several basic ideas. First, and most fundamentally, winter hydrodynamic, bottom boundary layer and sedimentary responses on the inner shelf of Louisiana are episodic, and are closely associated with extratropical storm passages. Second, these responses are highly dependent upon the characteristics of a particular storm. Finally, responses are variable over the course of individual storms, although the causes of this are not known. Clearly, these are complex issues that must be addressed through further research.

6. COMPARISON OF HYDRODYNAMICS, BOTTOM BOUNDARY LAYER PARAMETERS AND SEDIMENT TRANSPORT DURING STORMS AND FAIR WEATHER CONDITIONS

As noted in the introduction, coastal scientists have often used the distinction between storms and fair weather as an informative and convenient means by which to categorize hydrodynamic, bottom boundary layer and sediment transport regimes in a variety of environments. Although this approach is limited by the fact that it neglects both the various phases of individual storms and to some degree, the differences between storms, it can provide a basis by which to evaluate the long-term impact of atmospheric forcing, particularly if a long data record is available. Since several storms, with a variety of characteristics, occurred during this deployment, it appears to have been representative of a wide range of typical winter conditions in coastal Louisiana. This section is therefore devoted to quantifying the magnitude and variability associated with storms and fair weather conditions on the Louisiana coast.

Storm and Fair Weather Hydrodynamics

Hydrodynamic variables that exert direct influences on the bottom boundary layer and ultimately, on inner shelf sediment transport, include wave height and period, near-bed orbital velocity, and mean current velocity. These are summarized for Sites 1 and 2 in Tables 6.1 and 6.2, respectively. At both sites, hydrodynamic conditions during an average storm clearly differed from those that occurred during fair weather. As expected, wave height and current speed (both mean and oscillatory) generally increased during storms, while peak wave period decreased, presumably as a result of sea-like conditions that were generated by sudden increases in wind speed. Mean current direction at both sites was southwesterly during storms, and thus had an offshore component, although this is much more pronounced at Site 1 Fair- weather current direction was very close to westerly at the offshore site, while it was north-northwesterly at the nearshore site, indicating a strong onshore component. Some storms were clearly very energetic, and were characterized by hydrodynamic indices many times in excess of average fair weather conditions. Notably, however, there was considerable variability between storms. In the case of meteorologically weak events, such as Storm 3, and to some extent, Storm 5, waves and currents were actually less energetic than during typical fair weather conditions. Another notable point is that, even during powerful storms, wave and current hydrodynamic characteristics were not necessarily proportionately high—in other words, high waves and strong mean flows were not necessarily concurrent. For example, while waves at the offshore site during Storm 9 were more than twice as high as they were during Storm 1, mean current speed was measurably weaker. It is clear therefore, that while storms were usually responsible for generating comparatively high-energy hydrodynamic conditions, there was considerable variation between storms.

Table 6.1. Summary of storm and fair weather hydrodynamic measurements taken at Site 1 using System 1B (WADMAS). Hs is significant wave height, Tp is peak wave period, and Ub is orbital velocity, while Top, Mid, and Bot refer to the current meter velocity at heights of 100, 60 and 20 cm, respectively.

	Waves			***Currents***			
Meterology	***Hs (m)***	***Tp (s)***	***Ub(cms^{-1})***	***Top (cms^{-1})***	***Mid (cms^{-1})***	***Bot (cms^{-1})***	***Direction***
Storm 1	0.73	4.40	13.5	17.0	15.5	11.1	237
Storm 2	0.69	4.89	12.4	11.7	10.0	5.4	132
Storm 3	0.29	3.77	5.3	4.8	4.2	3.3	346
Storm 4	0.76	3.98	11.7	16.8	15.9	8.8	231
Storm 5	0.33	3.87	6.0	12.1	11.1	7.6	219
Storm 6	0.84	4.81	14.0	13.8	13.1	8.5	167
Storm 7	0.98	4.07	14.3	15.4	15.0	10.0	214
Storm 8	0.67	5.22	10.6	7.5	7.0	4.5	205
Storm 9	1.81	8.31	34.1	14.1	11.9	6.6	49
All Storms	**0.87**	**4.99**	**15.1**	**13.7**	**12.5**	**7.7**	**210**
Fair Weather	**0.52**	**5.46**	**9.1**	**6.2**	**5.3**	**3.6**	**260**

Table 6.2: Summary of storm and fair weather hydrodynamic measurements taken at Site 2 using System 2A. The U100 measurement is the current speed at 100 cm estimated using the Logarithmic profile method.

	Waves			***Currents***		
Meteorology	***Hs (m)***	***Tp (s)***	***Ub(cms^{-1})***	***U(cms^{-1})***	***U100(cms^{-1})***	***Direction***
Storm 1	0.53	3.85	12.3	9.9	16.0	288
Storm 2	0.73	5.35	15.8	9.4	21.6	146
Storm 3	0.24	3.56	5.6	7.4	11.7	301
Storm 4	0.59	3.87	12.2	11.2	20.1	274
Storm 5	0.23	3.95	6.3	8.7	12.8	191
Storm 6	0.62	4.70	13.2	10.6	22.0	173
Storm 7	0.73	3.75	14.0	12.8	24.4	262
All Storms	**0.57**	**4.27**	**12.3**	**10.3**	**19.5**	**250**
Fair Weather	**0.42**	**5.25**	**9.2**	**5.1**	**12.1**	**335**

Bottom Boundary Layer Parameters

Hydrodynamic differences between storms and fair weather obviously lead to differences in the bottom boundary layer regime, and these were evident at the deployment sites, as shown in Tables 6.3-6.5. Overall, current- and wave-current shear velocity were appreciably higher during storms than during fair weather, indicating an increased potential for sediment entrainment and transport during high-energy events. However, there was considerable variation between individual storms, largely as a result of their meteorological and hydrodynamic intensity. Not

surprisingly, the more powerful storms, such as Storms 2, 4, 6 and 7, were characterized by high shear velocity values.

Table 6.3. Summary of bottom boundary layer parameters (current, and wave-current, shear velocity, apparent bottom roughness, R-squared, wave friction factor, 100-cm drag coefficient, and wave boundary layer thickness) calculated based on the System 1B (WADMAS) data for storms and fair weather conditions.

	*u*c(cms^{-1})*	*u*cw(cms^{-1})*	*Zoc(cm)*	*r^2*	*fw*	*C_{D100}*	*WBL(cm)*
Storm 1	1.50	2.63	2.21	0.9716	0.0374	0.0114	1.41
Storm 2	1.61	2.42	5.73	0.9539	0.0404	0.0143	1.62
Storm 3	0.41	0.67	1.25	0.9676	0.0222	0.0157	0.31
Storm 4	1.54	2.62	1.36	0.9394	0.0455	0.0063	1.34
Storm 5	1.02	1.62	2.02	0.9301	0.0558	0.0135	0.81
Storm 6	1.36	2.31	2.89	0.8473	0.0328	0.0139	1.55
Storm 7	1.42	2.27	1.69	0.9102	0.0309	0.0072	1.15
Storm 8	0.85	1.38	3.72	0.7956	0.0230	0.0170	0.86
Storm 9	1.64	3.06	3.84	0.9714	0.0161	0.0106	3.25
All Storms	**1.41**	**2.37**	**3.00**	**0.9233**	**0.0352**	**0.0116**	**1.60**
Fair Weather	**0.64**	**1.09**	**3.23**	**0.8485**	**0.0276**	**0.0217**	**0.76**

Table 6.4. Summary of bottom boundary layer parameters (current, and wave-current, shear velocity, apparent bottom roughness, wave friction factor, 100-cm drag coefficient, and wave boundary layer thickness) calculated based on data from the offshore ADV (System 1A) for storms and fair weather conditions.

	*u*c (cms^{-1})*	*u*cw (cms^{-1})*	*Zoc(cm)*	*fw*	*C_{D100}*	*WBL(cm)*
Storm 1	1.20	2.18	2.19	0.0326	0.0094	1.18
Storm 2	1.89	3.08	3.11	0.0298	0.0094	1.96
Storm 3	0.45	0.73	5.91	0.0350	0.0463	0.36
Storm 4	1.06	1.54	0.69	0.0261	0.0048	0.70
Storm 5	0.89	1.56	0.97	0.0338	0.0074	0.77
Storm 6	2.03	3.21	1.52	0.0284	0.0052	2.00
Storm 7	2.43	3.66	1.05	0.0378	0.0031	1.83
Storm 8	2.28	3.61	3.25	0.0489	0.0061	2.54
All Storms	**1.66**	**2.67**	**2.11**	**0.0326**	**0.0090**	**1.58**
Fair Weather	**1.12**	**1.87**	**3.22**	**0.0311**	**0.0182**	**1.33**

Current shear velocity was in excess of 1.5 cm s^{-1}, and combined wave-current shear velocity exceeded 3.0 cm s^{-1}, during these events as calculated using the Reynolds Stress (RS) method. On the other hand, the shear velocity during Storm 3 and Storm 5 were weaker than during fair weather at two of the systems. Coefficient of determination (r^2) estimates, obtained by applying log-linear regression to the stacked current meter data from System 1B, were used to evaluate the degree to which flows were characterized by a well-organized logarithmic structure. Values

were generally higher during storms than during fair weather as has been reported previously for extratropical storm passages (Pepper et al., 1999). An increase in the statistical significance of logarithmic flow profiles did not always accompany strong currents, however, as illustrated by Storm 6, which was characterized by r^2 values similar to those during fair weather (~0.85). This was caused by a few extremely low r^2 values that occurred during the waning phases of the storm, when apparent bottom roughness (z_{0c}) was very high (10-15cm). However, the reason for these large z_{0c} values during the final hours of the storm is unknown.

Table 6.5. Summary of bottom boundary layer parameters (current, and wave-current, shear velocity, apparent bottom roughness, wave friction factor, 100-cm drag coefficient, and wave boundary layer thickness) calculated based on the System 2A (ADV) data for storms and fair weather conditions at Site 2.

	u*c (cm s^{-1})	***u*cw (cm s^{-1})***	***Z_{0c} (cm)***	***fw***	***CD100***	***WBL(cm)***
Storm 1	1.58	2.70	3.42	0.0462	0.0079	1.33
Storm 2	3.03	4.40	6.75	0.0383	0.0085	3.15
Storm 3	1.04	1.45	2.15	0.0540	0.0116	0.66
Storm 4	1.97	3.12	2.23	0.0557	0.0057	1.55
Storm 5	0.86	1.38	0.72	0.0457	0.0063	0.71
Storm 6	2.46	3.88	3.15	0.0472	0.0065	2.80
Storm 7	2.34	3.46	1.56	0.0490	0.0041	1.66
All Storms	**2.08**	**3.22**	**3.10**	**0.0481**	**0.0068**	**1.95**
Fair Weather	**1.58**	**2.50**	**5.76**	**0.0447**	**0.0168**	**1.76**

Apparent bottom roughness (z_{0c}) decreased during storm activity, in most cases, when values were generally less than 3.0 cm, as compared with mean fair weather values of 3.0-6.0 cm. Increased values were also observed, however, during some high-energy events, such as Storm 2. Drag coefficients at 100 cm above the bed (C_{D100}) decreased during storms, when mean values were near 0.01, roughly half the mean fair weather value, likely as a result of the decreased bottom roughness. The response of these factors to storm activity is thought to be a function of bed form changes during the deployment, as described previously by several authors (e.g., Amos et al, 1999). It is possible that during prolonged fair weather periods, wave ripples eventually formed, increasing the physical roughness of the bed, while high energy conditions caused bed forms to be washed out. Unfortunately, the limited observations made of the bed during this study neither confirm nor disprove this, and as such, further investigation of this question is necessary.

Wave friction factor (f_w), was higher during storms than during fair weather, although interestingly, it was high during one of the weakest events (Storm 3) and low during one of the strongest (Storm 9). It is somewhat unclear why this was the case, although it should be noted that wave friction factor was calculated numerically, based on a very complex set of interactions between bottom boundary layer variables, and thus generalizations based on meteorological conditions may not be entirely appropriate. Wave boundary layer (WBL) thickness, on the other hand, is strongly a function, as shown in Equation. 3.21, of combined wave-current shear velocity (u_{*cw}), and thus responded much more predictably, occasionally reaching values during strong storms that were twice that of mean fair weather conditions. As was the case with nearly all bottom boundary layer parameters, however, deviations from general patterns were

sometimes apparent. Not surprisingly, this variabilty was also apparent for sediment transport, as will be discussed in the next section.

Sediment Transport

Tables 6.6 through 6.9 show sediment transport predicted using a variety of models as well as bed level change for storms and fair weather at the two deployment sites. As noted in earlier sections, the absolute values of sediment transport predictions varied widely, and as such, they should be used chiefly as relative indices for the purposes of comparison. Generally speaking, the differences between storm and fair-weather conditions that were evident in hydrodynamic and bottom boundary layer parameters are also observable in the sediment transport data. According to nearly all indices, the predicted rate of sediment transport was higher during storms than during fair weather, with mean storm values calculated using certain methods exceeding fair-weather values by nearly an order of magnitude. Sediment transport values varied widely between storms as well. Storm 3 was characterized by little or no sediment transport, while strong storms, most notably Storm 6, caused sediment transport rates well over an order of magnitude in excess of fair-weather rates. It is apparent, therefore, that overall sediment transport was dominated by larger storms. It is also interesting that the mean sediment transport rate during fair weather was not zero as calculated by any of the techniques, indicating that sediment transport may occur at this location during mean winter fair weather conditions; previously, fair weather resuspension and transport of bottom sediment has often been considered unlikely for much of the Louisiana inner shelf (e.g. Adams et al., 1987; Wright et al., 1997).

Table 6.6. Summary of sediment transport estimates within and above the wave boundary layer for storms and fair weather conditions at the offshore site. These calculations are based on WADMAS data analyzed using the Grant-Madsen Model combined with Rouse Profiles (the GMR method).

	z<wbl		***z>wbl***		***Total***	
Meteorology	***Q (mg cm^{-1} s^{-1})***	***Direction***	***Q (mg cm^{-1} s^{-1})***	***Direction***	***Q (mg cm^{-1} s^{-1})***	***Direction***
Storm 1	0.330	238	0.608	248	0.934	245
Storm 2	0.235	125	0.591	112	0.822	116
Storm 3	0.000	9	0	-	0	9
Storm 4	0.207	247	0.398	231	0.600	237
Storm 5	0.053	253	0.040	257	0.092	255
Storm 6	0.433	152	2.237	135	2.655	138
Storm 7	0.160	190	0.083	202	0.241	194
Storm 8	0.028	161	0.001	179	0.029	162
Storm 9	0.055	37	0.399	9	0.448	12
All Storms	0.135	**175**	0.465	**141**	0.581	**148**
Fair Weather	0.072	**305**	0.113	**258**	0.170	**276**

Table 6.7. Predicted sediment transport and bed level change for Site 1 based on data from System 1A analyzed using several models.

	GMR		***MPM***		
	Q (mgcm^{-1}s^{-1})	***Direction***	***Q (mgcm^{-1}s^{-1})***	***Direction***	***Bed Change (cm)***
Storm 1	25.8	251	56.6	245	-6.3
Storm 2	213.3	119	82.1	113	1.1
Storm 3	0.0	343	0.3	343	0.2
Storm 4	0.7	227	5.5	203	-8.6
Storm 5	0.6	208	8.1	176	-0.3
Storm 6	1425.1	120	159.0	120	2.2
Storm 7	1157.8	185	355.2	165	-2.1
Storm 8	284.1	269	115.9	260	-0.2
All Storms	**549.1**	**139**	**97.8**	**145**	**-14.0**
Fair Weather	**138.7**	**298**	**85.6**	**253**	**40.5**

Table 6.8: Predicted sediment transport and bed level change for Site 2 based on several models.

	GMR		***MPM***		
	Q (mgcm^{-1}s^{-1})	***Direction***	***Q (mgcm^{-1}s^{-1})***	***Direction***	***Bed Change (cm)***
Storm 1	20.2	295	101.2	296	-0.5
Storm 2	887.8	129	451.4	66	8.3
Storm 3	4.8	276	20.8	309	-0.1
Storm 4	112.5	281	175.1	261	-2.7
Storm 5	0.7	309	12.0	324	0.1
Storm 6	2277.4	199	975.7	230	-1.6
Storm 7	544.8	268	267.7	237	-1.6
All Storms	**803.0**	**180**	**402.3**	**238**	**1.9**
Fair Weather	**579.0**	**54**	**325.6**	**351**	**11.1**

The direction of sediment transport also varied between storm and fair weather conditions, as well as between sites. The first point to note is that mean sediment transport during storms at both sites had a strong seaward (offshore) component as predicted by all methods. This was apparently the case both within and above the wave boundary layer, as indicated by columns 3 and 5 of Table 6.6. It was also true for both suspended and bed load transport, as shown by Tables 6.7 –6.9. Strong seaward components were most pronounced during more energetic storms, which, as noted previously, generally dominated overall transport. Landward transport was sometimes evident, however, during weaker events such as Storm 3. This was particularly notable at the nearshore site, where roughly half of the storms transported sediment onshore, although at generally lower rates than the seaward transport that occurred during the other of the storms. One exception to this was Storm 4, which was fairly energetic, but appeared to have a slight landward component (at Site 2), owing to the presence of mean west-north-westerly flowing currents. Across-shelf transport during fair weather, in contrast to energetic storm

conditions, had a landward component at all sites, according to the majority of prediction methods used.

Table 6.9. Cospectral estimates of suspended sediment transport (mg $cm^{-1}s^{-1}$) at System 1A (~20cm above the bed). Periods are Infragravity:=>10.25s;Wind-Wave: 2.15s-10.24s.

	Mean Transport		***Infragravity Transport***		***Wind-Wave Transport***		***Total Transport***	
	$mgcm^{-1}s^{-1}$	***Direction***	***$mgcm^{-1}s^{-1}$***	***Direction***	***$mgcm^{-1}s^{-1}$***	***Direction***	***$mgcm^{-1}s^{-1}$***	***Direction***
Storm 1	14.1	252	163.0	73	107.4	73	250.5	73
Storm 2	8.6	146	95.8	349	394.9	8	504.6	3
Storm 3	0.0	57	4.3	174	2.5	232	6.1	189
Storm 4	15.9	253	199.3	29	607.2	177	467.9	158
Storm 5	1.1	249	13.3	59	35.7	31	48.6	38
Storm 6	47.8	141	336.6	338	905.6	351	1536.5	346
Storm 7	2.8	171	91.1	157	496.6	237	496.2	227
Storm 8	0.2	273	11.8	39	8.5	75	18.6	50
All Storms	**11.4**	**165**	**119.8**	**4**	**139.2**	**345**	**322.7**	**353**
Fair Weather	**2.2**	**274**	**100.6**	**316**	**429.9**	**312**	**532.2**	**312**

Table 6.10. Cospectral estimates of suspended sediment transport (mg $cm^{-1}s^{-1}$) at System 2A (~20 cm above the bed). Periods are Infragravity:=>10.25s;Wind-Wave: 2.15s-10.24s.

	Mean Transport		***Infragravity Transport***		***Wind-Wave Transport***		***Total Transport***	
	$mgcm^{-1}s^{-1}$	***Direction***	***$mgcm^{-1}s^{-1}$***	***Direction***	***$mgcm^{-1}s^{-1}$***	***Direction***	***$mgcm^{-1}s^{-1}$***	***Direction***
Storm 1	21.6	294	84.3	116	96.3	167	145.0	147
Storm 2	30.6	141	106.3	321	77.3	359	180.4	334
Storm 3	0.8	279	3.2	103	1.7	103	4.2	102
Storm 4	31.7	287	110.2	94	71.7	106	165.3	97
Storm 5	0.1	353	0.3	167	0.4	179	0.7	175
Storm 6	151.1	140	152.5	314	791.4	71	757.2	69
Storm 7	49.2	265	150.5	79	154.9	107	283.6	93
All Storms	**32.9**	**155**	**40.1**	**7**	**214.5**	**74**	**232.7**	**70**
Fair Weather	**2.7**	**334**	**16.9**	**257**	**102.6**	**358**	**100.5**	**345**

Along-shelf transport varied somewhat according to the techniques used, and generalizations are difficult to make. Westerly transport predictions were more prevalent during storms than easterly predictions, although there was considerable variability between storms that did not seem to be related to intensity. During fair weather, easterly sediment transport predictions were somewhat more common than westerly predictions. In both cases, the causes of

this variability are unknown. It is possible that since east-west shifts in wind direction accompanying extratropical storms were not generally as regular or dramatic as north-south shifts, alongshore changes in hydrodynamic and sediment transport parameters were not as clear they were in the across-shelf. This suggests that, unlike many coastlines where along-shelf fluxes dominate, notably the Atlantic and Pacific coasts of North America, the northern coast of the Gulf of Mexico may be most strongly influenced by meteorological, hydrodynamic and sedimentary variations in the across-shelf direction.

Sediment Fluxes across Ship Shoal

It is apparent that Ship Shoal exerts a significant influence on regional hydrodynamic and sediment transport patterns, and as such, convergences and divergences (i.e. fluxes) of sediment are expected to occur during certain conditions. Calculating these fluxes is important, of course, in providing a clearer representation of the short-term modulating effect of the shoal on sediment transport patterns. However, since convergences and divergences indicate potential accretion and erosion of the shoal, calculation of flux is perhaps even more crucial in describing the long-term evolution of Ship Shoal, and ultimately, predicting its fate.

The issues discussed above are important for both theoretical and practical reasons. First, as noted earlier, Ship Shoal is a conspicuous and influential bathymetric feature on the Louisiana inner shelf that reduces wave energy and modulates current velocity. Changes to its morphology are therefore closely linked with regional changes in hydrodynamics and sediment transport. Furthermore, its sandy sedimentary composition is somewhat anomalous in the regional context of the otherwise muddy Louisiana coast, and it may therefore serve as an important source of sandy sediment to adjacent barrier islands and wetlands, either through natural processes or by means of human nourishment projects. Globally, the shoal is somewhat distinctive in terms of inner-shelf geology, since it formed recently as a result of exceptionally rapid rates of coastal transgression and barrier island submergence. In a sense, therefore, Ship Shoal may serve as a "laboratory" in which transgressive responses over short time scales reflect long-term barrier island responses to relative sea level rise on more "typical" coasts. In light of these regional, and global considerations, this section is therefore devoted to discussing the sedimentary fluxes across Ship Shoal associated with meteorological forcing.

There was considerable variability in flux during the deployment, as shown in Figures 6.1-6.4. This is not surprising, given the short-term variability in currents and sediment transport that occurred at each site individually. Figure 6.1 represents the current flux throughout the deployment, which appears to have been predominantly divergent, aside from a few convergent peaks, such as those accompanying Storms 2 and 6. The mean tendency toward divergence was presumably the result of the persistent seaward current component at Site 1 and landward current component at Site 2. The current convergence during Storms 2 and 6, on the other hand, occurred when flows were seaward at both sites, but were comparatively stronger at Site 2.

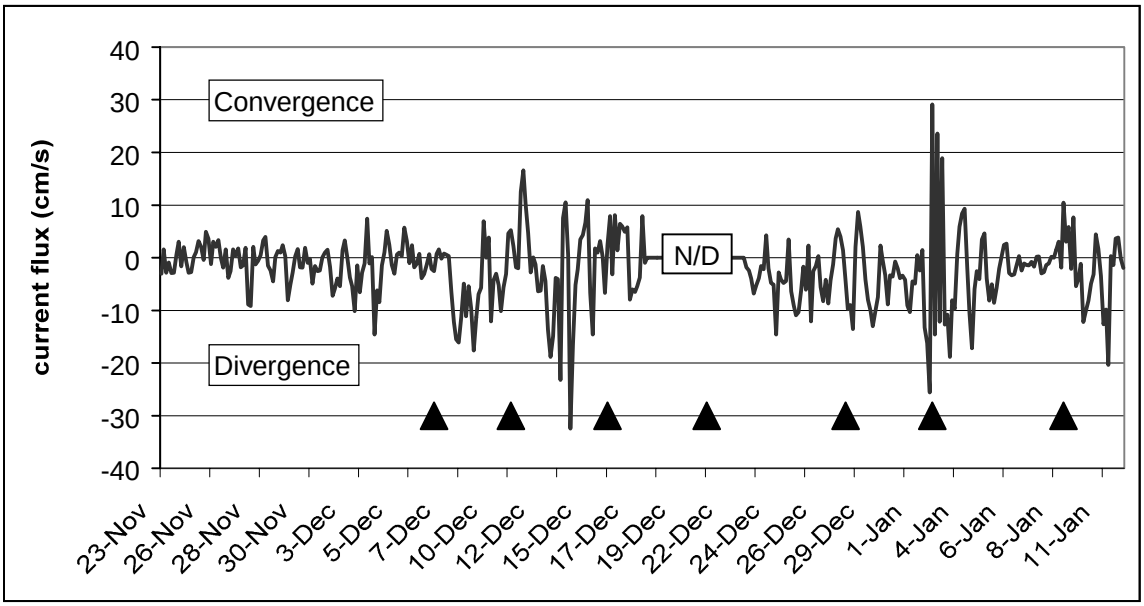

Figure 6.1. Current flux over Ship Shoal. The occurrence of storms is indicated with black arrows and N.D. represents a time for which no data are available, owing to sensor burial.

Figures 6.2-6.4 show the flux of sediment across the shoal as calculated using various methods. The pattern is similar in all cases—fairly low mean values were punctuated by high levels of episodic convergence or divergence. High-volume events often occurred in response to atmospheric storms, although this was not always the case. Such events were sometimes characterized by alternating periods of convergence and divergence, and, as will be demonstrated subsequently, net storm flux is therefore much lower in volume than would be expected. Clearly, therefore, sediment flux, like sediment transport at a particular point, is highly episodic. Table 6.11 shows the flux of sediment across Ship Shoal for the deployment, in the context of meteorological conditions. As expected, regularities in sediment flux over the shoal mirror those in sediment transport at the individual sites. Therefore, there was considerable variation in flux depending upon both the individual storm and the computational method used. Despite these sources of variability, however, the data clearly indicate that storms were most often associated with convergence of sediment over the shoal (accretion), while fair weather conditions were related to divergence (erosion). In particular, strong flux convergence occurred during Storms 2 and 6, apparently as a result of differences in sediment transport rate between the two sites. Specifically, although seaward transport occurred at both locations, the rate was much higher at the nearshore site. On the other hand, flux divergence occurred during Storm 7 for just the opposite reason—a higher rate of seaward transport at Site 1 than at Site 2. Fair weather conditions were characterized by flux divergence over the shoal, caused by high rates of landward transport at the nearshore location, accompanied by lower, and predominantly westward, sediment transport at the seaward site.

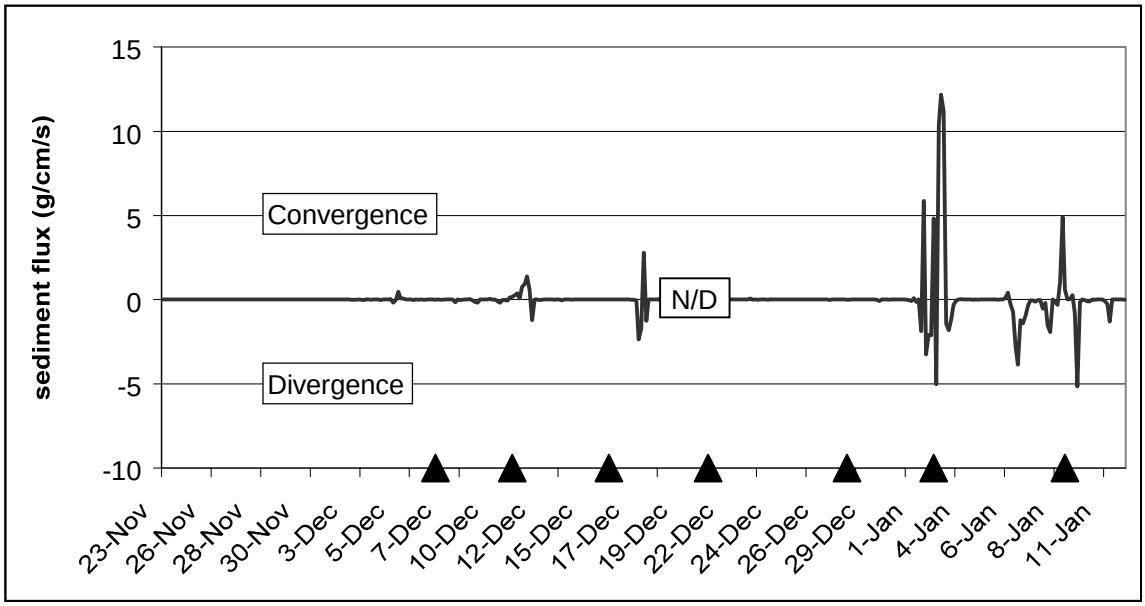

Figure 6.2. Flux of sediment across Ship Shoal as calculated using the GMR Method.

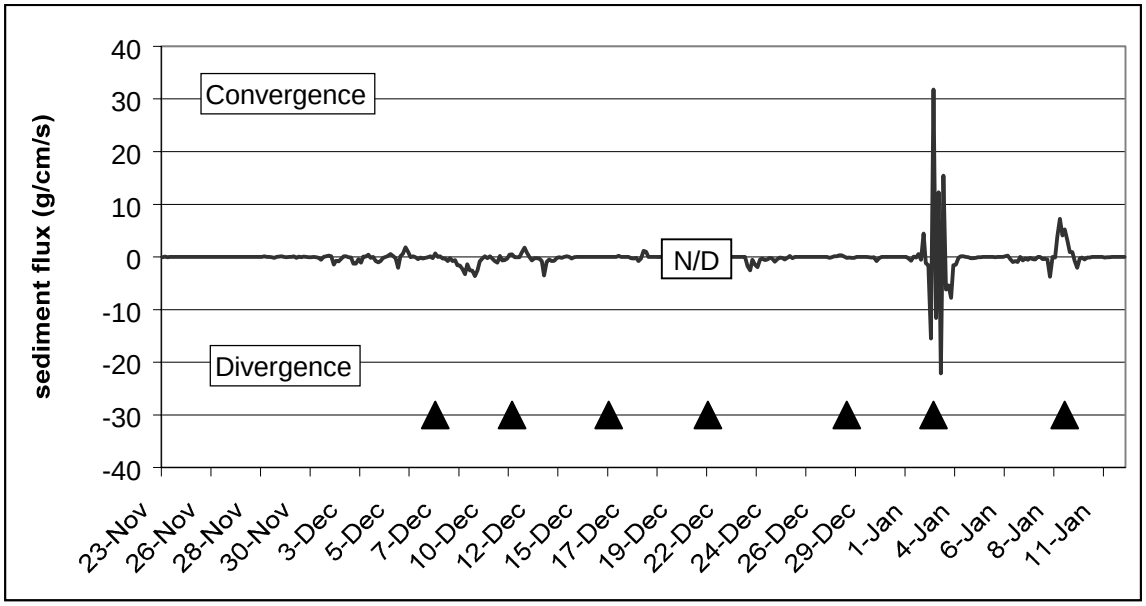

Figure 6.3. Flux of suspended sediment across Ship Shoal as calculated using the steady current/concentration (SCC) method.

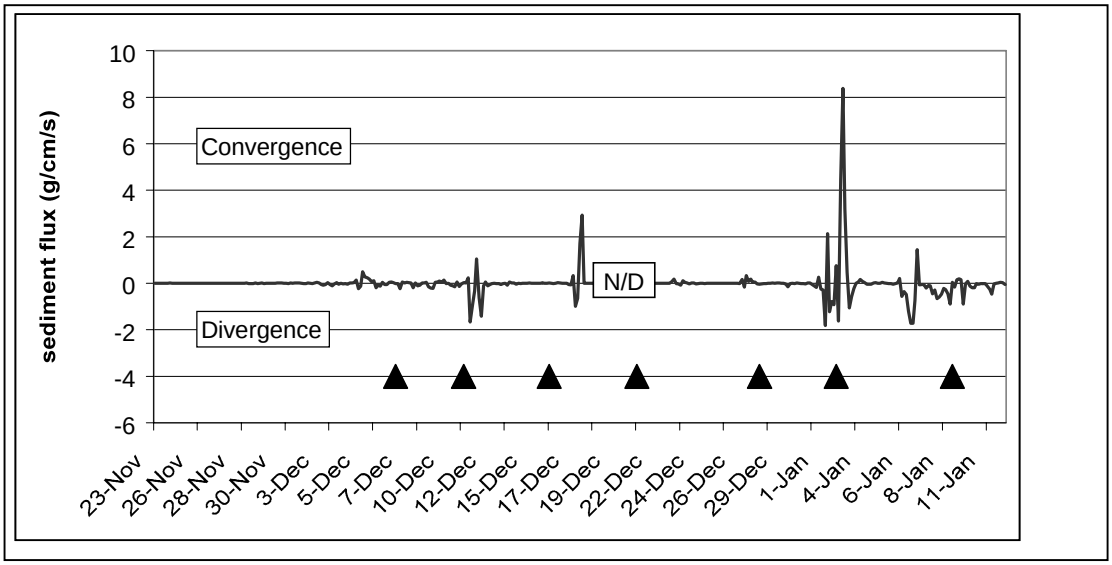

Figure 6.4: Flux of bed load across Ship Shoal as calculated using the Meyer-Peter and Muller (MPM) method**.**

Table 6.11. Sediment flux (in mg cm^{-1} s^{-1}) across Ship Shoal during storms and fair weather as predicted from Systems1A and 2A using spectral methods and the GMR and MPM models (outlined previously). Negative values indicate a divergence of sediment from the shoal while positive values indicate a convergence.

	Spectral				***Time-Averaged***	
	Mean	***Infragravity***	***Wind-wave***	***Sum***	***GMR***	***MPM***
Storm 1	-53.31	713.54	528.94	1160.25	-17.29	-41.62
Storm 2	-1.76	158.14	1093.63	1286.80	220.72	-177.46
Storm 3	0.68	-10.33	-12.86	-21.11	1.87	-2.54
Storm 4	-52.63	715.41	-1333.94	-405.05	4.43	11.99
Storm 5	-5.22	63.70	147.63	214.22	-0.55	-9.18
Storm 6	12.81	230.85	672.64	1207.16	1307.85	444.65
Storm 7	40.10	-191.00	-2477.24	-2548.22	-583.88	-66.03
All Storms	**-11.82**	**313.47**	**-32.02**	**408.22**	**281.34**	**57.75**
Fair Weather	**-11.08**	**-157.16**	**-933.56**	**-1132.63**	**-62.25**	**-30.28**

In summary, therefore, sediment flux on Ship Shoal tends to be divergence (potentially, erosion of the shoal) during fair weather, due largely to high rates of onshore transport on its landward side, and convergence (potentially, shoal accretion) during storms, due to strong offshore transport on the seaward side. The situation is somewhat analogous to the well-established model of surf zone storm sediment transport in which seaward transport during storms creates an offshore bar that is then steadily reworked landward during fair weather. This

comparison should not be carried too far, however, since the forcing mechanisms operating on Ship Shoal are poorly understood, and may be completely unrelated to those that operate in the nearshore. Furthermore, the sediment flux initiated by individual storms was highly variable, suggesting that a single “typical” pattern of flux due to storms may not be a realistic paradigm for of Ship Shoal. Nonetheless, it appears that the natural evolution of Ship Shoal is the result of balances between erosive fair weather influences, and aggradational winter-storm influences.

7. VALIDATION OF NUMERICAL WAVE MODEL *(STWAVE)*

Introduction

Phase 1 of this program concentrated on quantifying the impacts of sand removal at Ship Shoal on the wave field (Stone and Xu, 1996). In order to accomplish this goal, a number of state-of-the-art numerical wave models were evaluated (STWAVE v3, REF/DIF, REFDIFS, RCPWAVE). These models were compared against the following criteria: representation (scale), efficiency, accuracy, spectral capability, computational grid size requirement, breaking criteria, and wind-wave generating. STWAVE was given the highest composite score because of its spectral capability, inclusion of a wind-forcing function, high accuracy, and high efficiency.

STWAVE is a finite-difference model for near-coast time-independent spectral wave energy propagation simulations (Cialone *et al.*, 1992; McKee et al., 1999). It is based on a simplified spectral balance equation

$$\frac{\partial}{\partial x}\left(C\ C_g\ E(f,q)\right) + \frac{\partial}{\partial y}\left(C\ C_g\ E(f,\theta)\right) + \sum_{i=1}^{N} S_i = 0$$

where

$E(f,\theta)$	=spectral energy density
f	=frequency of spectral component
θ	=propagation direction of spectral component
S_i	=source terms (shoaling, refraction, wind forcing, wave-wave nonlinear interactions, bottom interaction, etc.) (see McKee et al., 1999 for a detailed description.)

STWAVE simulation requires a wave energy spectrum specified for the input boundary of the computational grid. It transforms the spectrum across the grid, including refraction and shoaling effects. The spectrum is modified to include the effects of bottom diffraction and the convergence/divergence of energy influenced by the local bathymetry. Wind-wave generation, nonlinear energy transfer, wave field and wave-bottom dissipation and wave breaking are considered. The model is computationally efficient because of its assumption that only wave energy directed into the computational grid is significant, i.e., wave energy not directed into the grid is neglected.

Validation Methods

The output from STWAVE version 3 was tested for two CSI field deployments in 1998/1999 and 2000. Two stations were established for the first deployment (offshore and inshore on Figure 7.1) and a third station mid-way between the former during the 2000 deployment. For both deployments, wave information measured at the offshore station was selected as the input boundary condition for the model. The wind conditions for the 1998/99 deployment were obtained from Grand Isle, Louisiana, and a Terrebonne

Bay site for the 2000 deployment. The input wave spectra (JONSWAP) were calculated by STWAVE from measured significant wave heights, peak wave period, and wave direction and corresponding wind information. A range of 15 frequencies was applied over 35 approach angles. Peak, low, and high cut off frequencies were dependant on the individual measured wave parameters at the boundary station. Because STWAVE is a half-plane model (i.e., wave energy can only propagate from offshore to onshore or +/- 87.5 degrees from the grid x axis), wind generated waves from the north are neglected. The bathymetric grid at Ship Shoal had the dimensions 16.6 km by 27.1 km. As shown on Figure 7.1, the offshore station was located on the south side boundary of modeling area, and the mid and inshore stations to the north. The bathymetric grid was generated from surveys conducted in the 1980's by the United States Geological Survey. Bathymetry for the west and north west part of the study site was obtained from the National Ocean Service. The grid size is 166 by 271 with 100 meters spacing. Measured wave and wind data were input to the model for both time series every 3 hours for the 1998/99 time series and 4 hours for the 2000 time series. A total of 590 models runs were conducted and the data are presented in Figures 7.2-7.17 as scatter plots of measured and numerically derived H_s along with the respective coefficient of determination (r^2), and time series plots of measured and computed H_s. Plots of all wind directions for both deployments are presented in addition to wind directions from the SW, S and SE.

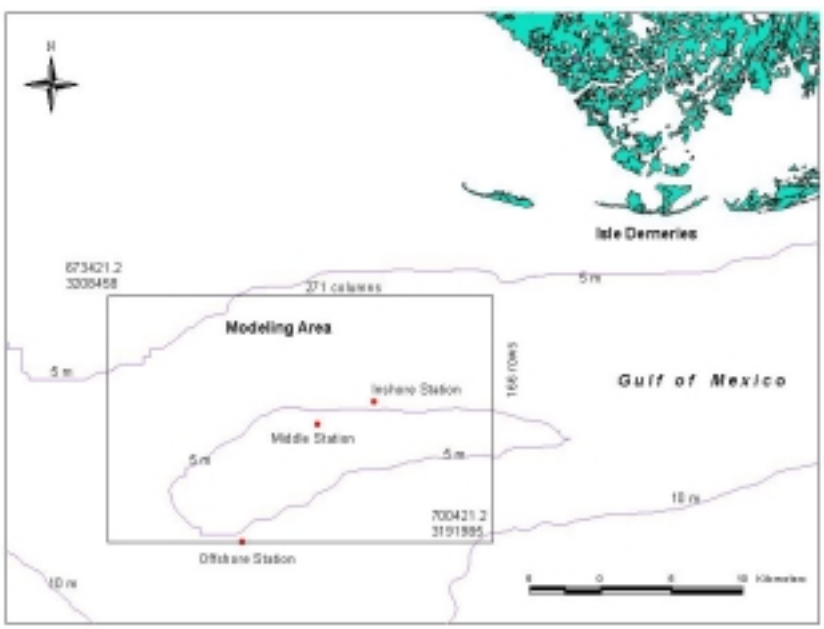

Figure 7.1. Location of the modeling area at Ship Shoal and instrumentation deployment sites.

Comparison of *In Situ* and Modeled Data

High r^2 values of 0.85 and 0.89 were obtained for all comparisons in both deployments at the Inshore station indicating that STWAVE has performed well in predicting H_s (Table 7.1 and Figures 7.2 and 7.3). As shown in Figures 7.4 -7.7, the

measured and predicted values are in good agreement throughout the entire range of wave heights measured, 0.1 to 1.6m. At both stations for each deployment, the model over predicts wave height by between 23 and 24% (Table 7.1). At the Middle station for the 2000 deployment, the r^2 value is 0.76 (Figures 7.8 and 7.9) for all wind directions and the percentage over prediction is 13% (Table 7.1) for H_s values ranging between 0.1 to 1.2 m.

Table 7.1. Percentage of over prediction of H_s by STWAVE when compared to i*n situ* measurements at two locations on Ship Shoal, based on 590 model runs.

Wind Direction	**1998/1999 Deployment (*Inshore*)**		**2000 Deployment (*Inshore*)**		**2000 Deployment (*Middle*)**	
	Percentage	**r^2**	**Percentage**	**r^2**	**Percentage**	**r^2**
From: SW, S, SE	14.1	0.90	23.4	0.81	7.6	0.56
From: SW	No waves from this direction		19.4	0.79	6.4	0.79
All Data	24.2	0.85	23.4	0.89	13.1	0.76

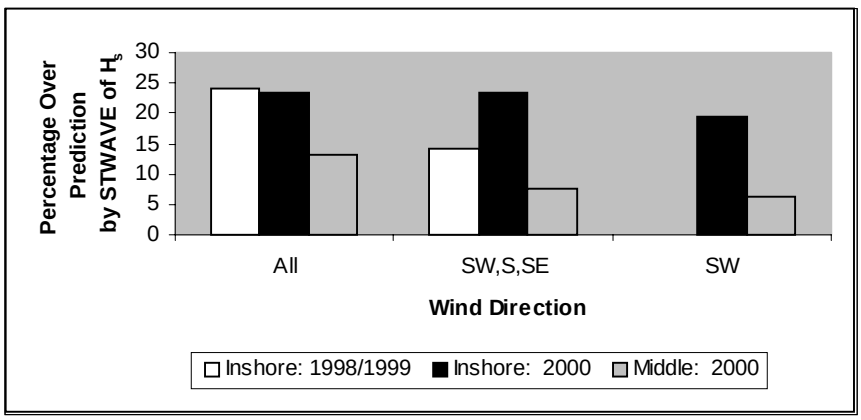

Figure 7.2: Summary of % over prediction of H_s by STWAVE for all stations.

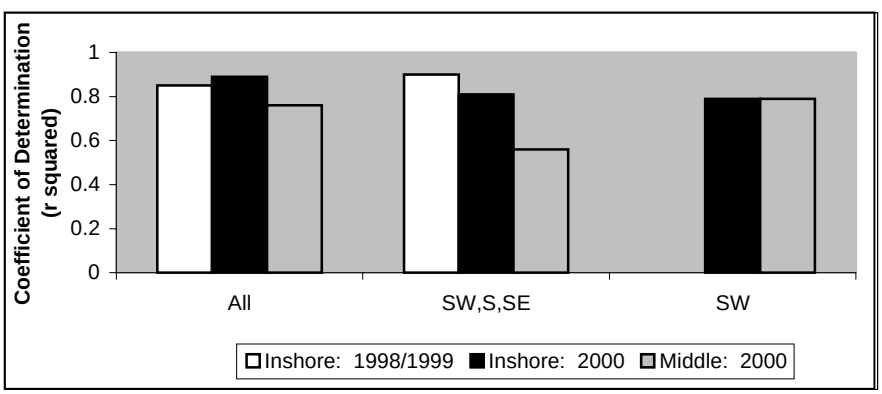

Figure 7.3: Summary of r^2 values for measured and modeled H_s for all stations.

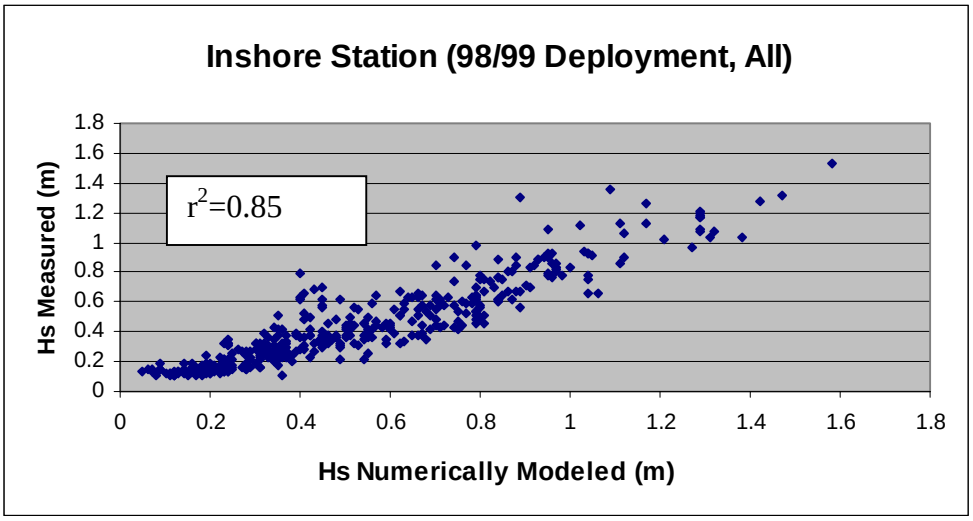

Figure 7.4. Scatter plot of significant wave heights for 1998/99 deployment for all wind directions at Inshore station.

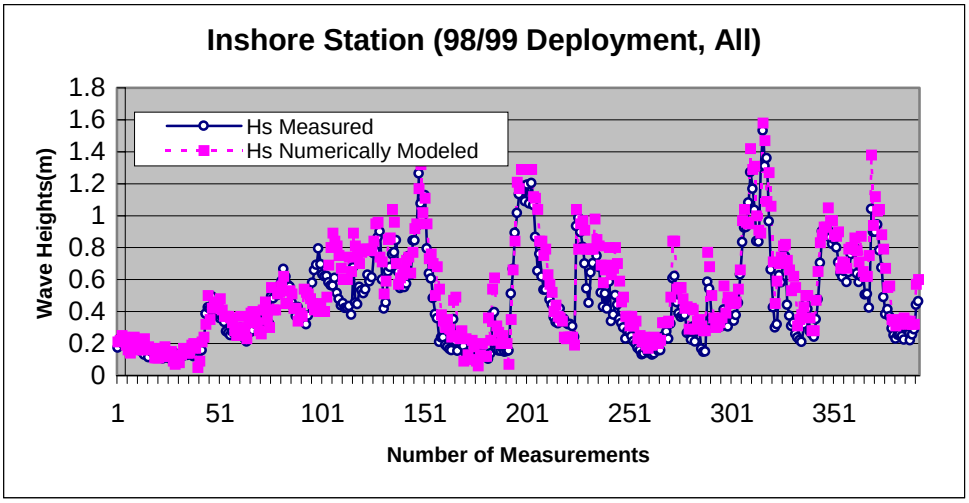

Figure 7.5. Comparison of measured and numerically modeled wave heights for all wind directions in 1998/99 deployment at Inshore station.

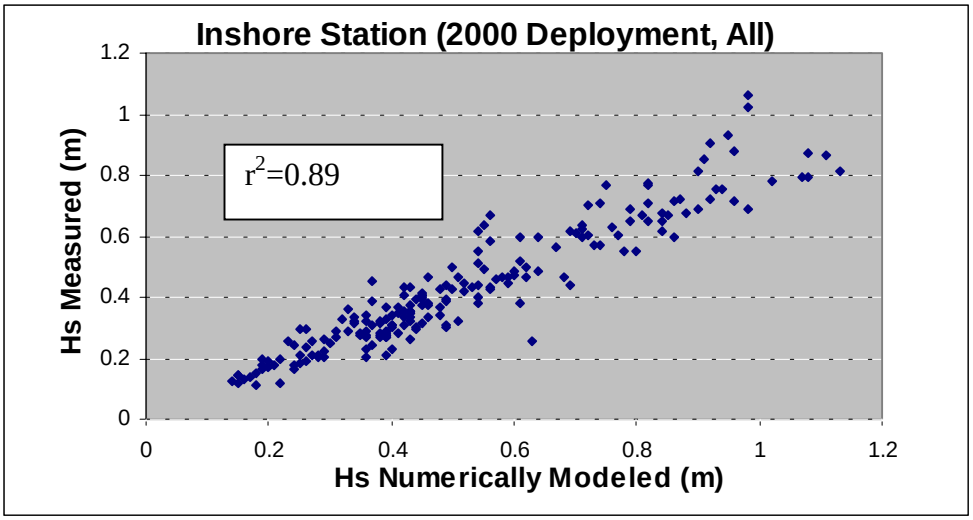

Figure 7.6. Scatter plot of significant wave heights for all wind direction at Inshore station for 2000 deployment.

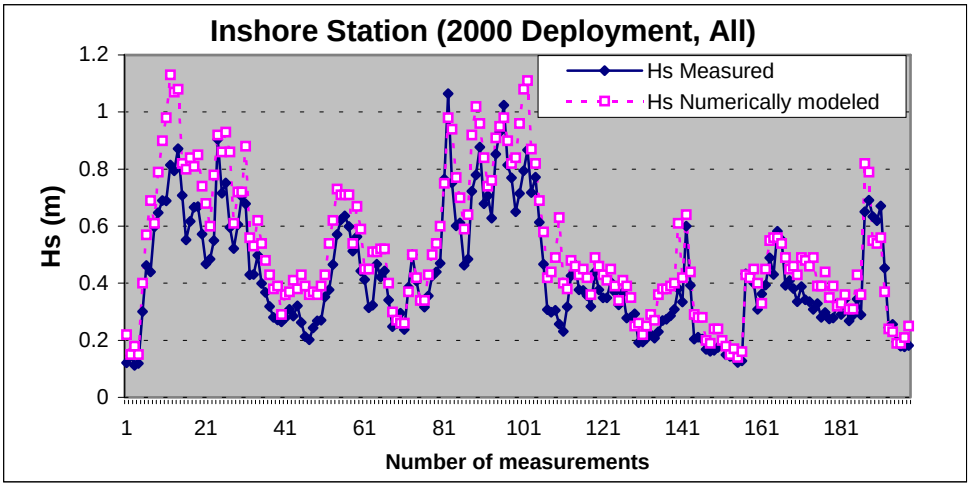

Figure 7.7. Comparison diagram of numerically modeled and measured wave heights for all wind directions at Inshore station for 2000 deployment.

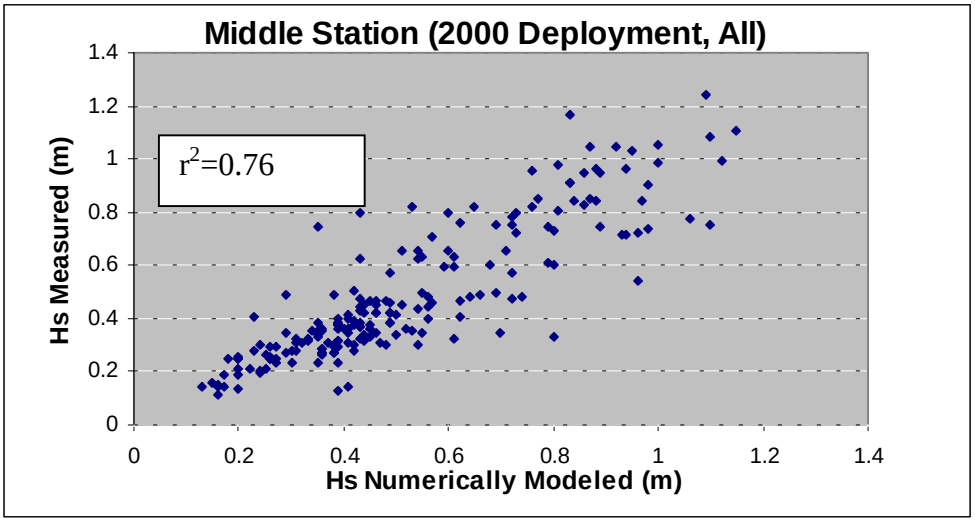

Figure 7.8. Scatter plot of Hs measured vs. Hs numerically modeled for 2000 deployment at Middle station.

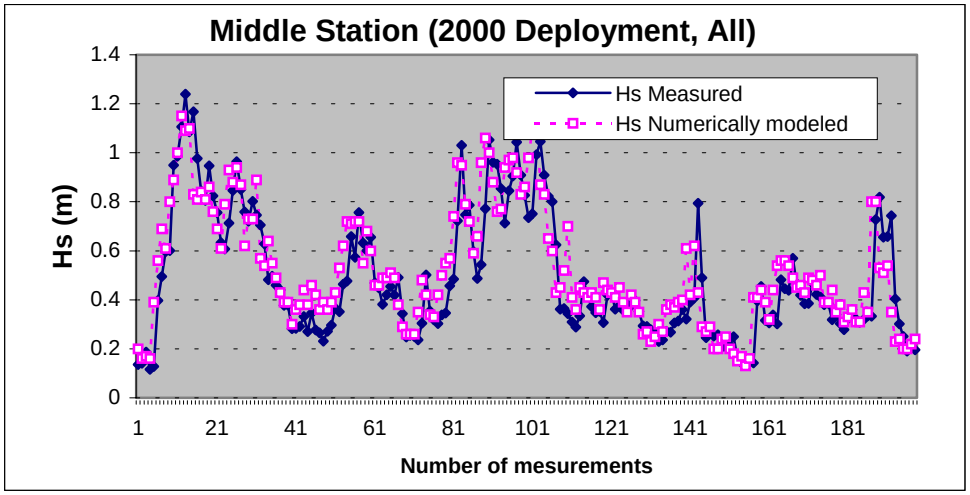

Figure 7.9. Comparison diagram of numerically modeled and measured wave heights for all wind directions at Middle station for 2000 deployment.

Given that STWAVE does not account for waves generated and propagated from the north, input wave parameters of waves approaching from the southwest, south and southeast were extracted from the measured data sets and input to the model. For the 1998/99 deployment at the Inshore station, the r^2 value increased to 0.9 and the percentage over prediction of H_s decreased to 14.1% when compared to all data (i.e., winds from all four quadrants) (Figures 7.10 and 7.11).. For the 2000 deployment, however, the r^r value decreased slightly to 0.81 and the percentage over prediction remained the same (23.4%) (Figures 7.12 and 7.13). Data obtained from the Middle station showed a marked decrease in over prediction from 13.1% down to 7.6% and a decrease in the r^2 value from 0.76 to 0.56 (Figures 7.14 and 7.15).

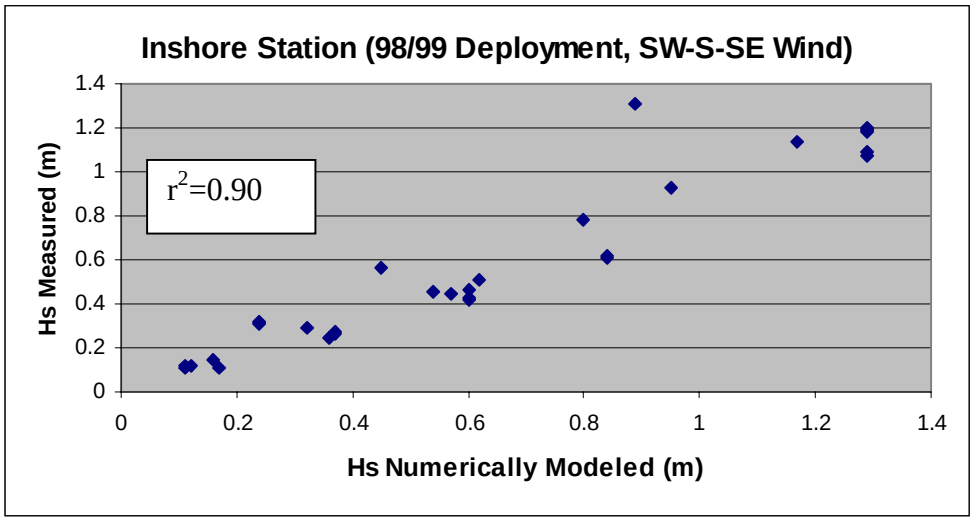

Figure 7.10. Scatter plot of measured and modeled H_s for wind blowing from southwest, south and southeast for 1998/99 deployment at Inshore station.

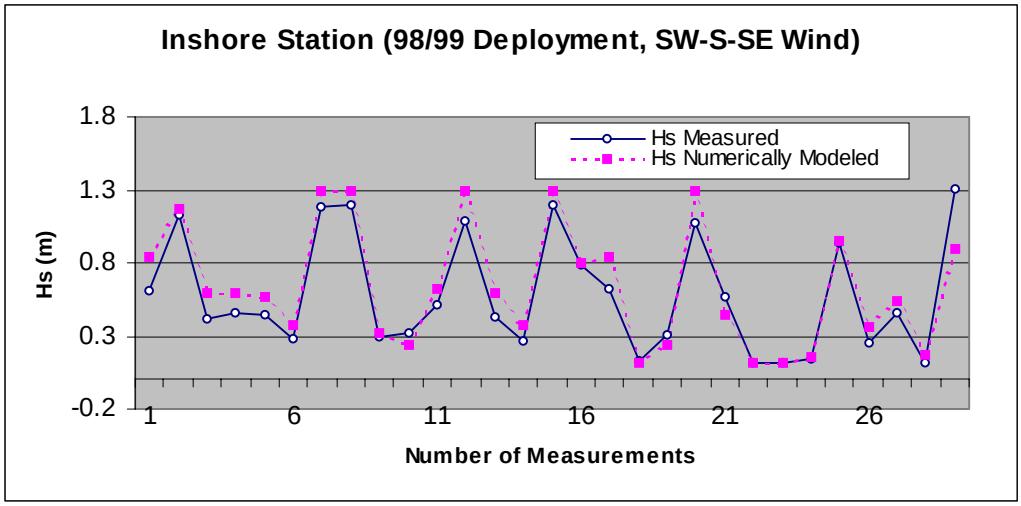

Figure 7.11. Comparison diagram of numerically modeled and measured wave heights for selected southwest, south and southeast winds at Inshore station for 1998/99 deployment.

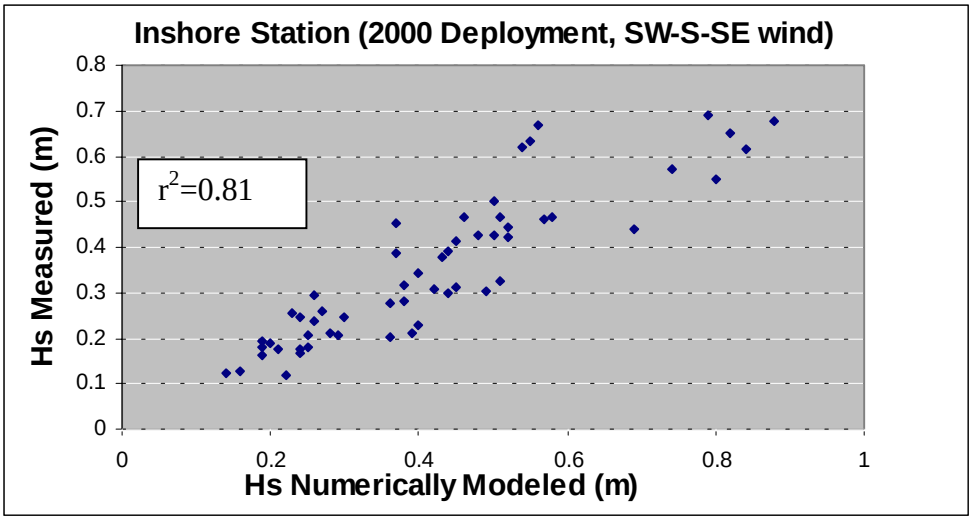

Figure 7.12. Scatter plot of Hs measured vs. Hs numerically modeled at Inshore station for southwest, south and southeast wind directions for 2000 deployment.

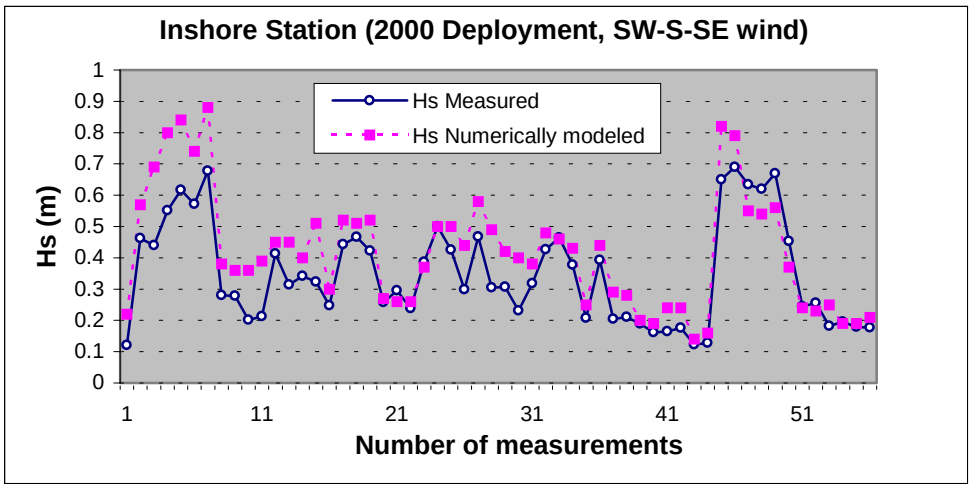

Figure 7.13: Comparison diagram of numerically modeled and measured wave heights for southwest, south and southeast wind directions at Inshore station for 2000 deployment.

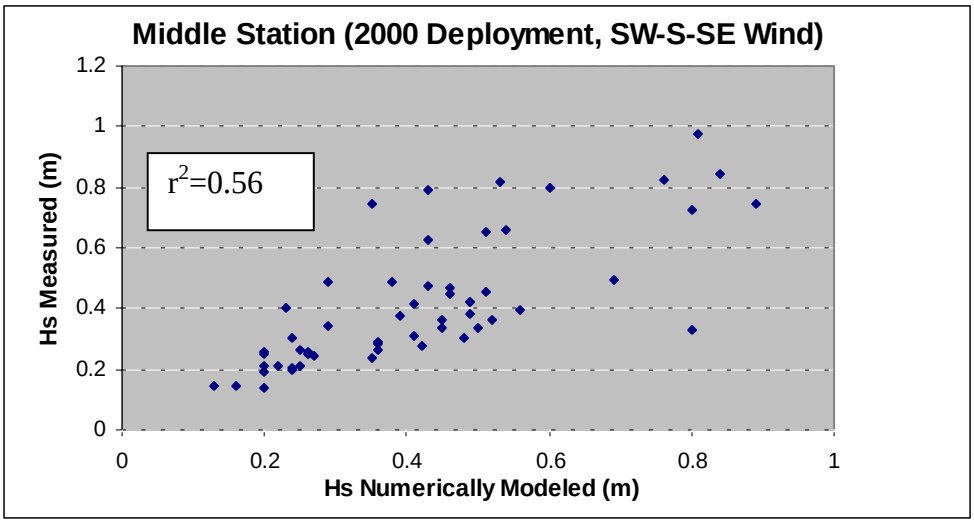

Figure 7.14. Scatter plot of Hs measured vs. numerically modeled Hs at Middle station for southwest, south and southeast winds foe 2000 deployment.

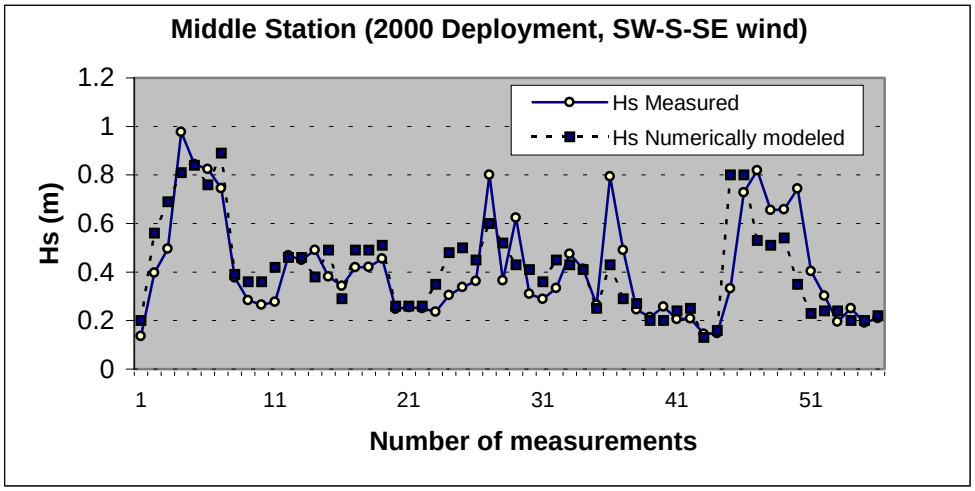

Figure 7.15. Relationship between numerically modeled and measured significant wave heights at Middle station for southwest, south and southeast winds.

To test the model further, waves approaching from the southwest were extracted from the time series and used as input. This was done to test if the orientation of the instrumentation array (slightly southwest to northeast) and wave refraction effects across the seaward flank of Ship Shoal were of significance in the comparisons of data sets. During the 1998/1999 deployment waves did not approach from the southwest, a common phenomenon during winter months off the Louisiana coast. For the 2000 deployment at the Inshore station, the r^2 value decreased slightly when compared to SW,

S and SE approaches from 0.81 to 0.79 (Figures 7.16 and 7.17). The percent over prediction in H_s decreased by 4% to 19.4%. At the Middle station, the r^2 value increased from 0.56 to 0.79, and the percent over prediction of H_s decreased by 1.2% to 6.4% (Figures 7.18 and 7.19).

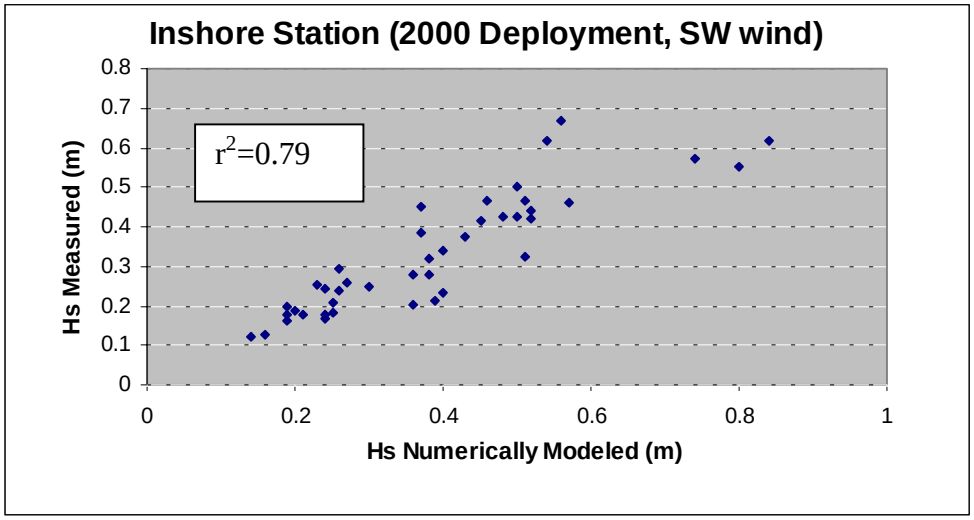

Figure 7.16. Scatter plot of Hs measured vs. Hs numerically modeled for southwest wind only at Inshore station for 2000 deployment.

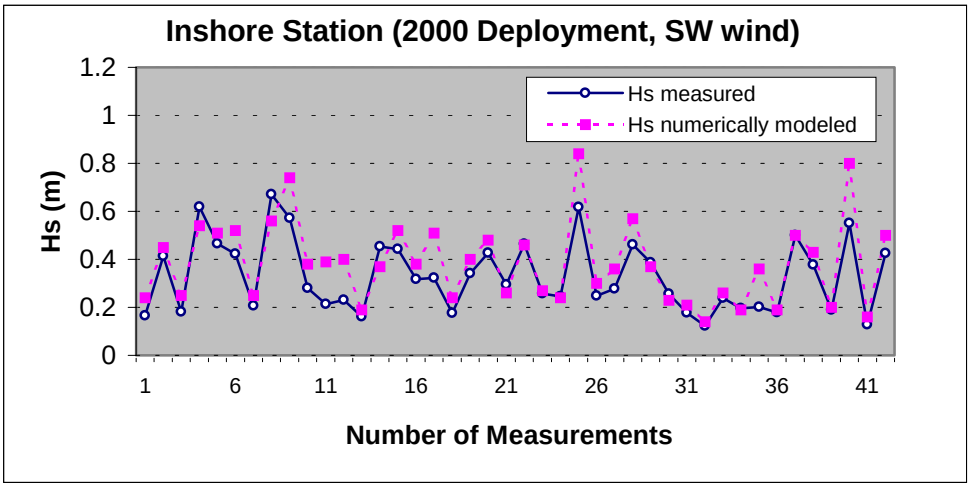

Figure 7.17. Relationship between numerically modeled and measured significant wave heights for south-west wind only at Inshore station.

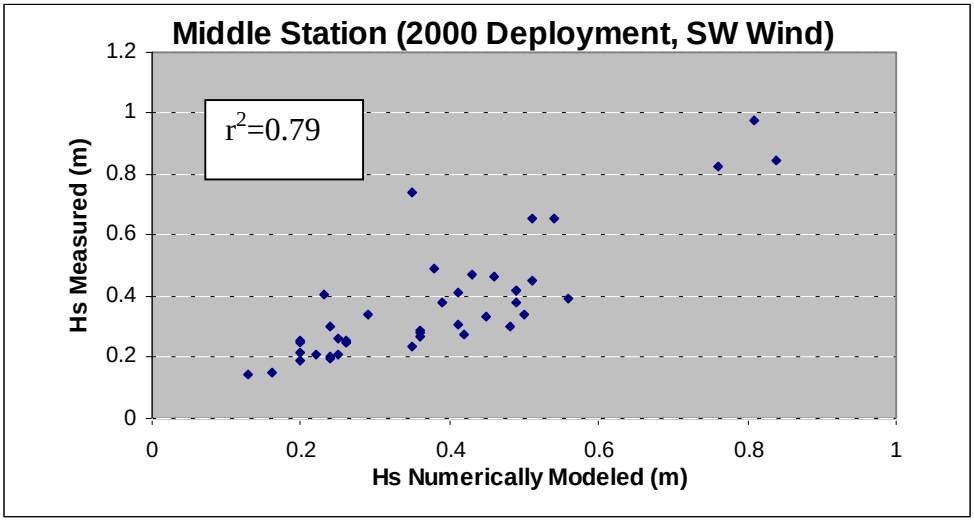

Figure 7.18. Scatter plot of Hs measured vs. Hs numerically modeled for southwest wind only at Middle station for 2000 deployment.

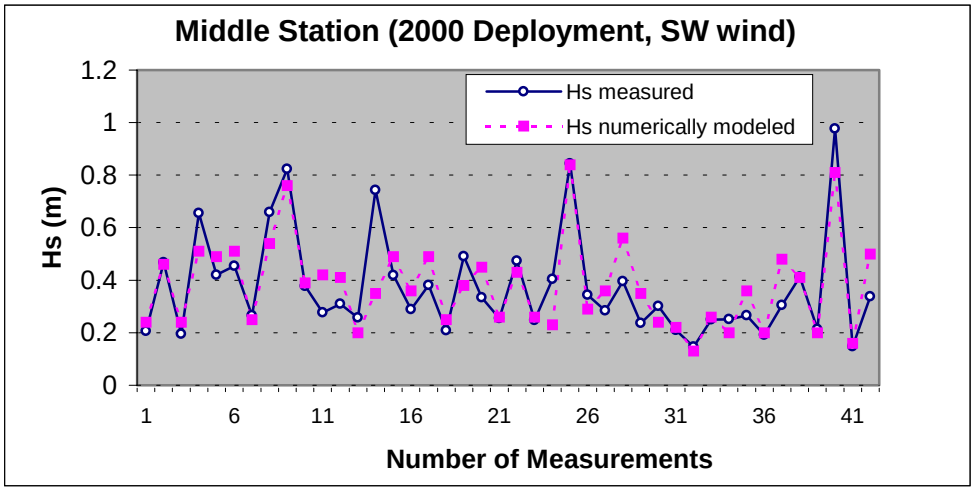

Figure 7.19. Relationship between numerically modeled and measured significant wave heights for south-west wind only at Middle station.

As summarized in Table 7.1 and Figures 7.2 and 7.3, the data presented indicate that STWAVE over predicts H_s by between 6 and 24%. Over prediction shows a general decrease when winds from the northern two quadrants are removed from the time series. Modeling waves propagating from the southwest to incorporate possible refraction effects across the shoal does not significantly alter either the over prediction percentage or r^2

value when compared to wave approaches from both southern quadrants. Overall, the model has predicted H_s very well over a substantial spectrum of wave conditions for the northern Gulf of Mexico.

8. CONCLUSIONS

Based on the data presented, the following conclusions are made:

1. Hydrodynamic, bottom boundary layer, and sedimentary variability on the Louisiana inner shelf during the winter is episodic, and is largely the result of recurring extratropical storm passages.

2. Considerable variability between storms, as well as during storms themselves, is reflected in hydrodynamic, bottom boundary layer, and sedimentary parameters. Some indices are several orders of magnitude greater during strong storms than during fair weather, while in the case of weak storms, the same parameters may actually be weaker.

3. Despite this considerable variability, storms are generally characterized by increases in: wave height, near-bed orbital, and mean current speed, shear velocity, suspended sediment concentration, and sediment transport. Decreases in wave period and apparent bottom roughness are also apparent.

4. Sediment transport during the winter is dominated by the strongest storms, when net sediment flux tends to be seaward.

5. Differences between the seaward and landward flanks of Ship Shoal are apparent. Waves tend to be higher and longer in period on the seaward side, while mean currents are generally higher landward, where they are directed onshore, in comparison with the seaward currents that predominate at the offshore site. It is apparent, therefore, that Ship Shoal exerts a significant influence on regional hydrodynamics, reducing wave energy and modulating current velocity.

6. The long-term evolution of Ship Shoal appears to be the result of a balance between fair weather influences, which cause erosion, and winter storm influences, which cause accretion. Superficially, this closely follows the commonly-held notions of nearshore storm/fair weather sediment transport on barred, but direct parallels are avoided for the moment since the details of process and response require further investigation.

7. The numerical wave model STWAVE version 3, appears to represent the wave field across Ship Shoal very well and on considering the complexity of wave-wave/current interactions at the site, the tendency for over prediction is relatively minor.

8. There is a considerable amount of additional experimentation that should be conducted at the site, particularly to answer questions pertaining to large-scale sedimentation patterns and event-scale morphodynamics.

9. REFERENCES

Adams, C.E., Jr., D.J.P. Swift and J.M. Coleman. 1987. Bottom Currents and Fluviomarine Sedimentation on the Mississippi Prodelta Shelf: February-May 1984. Journal of Geophysical Research 92(C13):14595-14609.

Adams, C.E., Jr. and G. Weatherly. 1981. Suspended-sediment transport and benthic boundary-layer dynamics. Marine Geology 42:1-18.

Agrawal, Y.C. and D.G. Aubrey. 1992. Velocity observations above a rippled bed using laser doppler velocimetry. Journal of Geophysical Research 97(C12):20249-20259.

Amos, C.L., A.J. Bowen, D.A. Huntley and C.F.M. Lewis. 1988. Ripple generation under the combined influences of waves and currents on the Canadian continental shelf. Continental Shelf Research 8(10):1129-1153.

Amos, C.L. and J.T. Judge. 1991. Sediment transport on the eastern Canadian continental shelf. Continental Shelf Research 11:1037-1068.

Armbruster, C.K., G.W. Stone and J.P. Xu. 1995. Episodic atmospheric forcing and bayside foreshore erosion: Santa Rosa Island, Florida. Gulf Coast Association of Geological Societies Transactions 45:31-37.

Biocourt, W.C., W.J. Wiseman Jr., A. Valle-Levinson and L.P. Atkinson. 1998. Continental shelf of southeastern United States and Gulf of Mexico. In: Robinson, A.R. and K.H. Brink (eds.), The Sea. Vol. 11. New York: Wiley and Sons, pp. 135-182.

Boon, J.D., M.O. Green and K.D. Suh. 1996. Bimodal wave spectra in lower Chesapeake Bay, sea bed energetics and sediment transport during winter storms. Continental Shelf Research 16(15):1965-1988.

Cacchione, D.A. and D.E. Drake. 1990. Shelf sediment transport: An overview with applications to the northern California shelf. In: Hanes, D. and B. LeMehaute (eds.), The Sea. Vol. 9. New York: Wiley and Sons, pp. 729-773.

Cacchione, D.A. and D.E. Drake. 1982. Measurements of storm-generated bottom stresses on the continental shelf. Journal of Geophysical Research 87(C3):1952-1960.

Cacchione, D.A., D.E. Drake, J.T. Ferreira and G.B. Tate. 1994. Bottom stress estimates and sand transport on northern California inner continental shelf. Continental Shelf Research 14(10/11):1273-1289.

Cacchione, D.A., W.D. Grant, D.E. Drake and S.M. Glenn. 1987. Storm-dominated bottom boundary layer dynamics on the northern California continental shelf: Measurements and predictions. Journal of Geophysical Research 92(C2):1817-1827.

Chaney, P.L. 1999. Extratropical storms of the Gulf of Mexico and their effects along the northern coast of a barrier i sland: West Ship Island, Mississippi. Unpublished project. Baton Rouge: Louisiana State University, 211 pp.

Coleman, J.M., H.H. Roberts and G.W. Stone. 1998. Mississippi River delta: an overview. Journal of Coastal Research 14(3):698-716.

Crout, R.L. and R.D. Hamiter. 1981. Response of bottom waters on the west Louisiana shelf to transient wind events and resulting sediment transport. Transactions of the Gulf Coast Association of Geological Societies 31:273-277.

Daddio, E. 1977. Respo nse of coastal waters to atmospheric frontal passage in the Mississippi Delta region. Technical Report 234, Coastal Studies Institute, Center for Wetland Resources, Baton Rouge: Louisiana State University, 38 pp.

Davidson, M.A., P.E. Russell, D.A. Huntley and J. Hardisty. 1993. Tidal asymmetry in suspended sand transport on a macrotidal intermediate beach. Marine Geology 110: 333-353.

Davies, A.G. 1995. Effects of unsteadiness on the suspended sediment flux in co-linear wave-current flow. Continental Shelf Research 15(8):949-979.

Davies, A.G. and Z. Li. 1997. Modelling sediment transport beneath regular symmetrical and asymmetrical waves above a plane bed. Continental Shelf Research 17(5):555-582.

Dingler, J.R., T.E. Reiss and N.G. Plant. 1993. Erosional patterns of the Isles Dernieres, Louisiana, in relation to meteorological influences. Journal of Coastal Research 9(1):112-125.

Dolan, R. and R.E. Davis. 1992a. Rating northeasters. *Mariners Weather Log* 36(1):4-11.

Dolan, R. and R.E. Davis. 1992b. An intensity scale for Atlantic coast northeast storms. Journal of Coastal Research 8(4):840-853.

Drake, D.E. and D.A. Cacchione. 1992. Wave-current interaction in the bottom boundary layer during storm and non-storm conditions: observations and model predictions. Continental Shelf Research 12(12):1331-1352.

Drake, D.E. and D.A. Cacchione. 1986. Field observations of bed shear stress and sediment resuspension on continental shelves, Alaska and California. Continental Shelf Research 6(3):415-429.

Dyer, K.R. and R.L. Soulsby. 1988. Sand transport on the continental shelf. Annual Review of Fluid Mechanics 20:295-324.

Earle, M.D., D. McGehee, and M. Tubman. 1995. Field Wwave gaging program, wave data analysis standard. U.S. Army Corps of Engineers Instruction Report, CERC-95-1, 33 pp.

Frazier, D.E. 1967. Recent deltaic deposits of the Mississippi River, their development and chronology. Transactions of the Gulf Coast Association of Geological Societies 17:287-315.

Glenn, S.M. and W.D. Grant. 1987. A suspended sediment stratification correction for combined Wave and current flows. *Journal of Geophy sical Research* 92(C8):8244-8264.

Grant, W.D. and O.S. Madsen. 1986. The continental-shelf bottom boundary layer. Annual Review of Fluid Mechanics 18:265-305.

Grant, W.D. and O.S. Madsen. 1982. Movable bed roughness in unsteady oscillatory flow. *Journal of Geophy sical Research* 87(C1):469-481.

Grant, W.D. and O.S. Madsen. 1979. Combined wave and current interaction with a rough bottom. Journal of Geophysical Research 84(C4):1797-1807.

Green, M.O. 1992. Spectral estimates of bed shear stress at subcritical Reynolds numbers in a tidal boundary layer. Journal of Physical Oceanography 22:903-917.

Green, M.O, C.E. Vincent, I.N. McCave, R.R. Dickson, J.M. Rees and N.D. Pearson. 1995. Storm sediment transport: observations from the British North Sea shelf. Continental Shelf Research 15:889-912.

Gross, T.F., A.E. Isley and C.R. Sherwood. 1991. Estimation of stress and bed roughness during storms on the northern California shelf. Continental Shelf Research 12:389-413.

Gust, G. and J.B. Southard. 1983. Effects of weak bedload on the universal law of the wall. Journal of Geophysical Research 88(C10):5939-5952.

Halper, F.B. and D.W. McGrail. 1988. Long-term measurements of near-bottom currents and suspended sediment concentration on the outer Texas-Louisiana continental shelf. *Continental Shelf Research* 8(1):23-36.

Henderson-Sellers, A. and P.J. Robinson. 1986. Contemporary Climatology, United Kingdom: Longman Scientific and Technical, 439 pp.

Huntley, D.A., R.J. Nicholls, C. Liu and K.R. Dyer. 1994. Measurements of the semi-diurnal drag coefficient over sand waves. Journal of Geophysical Research 14(C5):437-456.

Hsu, S.A. 1993. The Gulf of Mexico—A breeding ground for winter storms. *Mariners Weather Log* 37(2):4-11.

Jaffe, B.E., J.H. List and A.H. Sallenger, Jr. 199. Massive sediment bypassing on the lower shoreface offshore of a wide tidal inlet–Cat Island Pass, Louisiana. Marine Geology 136:131-149.

Kim, S.-C, L.D. Wright and B.-O. Kim. 1997. The combined effects of synoptic scale and local-scale meteorological events on bed stress and sediment transport on the inner shelf of the Middle Atlantic Bight. Continental Shelf Research 17(4):407-433.

Kolb, C.R. and J.R. Van Lopik. 1958. Geology of the Mississippi deltaic plain-southeastern Louisiana. New Orleans: U.S. Army Corps of Engineers Technical Report 2, 482 pp.

Komar, P.D. and M.C. Miller. 1975. On the comparison between the threshold of sediment motion under waves and unidirectional currents with a discussion of the practical evaluation of the threshold. Journal of Sedimentary Petrology 43:362-367.

Lesht, B.M. 1980. Benthic boundary-layer velocity profiles: dependence on averaging period. Journal of Physical Oceanography 10:985-991.

Li, M.Z. and C.L. Amos. 1999. Sheet flow and large wave ripples under combined waves and currents: field observations, model predictions and effects on boundary layer dynamics. Continental Shelf Research 19:637-663.

Li, M.Z., C.L. Amos and D.E. Heffler. 1997. Boundary layer dynamics and sediment transport under storm and non-storm conditions on the Scotian Shelf. Marine Geology 141:157-181.

Li, M.Z., L.D. Wright and C.L. Amos. 1996. Predicting ripple roughness and sand resuspension under combined flows in a shoreface environment. Marine Geology 130:139-161.

Long, C.E, and J.M. Oltman-Shay. 1991. Directional characteristics of waves in shallow water. New Orleans: U.S. Army Corps of Engineers Instruction Report CERC-95-1, 130 pp.

Longuet-Higgins, M.S. 1980. On the distribution of the heights of sea waves: some effects of nonlinearity and finite bandwidth. Journal of Geophysical Research 85:1519-1523.

Lynch, J.f., T.F Gross, C.R. Sherwood, J.D Irish and B.H. Brumley. 1996. Acoustical and optical backscatter measurements of sediment transport in the 1988-1989 STRESS experiment. Continental Shelf Research 17(4):337-366.

Lyne, V.D., B. Butman and W.D. Grant. 1990a. Sediment movement along the U.S. east coast continental shelf—I. estimates of bottom stress using the Grant-Madsen model and near-bottom wave and current measurements. Continental Shelf Research 10(5):397-428.

Lyne, V.D., B. Butman and W.D. Grant. 1990b. Sediment movement along the U.S. east coast continental shelf—II. modelling suspended sediment concentration and transport rate during storms. Continental Shelf Research 10(5):429-460.

Madsen, O.S., L.D. Wright, J.D. Boon and T.A. Chisolm. 1993. Wind stress, bed roughness and sediment suspension on the inner shelf during an extreme storm event. *Continental Shelf Research* 13(11):1303-1324.

Manighetti, B., and L. Carter. 1999. Across-shelf sediment dispersal, Hauraki Gulf, New Zealand. *Marine Geology* 160:271-300.

McKee Smith, J., D.T. Resio and A.K. Zundel. 1999. STWAVE: steady-state spectral wave model. Report 1, User's Manual. Vicksbueg, MS: USACOE, IR CHL 99-1, 45 pp.

Niedoroda, A.W. and D.J.P. Swift. 1981. Maintenance of the shoreface by wave orbital currents and mean flow: observations from the Long Island coast. Geophysical Research Letters 8(4):337-340.

Niedoroda, A.W., D.J.P. Swift, T.S. Hopkins and C.-M. Ma. 1984. Shoreface morphodynamics on wave dominated coasts. Marine Geology 60:331-354.

Nittrouer, C.A. and L.D. Wright. 1994. Transport of particles across continental shelves. Reviews of Geophysics 32:85-113.

Osborne, P.D. and B. Greenwood. 1993. Sediment suspension under waves and currents: time scales and vertical structure. Sedimentology 40:599-622.

Osborne, P.D. and C.E. Vincent. 1996. Vertical and horizontal structure in suspended sand concentrations and wave-induced fluxes over bedforms. Marine Geology 131:195-208.

Penland, S., R. Boyd and J.R. Suter. 1988. Transgressive depositional systems on the Mississippi Delta Plain: a model for barrier shoreline and shelf sand development. Journal of Sedimentary Petrology 58(6):932-949.

Penland, S. and K. Ramsey. 1990. Relative sea level rise in Louisiana and the Gulf of Mexico: 1908-1988. Journal of Coastal Research 6(2):323-342.

Pepper, D.A., G.W. Stone, and P. Wang. 1999. Bottom boundary layer parameters and sediment transport on the Louisiana inner-shelf during cold front passages. Transactions of the Gulf Coast Association Geological Societies 49:432-439.

Pond, S. and G.L Pickard. 1983. Introductory Dynamical Oceanography, 2nd Edition. United Kingdom: Butterworth-Heinemann, 329 pp.

Ritchie, W. and S. Penland. 1988. Rapid dune changes associated with overwash processes on the deltaic coast of south Louisiana. Marine Geology 81:97-122.

Roberts, H.H., O.K. Huh, S.A. Hsu, L.J. Rouse, Jr. and D. Rickman. 1987. Impact of cold-front Passages on geomorphic evolution and sediment dynamics of the complex Louisiana coast. Proceedings of Coastal Sediments '87, *ASCE* 2, pp. 1950-1963.

Scruton. 1960. Delta Building and the Deltaic Sequence. Recent Sediments, Northwest Gulf of Mexico, AAPG Symposium: pp. 82-102.

Shauer, U. 1987. Determination of bottom boundary layer parameters at two shallow sea sites using the profile method. Continental Shelf Research 7(10):1211-1230.

Smith, J.D. and S.R. McLean. 1977. Spatially averaged flow over a wavy surface. Journal of Geophysical Research 82(C12):1735-1746.

Stone, G. W., J. P. Xu and X. Zhang. 1995 Estimation of the wave field during Hurricane Andrew and morphological change along the Louisiana coast. Journal of Coastal Research 18:234-253.

Stone, G.W. and Xu, J. 1996. Wave climate modeling and evaluation relative to sand mining on Ship Shoal, offshore Louisiana, for coastal restoration and barrier island restoration. OCS Study MMS 960059, 170 pp.

Stone, G.W., J.M. Grymes III, J.R Dingler and D.A. Pepper. 1997. Overview and significance of Hurricanes on the Louisiana coast, U.S.A. Journal of Coastal Research 13(3):656-659.

Stone, G.W. and R. A. McBride. 1998. Louisiana barrier Islands and their importance in wetland protection: forecasting shoreline change and subsequent response of wave climate. Journal of Coastal Research 14(3):900-915.

Vincent, C.E. and M.O. Green. 1990. Field measurements of the suspended sand concentration profiles and fluxes and of the resuspension coefficient $_0$ over a rippled bed. Journal of Geophysical Research 95(C7):11591-11601.

Vincent, C.E., R.A. Young and D.J.P. Swift. 1983. Sediment transport on the Long Island shoreface, North American Atlantic Shelf: role of waves and currents in shoreface maintenance. Continental Shelf Research 2(2/3):163-181.

Wiberg., P.L., D.E. Drake and D.A. Cacchione. 1994. Sediment resuspension and bed armoring during high bottom stress events on the northern California inner continental shelf: measurements and predictions. Continental Shelf Research 14(10/11):1191-1219.

Williams, S. J., S. Penland and A. H. Sallenger Jr. 1992. Louisiana barrier island erosion study: Atlas of shoreline changes in Louisiana from 1853 to 1989. USGS Miscellaneous Investigations Series I-2150-A, 103 pp.

Wright, L.D. (1995) *Morphodynamics of Inner Continental Shelves* CRC Press Inc., Boca Raton, FL, USA.

Wright, L.D., J.D. Boon, III, M.O. Green and J.H. List. 1986. Response of the mid shoreface of the southern mid-Atlantic bight to a “northeaster.” Geo-Marine Letters 6:153-160.

Wright, L.D., J.D. Boon, III, S.C Kim and J.H. List. 1991. Modes of cross-shore sediment transport on the shoreface of the Middle Atlantic Bight. Marine Geology 96:19-51.

Wright, L.D., C.R. Sherwood and R.W. Sternberg. 1997. Field measurements of fairweather bottom boundary layer processes and sediment suspension on the Louisiana inner continental shelf. Marine Geology 140:329-345.

Wright, L.D., J.P. Xu and O.S. Madsen. 1994. Across-shelf benthic transports on the inner shelf of the Middle Atlantic Bight during the "Halloween storm" of 1991. Marine Geology 118:61-77.

Xu, J.P. and L.D Wright. 1998. Observations of Wind-generated shoreface currents off Duck, North Carolina. Journal of Coastal Research 14(2):610-619.